Doklady Physics, Vol. 48, No. 10, 2003, pp. 537–539. Translated from Doklady Akademii Nauk, Vol. 392, No. 4, 2003, pp. 467–469.

PHYSICS

On the Solution of the Self-Consistent Problem for the Bunch of Charged Particles in a Penning Trap

N. D. Naumov

Presented by Academician A.F. Andreev May 26, 2003

Received April 14, 2003

Construction of analytical solutions of a self-consistent problem is one of the methods of studying the properties of a nonlinear system such as a gas of charged particles. In this study, it is shown that, under certain conditions, it is possible to obtain the solution of the Vlasov equation for a spatially limited distribution of charged particles. This equation describes both the pulsations of a uniform bunch of particles in a Penning trap and the initial stage of pulsations of a nonuniform bunch.

The external magnetic field used in the Penning trap is the superposition of the uniform magnetic field $\mathbf{B} = B\mathbf{e}_z$ and the nonuniform electric field whose potential in a cylindrical coordinate system has the form

$$\Phi_0 = A(\rho^2 - 2z^2).$$

Such an electric field can be produced by hyperbolic electrodes consisting of two surfaces $2z^2 = \rho^2 + 2d^2$ with potential $-V$ and surface $\rho^2 = 2z^2 + 2d^2$ with potential V. In this case, $A = \frac{V}{2d^2}$.

Before proceeding to the construction of the solution of the Vlasov equation, let us discuss the conditions under which a function $g(P_\theta, P_\varphi) = \delta(P_\theta)\delta(P_\varphi)$ of dynamical variables can be an integral of motion for a spherically symmetric distribution of a gas of charged particles in a Penning trap. Here, P_θ and P_φ are the components of the generalized momentum in the spherical coordinate system. To this end, we write the Hamiltonian of a particle in the combination of the external and collective fields:

$$H = \frac{1}{2m}\left[P_r^2 + \frac{P_\theta^2}{r^2} + \left(\frac{P_\varphi}{\sin\theta} - m\Omega r\sin\theta\right)^2\right] + eAr^2(1 - 3\cos^2\theta) + e\Phi,$$

where $\Omega = \frac{eB}{2mc}$ and Φ is the potential of the self-electric field. The Poisson brackets of the function g and this Hamiltonian has the form

$$\{Hg\} = -\frac{1}{2}r^2\sin 2\theta(m\Omega^2 + 6eA)\delta(P_\varphi)\frac{\partial}{\partial P_\theta}\delta(P_\theta).$$

Hence, the function g is an integral of motion if $A = -\frac{m\Omega^2}{6e}$. In what follows, this condition is assumed to be satisfied.

Let the initial state of the bunch of particles be described by the distribution function

$$F_0 = f_0(r, p_r)g(P_\theta, P_\varphi),$$
$$f_0 = \frac{n_0}{4\pi}r^2 w(r)\delta(p_r - mv(r)). \qquad (1)$$

This function corresponds to a spherical bunch that rotates as a whole with the Larmor frequency and has a nonuniform distribution of the particle density and radial velocity. This follows from the following expressions for the particle density and the components of gasdynamic velocity:

$$n = \int F_0 d^3p = n_0 w(r),$$
$$V_r = \frac{1}{mn}\int p_r F_0 d^3p = v(r),$$
$$V_\theta = \frac{1}{mn}\int p_\theta F_0 d^3p = 0,$$
$$V_\varphi = \frac{1}{mn}\int p_\varphi F_0 d^3p = -\Omega r\sin\theta.$$

Here, p_r, p_θ, and p_φ are the components of the kinetic momentum in the spherical coordinate system.

Since the function $g(P_\theta, P_\varphi)$ is an integral of motion (under the condition mentioned above), the distribution function of the pulsating bunch can be sought in the form

$$F = f(r, p_r, t)g(P_\theta, P_\varphi). \qquad (2)$$

Substituting expression (2) into the Vlasov equation written in the spherical coordinate system, we find that the function $f(r, p_r, t)$ obeys the equation

$$\mathrm{L}f \equiv \left(\frac{\partial}{\partial t} + \frac{p_r}{m}\frac{\partial}{\partial r} - \frac{\partial U}{\partial r}\frac{\partial}{\partial p_r}\right)f = 0, \tag{3}$$

where $U = e\Phi + m\Omega^2 r^2/2$.

The solution of Eq. (3) can be constructed by the method of a singular solution that plays the role of the Green's function of the operator L [1]. This is possible because the time-dependent self-consistent problem in this case virtually reduces to calculation of the radial motion of the cold gas of charged particles in the external and collective fields. For the problem under consideration, this method is formulated as follows:

$$H(t)f(X, t) = \int G(X, X_0, t) f_0(X_0) r_0^2 dX_0,$$

$$\mathrm{L}G(X, X_0, t) = \delta(t)\delta(X - X_0),$$

$$G(X, X_0, t)$$

$$= H(t)\delta(r - r(t;\, X_0))\delta(p_r - p_r(t;\, X_0)).$$

Here, $H(t)$ is the Heaviside step function; $r(t; X_0)$ and $p_r(t; X_0)$ present the radial motion law for an individual particle (in a field with the potential energy U) that meets the initial conditions

$$r(0; X_0) = r_0 \text{ and } p_r(0; X_0) = p_{r0},$$

and X denotes the set of the variables r and p_r.

When layers of particles sequentially (without overtaking one another) move in the radial direction, the potential of the collective field acting on a particle is determined by both the initial position of the particle r_0 and the given initial particle-density distribution $n(r, 0) = n_0 w(r)$:

$$\Phi = 4\pi n_0 \frac{e}{r} W(r_0) \text{ and } W(r_0) = \int_0^{r_0} w(x) x^2 dx.$$

Finally, the distribution function of the bunch of charged particles has the form

$$F = \frac{n_0}{4\pi} w(\xi(r, t))$$

$$\times \frac{\xi^2(r, t)}{Q(r, t)} \delta(p_r - mV_r(r - t)) g(P_\theta, P_\varphi). \tag{4}$$

Here, the function $\xi(r, t)$ is the solution of the transcendental equation $s(t, \xi) = r$, where the function s is defined as $s(t, r_0) = r[t; r_0, mv(r_0)]$;

$$Q(r, t) = R(t, \xi(r, t)), \quad R(t, r_0) = \frac{\partial s(t, r_0)}{\partial r_0},$$

$$\text{and } V_r(r, t) = \dot{s}(t, \xi(r, t)).$$

Hereafter, the dot over a symbol means the time derivative.

Distribution function (4) describes the pulsations of the rotating nonuniform bunch of particles in the Penning trap. The result is considerably simplified for the uniform bunch and for the initial velocity proportional to the distance from the center of symmetry: $v(r) = kr$, where k is a constant. For $w(r) = H\left(1 - \frac{r}{a_0}\right)$, the radial motion law of a particle has the form $s(t, r_0) = r_0 R(t)$. Here, a_0 is the initial radius of the bunch and the function R is the solution of the equation

$$3\ddot{R} + 2\Omega^2 R - \frac{\omega^2}{R^2} = 0, \tag{5}$$

where $\omega^2 = \frac{4\pi n_0 e^2}{m}$. The initial conditions for Eq. (5) have the form $R_0 = 1$ and $\dot{R}_0 = k$.

In this case, $\xi(r, t) = \frac{r}{R(t)}$ and distribution function (4) reduces to the form

$$F = \frac{n_0 r^2}{4\pi R^3} H\left(1 - \frac{r}{a_0 R}\right) \delta\left(p_r - mr\frac{\dot{R}}{R}\right) g(P_\theta, P_\varphi).$$

Thus, if the initial gas velocity is proportional to the distance from the bunch center, this distribution remains in the uniform bunch during its pulsations.

For the nonuniform bunch, it is more convenient to use the Lagrangian description of gas motion. It is easy to understand that the function $s(t, r_0)$ introduced above represents the Lagrangian variable characterizing the position of the gas layer that was at distance r_0 from the bunch center at the initial time. As was mentioned above, this function satisfies the equation

$$\ddot{s} = \frac{\omega^2}{s^2} W(r_0) - \frac{2}{3}\Omega^2 s \tag{6}$$

with the initial conditions $s(0, r_0) = r_0$ and $\dot{s}(0, r_0) = v(r_0)$.

The condition of layer-mass conservation in gas motion has the form

$$4\pi n(t, r_0) s^2 ds = 4\pi n_0 w(r_0) r_0^2 dr_0.$$

Hence, the density of particles is determined as

$$n(t, r_0) = n_0 \frac{r_0^2 w(r_0)}{s^2 R(t, r_0)}. \tag{7}$$

To derive the equation for the function $R(t, r_0)$, Eq. (6) should be differentiated with respect to r_0:

$$\ddot{R} = \omega^2 w(r_0) \frac{r_0^2}{s^2} - 2\left[\frac{1}{3}\Omega^2 + W(r_0)\frac{\omega^2}{r^3}\right] R. \tag{8}$$

It is evident that the initial conditions for Eq. (8) have the form

$$R(0, r_0) = 1 \text{ and } \dot{R}(0, r_0) = \frac{dv(r_0)}{dr_0}.$$

Unfortunately, the solution of Eqs. (6) and (8) provides the gasdynamic characteristics of the nonuniform bunch only up to a certain time t_k. The domain of applicability of the results is limited, because the initial assumption that particle layers move without overtaking one another can be violated in bunch pulsations. Overtaking means that $R(t_k, r_0) = 0$ for a certain layer. As a result, the particle density at the time $t = t_k$ of overtaking tends to infinity (the so-called gradient catastrophe [2, 3]).

The formation of the peak in the particle density is illustrated in the figure, which shows the particle-density distribution in the bunch calculated by Eqs. (6)–(8) for τ = (*2*) 0.6, (*3*) 1.2, and (*4*) $\tau = 1.38$. Here, $\tau = \Omega t$ and curve *1* corresponds to the initial particle-density distribution:

$$w(r) = \begin{cases} 1 - \left(\dfrac{r}{a_0}\right)^2, & r \le a_0 \\ 0, & r > a_0. \end{cases}$$

The calculations were performed for $v(r) = 0$ and $\omega^2 = 2\Omega^2$.

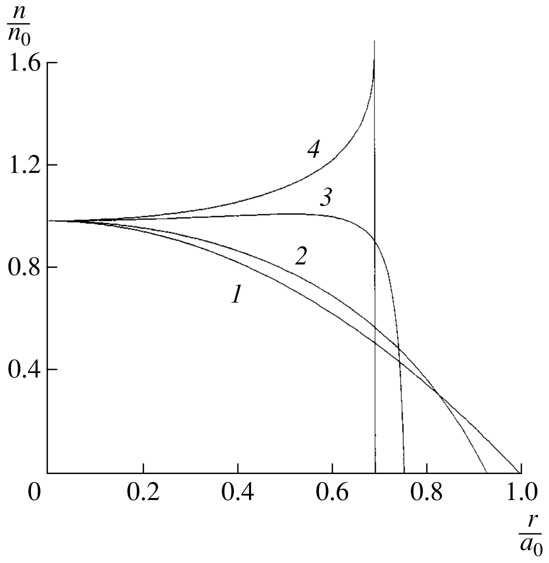

Formation of the peak in the particle density.

Thus, under the above conditions, calculation of pulsations of a uniform bunch of charged particles in a Penning trap reduces to the solution of an ordinary differential equation. Calculation of the initial stage of pulsations in a nonuniform bunch reduces to the solution of two such equations.

REFERENCES

1. N. D. Naumov, Dokl. Akad. Nauk **357**, 758 (1997) [Phys. Dokl. **42**, 670 (1997)].
2. V. P. Bykov, A. V. Gerasimov, and V. O. Turin, Usp. Fiz. Nauk **165**, 955 (1995) [Phys. Usp. **38**, 911 (1995)].
3. A. A. Samarskiĭ and A. P. Mikhaĭlov, *Mathematical Simulation* (Nauka, Moscow, 1997).

Translated by Yu. Vishnyakov

Doklady Physics, Vol. 48, No. 10, 2003, pp. 540–544. Translated from Doklady Akademii Nauk, Vol. 392, No. 5, 2003, pp. 614–617.
Original Russian Text Copyright © 2003 by Boyev, Sumbatyan.

PHYSICS

Short-Wave Diffraction on Bodies with an Arbitrary Smooth Surface

N. V. Boyev and M. A. Sumbatyan

Presented by Academician V.A. Babeshko April 24, 2003

Received June 5, 2003

The classical problem of the scattering of a high-frequency acoustic wave emitted by a point source is analyzed. The scattering occurs on an arbitrary smooth surface S of an obstacle. Below, we consider the time dependence of pressure to be monochromatic, i.e.,

$$p(x, y, z, t) = \mathrm{Re}[p(x, y, z)\exp(-i\omega t)],$$

and the boundary S of the obstacle to be acoustically solid:

$$\left.\frac{\partial p}{\partial n}\right|_S = 0.$$

In the case of single reflection, the solution to this problem in the two-dimensional case was obtained by various asymptotic methods in [1–3]. In [3], explicit asymptotic formulas were derived in the two-dimensional case for pressure in a reflected wave undergoing an arbitrary number of secondary reflections from the curvilinear boundary. In the three-dimensional case [4], the short-wave approximation was developed to determine pressure in the single-reflection case. In the present paper, we develop a method of investigating short-wave diffraction on obstacles with a complicated shape, which have an arbitrary smooth surface. This method is based on the estimate of Kirchhoff diffraction integrals, which uses the approach of many-dimensional stationary phase. The developed method makes it possible to determine for the first time and in closed form the amplitude of a multiply reflected high-frequency acoustic wave.

1. Let a spherical high-frequency monochromatic wave emitted from point x_0 of an acoustic medium impinge upon the surface S of an obstacle. For interaction of the wave with convex parts of the surface S, there exist only points of simple mirror reflection. On concave parts of the surface S, the diffraction pattern is more complicated than in the previous case and is stipulated by possible secondary reflections of the incident wave [2]. It is well known that the pressure in the reflected high-frequency wave at the point x is determined by the direction of wave incidence and by the small vicinity of the mirror-reflection point y^* of surface S. Therefore, with increasing frequency, the amplitude of the reflected signal can be determined in the framework of the beam representation using the stationary-phase method.

If a beam of the form $x_0 - y - x$ is reflected from the surface S ($y \in S$) only once, then, in accordance with the Kirchhoff diffraction theory, pressure $p(x)$ in the “illuminated” zone for an acoustically solid surface is determined by the following integral [5]:

$$p(x) = \iint_S 2p^{inc}(y)\frac{\partial \Phi}{\partial n_y}dS. \tag{1}$$

Here, $p^{inc}(y)$ is the pressure in the incident wave at the boundary S; Φ is the potential of the fundamental solution (Green function); n_y is the external normal to the surface S at the point y in the small vicinity of the point y^* of the beam mirror reflection; k is the wave number; γ is the angle between the normal n_y and direction of incidence of the $x_0 - y$ beam; and

$$\begin{aligned} p^{inc}(y) &= |x_0 - y|^{-1}e^{ik|x_0 - y|}, \\ \Phi &= (4\pi)^{-1}|x - y|^{-1}e^{ik|x - y|}. \end{aligned} \tag{2}$$

As $k \to \infty$,

$$\frac{\partial \Phi}{\partial n_y} = ik\cos\gamma(4\pi)^{-1}|x - y|^{-1}e^{ik|x - y|}[1 + O(k^{-1})]. \tag{3}$$

With allowance for the fact that the incident $x_0 - y^*$ and reflected $y^* - x$ beams lie in the same plane with the normal to the surface at the mirror reflection point y^*, we can obtain from expressions (1)–(3) the following basic relationship (after the nonoscillating functions have been taken out from the integral in the short-wave approximation):

$$p(x) = \frac{ik}{2\pi}\frac{\cos\gamma}{L_0 L}\iint_S e^{ik\varphi}dS. \tag{4}$$

Rostov State University,
ul. Bol'shaya Sadovaya 105, Rostov-on-Don, 344066 Russia
e-mail: boyev@math.rsu.ru; sumbat@math.rsu.ru

Here,

$$\begin{aligned} \varphi &= |x_0 - y| + |y - x|, \\ |x_0 - y^*| &= L_0, \quad |y^* - x| = L. \end{aligned} \tag{5}$$

The beam representation can be obtained from formula (4) on the basis of the stationary-phase method of [6].

We now associate the surface S with a local Cartesian coordinate system determined by both the normal n and surface curvature lines at the point $y^* \in S$. In this case, an arbitrary point $y \in S$ has coordinates

$$y(\Delta s_1, \Delta s_2, -0.5(k_1(\Delta s_1)^2 + k_2(\Delta s_2)^2)),$$

where Δs_1 and Δs_2 are arc increments along the curvature lines; $k_1 = R_1^{-1}$ and $k_2 = R_2^{-1}$ are the principal curvatures; R_1 and R_2 are the principal curvature radii at the point y^*; and $k_1(\Delta s_1)^2 + k_2(\Delta s_2)^2$ is the second quadratic form of the surface.

Employing the cosine theorem for the triangles x_0y^*y and xy^*y and ignoring quantities small compared to $(\Delta s_1)^2$, $\Delta s_1 \Delta s_2$, and $(\Delta s_2)^2$, we arrive at the following representations for distances $|x_0 - y|$ and $|x - y|$:

$$\begin{aligned} |x_0 - y| &= L_0 - \Delta s_1 \cos\alpha - \Delta s_2 \cos\beta \\ &+ 0.5(L^{-1}\sin^2\alpha + k_1\cos\gamma)(\Delta s_1)^2 \\ &- L_0^{-1}\cos\alpha\cos\beta\Delta s_1 \Delta s_2 \\ &+ 0.5(L_0^{-1}\sin^2\beta + k_2\cos\gamma)(\Delta s_2)^2, \end{aligned} \tag{6}$$

$$\begin{aligned} |x - y| &= L + \Delta s_1 \cos\alpha + \Delta s_2 \cos\beta \\ &+ 0.5(L_0^{-1}\sin^2\alpha + k_1\cos\gamma)(\Delta s_1)^2 \\ &- L^{-1}\cos\alpha\cos\beta\Delta s_1 \Delta s_2 \\ &+ 0.5(L^{-1}\sin^2\beta + k_2\cos\gamma)(\Delta s_2)^2. \end{aligned} \tag{7}$$

Substituting expressions (6) and (7) into formula (5), we obtain

$$\begin{aligned} \varphi &= L_0 + L + 0.5 d_{11}(\Delta s_1)^2 \\ &+ d_{12}\Delta s_1 \Delta s_2 + 0.5 d_{22}(\Delta s_2)^2, \\ d_{11} &= (L_0^{-1} + L^{-1})\sin^2\alpha + 2k_1\cos\gamma, \\ d_{12} &= -(L_0^{-1} + L^{-1})\cos\alpha\cos\beta, \\ d_{22} &= (L_0^{-1} + L^{-1})\sin^2\beta + 2k_2\cos\gamma. \end{aligned} \tag{8}$$

The absence of the first powers of Δs_1 and Δs_2 in relationships (8) testifies to the fact that the point y^* of direct beam reflection corresponds to a stationary value of the phase φ. Thus, as $k \to \infty$, the principal term in the asymptotic form of integral (4) is determined by the coefficients of the terms $(\Delta s_1)^2$, $\Delta s_1 \Delta s_2$, and $(\Delta s_2)^2$, which can be found from expression (4) using the method of [6] for the two-dimensional stationary phase:

$$p(x) = \frac{\exp\left\{i\left[k(L_0 + L) + \frac{\pi}{4}(\delta_2 + 2)\right]\right\}}{L_0 L\sqrt{|\det(D_2)|}}, \tag{9}$$

where D_2 is the Hessian of the symmetric structure ($d_{ij} = d_{ji}$, $i, j, = 1, 2$) with elements (8). In order to analyze the pressure in the case of single reflection, we represent formula (9) in the explicit form

$$p(x) = \frac{\exp\left\{i\left[k(L_0 + L) + \frac{\pi}{4}(\delta_2 + 2)\right]\right\}}{\sqrt{|(L_0 + L)^2 + 2L_0 L(L_0 + L)(k_2\sin^2\alpha + k_1\sin^2\beta)\cos^{-1}\gamma + 4L_0^2 L^2 K|}}. \tag{10}$$

Here, $K = k_1k_2$ is the Gaussian curvature; $\{-\cos\alpha, -\cos\beta, -\cos\gamma\}$ is the vector determining the direction of the incidence of the $x_0 - y^*$ beam in the chosen coordinate system; δ_2 is the difference between the number of positive and negative eigenvalues of the matrix of the Hessian D_2.

Formula (10) is derived for the case when the high-frequency wave impinges upon a convex surface. If the wave impinges upon a concave surface, then the principal curvatures k_1 and k_2 are taken to be negative.

We define two limiting cases of formula (10). If $k_1 = k_2 = 0$, then from (10) follows the well-known result for pressure in a wave reflected from a plane:

$$p(x) = -(L_0 + L)^{-1}\exp[ik(L_0 + L)].$$

In the case of inverse far-field scattering, formula (10) coincides with the representation of [5]:

$$p(x) = 0.5iL_0^{-2}\sqrt{R_1R_2}\exp\left[i\left(2kL_0 + \frac{\pi}{4}\delta_2\right)\right].$$

2. In the case of reiterated reflection of the $x_0 - y_1^* - y_2^* - x_3$ beam emitted from the point x_0 and received at the point x_3, the pressure $p(x_3)$ at the reception point is given by the formula

$$p(x_3) = \iint\limits_{S_2} 2p(y_2)\frac{\partial\Phi}{\partial n_2}dS_2,$$

$$p(y_2) = \iint\limits_{S_1} 2p^{inc}(y_1)\frac{\partial\Phi}{\partial n_1}dS_1.$$

Here, $p(y_2)$ is the pressure in the incident wave, which is determined after the first reflection in the vicinity of S_1. With allowance for (2) and (3), we arrive at the following basic representation:

$$p(x_3) = -\left(\frac{k}{2\pi}\right)^2\frac{\cos\gamma_1\cos\gamma_2}{L_0L_1L_2}\iint\limits_{S_2}\iint\limits_{S_1}e^{ik\varphi}dS_1dS_2, \quad (11)$$

where

$$\begin{gathered}\varphi = |x_0 - y_1| + |y_1 - y_2| + |y_2 - x_3|,\\ |x_0 - y_1^*| = L_0, \quad |y_1^* - y_2^*| = L_1, \quad (12)\\ |y_2^* - x_3| = L_2.\end{gathered}$$

Here, y_1 and y_2 are arbitrary points of the surface in the vicinities S_1 and S_2 of the mirror reflection points y_1^* and y_2^*.

We associate the vicinities S_1 and S_2 of the mirror reflection points y_1^* and y_2^* with right-hand Cartesian coordinate systems determined by the normals n_1 and n_2 and by surface curvature lines at the points y_1^* and y_2^*. Arc lengths $\Delta s_1^{(i)}$ and $\Delta s_2^{(i)}$ are counted off from the points y_i^* $(i = 1, 2)$ along the curvature lines.

The first $|x_0 - y_1|$ and the last $|y_2 - x_3|$ terms entering into the expression (12) for the phase φ have the same structure as terms in formulas (6) and (7). The second term in expression (12) has the form

$$\begin{gathered}|y_1 - y_2| = L_1 + \sum_{i=1}^{2}\Big[(-1)^{i+1}\{\Delta s_1^{(i)}\cos\alpha_i\\ + \Delta s_2^{(i)}\cos\beta_i + b_i^{(1)}(\Delta s_i^{(1)})^2 + b_i^{(2)}(\Delta s_i^{(2)})^2\}\\ - L_1^{-1}\cos\alpha_i\cos\beta_i\Delta s_1^{(i)}\Delta s_2^{(i)} + \sum_{j=1}^{2}m_{ij}\Delta s_i^{(1)}\Delta s_j^{(2)}\Big],\end{gathered}$$

$$\begin{gathered}b_i^{(j)} = 0.5[L_1^{-1}\sin^2\delta_i^{(j)} + (-1)^{(j+1)}k_i^{(j)}\cos\gamma_j],\\ i, j = 1, 2, \quad \delta_1^{(1)} = \alpha_1, \quad \delta_2^{(1)} = \beta_1, \quad (13)\\ \delta_1^{(2)} = \alpha_2 + \frac{\pi}{2}, \quad \delta_2^{(2)} = \beta_2 + \frac{\pi}{2}, \quad m_{ij} = (\mathbf{u}_1^{(i)}, \mathbf{u}_2^{(j)}),\\ \mathbf{u}_i^{(1)} = (L_1G_{12})^{-\frac{1}{2}}\{\cos\beta_i; (-1)^i\sqrt{Q_{12}}\cos\alpha_i\},\\ \mathbf{u}_i^{(2)} = (L_1G_{12})^{-\frac{1}{2}}\{-\cos\alpha_i; (-1)^i\sqrt{Q_{12}}\cos\beta_i\},\\ G_{12} = \sin\gamma_1\sin\gamma_2, \quad Q_{12} = \cos\gamma_1\cos\gamma_2.\end{gathered}$$

In the formula given above, $k_1^{(i)}$ and $k_2^{(i)}$ are principal curvatures at the points y_i^*; $i = 1, 2$; $\{-\cos\alpha_1, -\cos\beta_1, -\cos\gamma_1\}$ is the direction of the beam incident from the point x_0 with respect to the coordinate system with its origin at the point y_1^*; $\{-\cos\alpha_2, -\cos\beta_2, -\cos\gamma_2\}$ is the direction of the beam reflected at the point y_1^* with respect to the coordinate system with its origin at the point y_2^*. The structures of the terms entering into expression (12) for the phase φ show that, in this expression, terms $\Delta s_j^{(i)}$, $(i, j = 1, 2)$ containing the first powers are absent. This proves that points y_1^* and y_2^* of the direct beam reflection correspond to the stationary phase φ (12). The final result can be obtained from expression (11) by application of the four-dimensional stationary phase given in [6]:

$$p(x_3) = \frac{\exp\left\{i\left[k(L_0 + L_1 + L_2) + \frac{\pi}{4}(\delta_4 + 4)\right]\right\}}{L_0L_1L_2\sqrt{|\det(D_4)|}}. \quad (14)$$

Here, $D_4 = (d_{ij})$, $i, j = 1, 2, 3, 4$ is the Hessian of the symmetric structure with elements d_{ij}, $i \le j$;

$$\begin{gathered}\left\{\begin{matrix}d_{11}\\ d_{22}\end{matrix}\right\} = (L_0^{-1} + L_1^{-1})\left\{\begin{matrix}\sin^2\alpha_1\\ \sin^2\beta_1\end{matrix}\right\} + 2\left\{\begin{matrix}k_1^{(1)}\\ k_2^{(1)}\end{matrix}\right\}\cos\gamma_1,\\ \left\{\begin{matrix}d_{33}\\ d_{44}\end{matrix}\right\} = L_2^{-1}\left\{\begin{matrix}\sin^2\alpha_2\\ \sin^2\beta_2\end{matrix}\right\}\\ - L_1^{-1}\left\{\begin{matrix}\cos^2\alpha_2\\ \cos^2\beta_2\end{matrix}\right\} + 2\left\{\begin{matrix}k_1^{(2)}\\ k_2^{(2)}\end{matrix}\right\}\cos\gamma_2, \quad (15)\\ d_{12} = -(L_0^{-1} + L_1^{-1})\cos\alpha_1\cos\beta_1,\\ d_{34} = -(L_1^{-1} + L_2^{-1})\cos\alpha_2\cos\beta_2,\\ d_{13} = m_{11}, \quad d_{14} = m_{12}, \quad d_{23} = m_{21},\\ d_{24} = m_{22};\end{gathered}$$

δ_4 is the difference between the numbers of positive and negative eigenvalues of D_4.

3. If the number N of secondary reflections is arbitrary, then the general result for this case can be found on the basis of the same method. Thus, we arrive at the estimate of the following integral:

$$p(x_{N+1}) = \left(\frac{ik}{2\pi}\right)^N L_0^{-1} \prod_{n=1}^{N} L_n^{-1} \cos\gamma_n$$
$$\times \iint\limits_{S_N} \iint\limits_{S_{N-1}} \ldots \iint\limits_{S_1} e^{ik\varphi} dS_1 \ldots dS_{N-1} dS_N, \qquad (16)$$

where

$$\varphi = |x_0 - y_1| + |y_1 - y_2|$$
$$+ \ldots + |y_{N-1} - y_N| + |y_N - x_{N+1}|. \qquad (17)$$

Here, L_0 is the distance between an emitter x_0 and the first point y_1^* of the mirror reflection; L_N is the distance between the reception point x_{N+1} and the last point y_N^* of the mirror reflection; L_i, ($i = 1, 2, 3, \ldots, N-1$) is the distance between the mirror-reflection points y_{i-1}^* and y_i^*.

The first $|x_0 - y_1|$ and the last $|y_N - x_{N+1}|$ terms entering into expression (17) for the phase φ have the same structure as the terms in formulas (6) and (7), whereas the structure of the other terms is analogous to that of terms in (13). Using the method of the many-dimensional ($2N$-dimensional) stationary phase given in [6] for estimating a $2N$-multiple Kirchhoff integral as $k \to \infty$, we can find the amplitude of the wave reflected N times:

$$p(x_{N+1}) = \frac{\exp\left\{i\left[k\sum\limits_{n=0}^{N} L_n + \frac{\pi}{4}(\delta_{2N} + 2N)\right]\right\}}{\prod\limits_{n=0}^{N} L_n \sqrt{|\det(D_{2N})|}}. \qquad (18)$$

Here, δ_{2N} is the difference between the numbers with the positive and negative eigenvalues of the matrix of the Hessian $D_{2N} = (d_{ij})$, $i, j = 1, 2, \ldots, 2N$, which is band-shaped (with the bandwidth equal to 7) and symmetric, i.e., $d_{ij} = d_{ji}$, and has the following elements d_{ij}, $i \le j$ [the values of d_{11} and d_{22} are written out in formulas (15)]:

$$\begin{Bmatrix} d_{2n+1,\,2n+1} \\ d_{2n+2,\,2n+2} \end{Bmatrix} = L_{n+1}^{-1} \begin{Bmatrix} \sin^2\alpha_{n+1} \\ \sin^2\beta_{n+1} \end{Bmatrix}$$
$$- L_n^{-1} \begin{Bmatrix} \cos^2\alpha_{n+1} \\ \cos^2\beta_{n+1} \end{Bmatrix} + 2 \begin{Bmatrix} k_1^{(n+1)} \\ k_2^{(n+1)} \end{Bmatrix} \cos\gamma_{n+1},$$
$$d_{2n-1,\,2n} = -(L_{n-1}^{-1} + L_n^{-1}) \cos\alpha_n \cos\beta_n,$$
$$d_{2n-1,\,2n+1} = m_{11}(n, n+1),$$
$$d_{2n-1,\,2n+2} = m_{12}(n, n+1),$$
$$d_{2n,\,2n+1} = m_{21}(n, n+1),$$
$$d_{2n,\,2n+2} = m_{22}(n, n+1),$$
$$m_{ij}(n, n+1) = (\mathbf{u}_1^{(i)}(n, n+1), \mathbf{u}_2^{(j)}(n, n+1)), \qquad (19)$$
$$\mathbf{u}_i^{(1)}(n, n+1) = (L_n G_{n,\,n+1})^{-\frac{1}{2}}$$
$$\times \{-\cos\beta_i^*;\ (-1)^i \sqrt{Q_{n,\,n+1}} \cos\alpha_i^*\},$$
$$\mathbf{u}_i^{(2)}(n, n+1) = (L_n G_{n,\,n+1})^{-\frac{1}{2}}$$
$$\times \{-\cos\alpha_i^*;\ (-1)^i \sqrt{Q_{n,\,n+1}} \cos\beta_i^*\}, \quad i = 1, 2;$$
$$\alpha_1^* = \alpha_n, \quad \alpha_2^* = \alpha_{n+1}, \quad \beta_1^* = \beta_n,$$
$$\beta_2^* = \beta_{n+1}, \quad G_{n,\,n+1} = \sin\gamma_n \sin\gamma_{n+1},$$
$$Q_{n,\,n+1} = \cos\gamma_n \cos\gamma_{n+1}, \quad n = 1, 2, 3, \ldots, N-1.$$

Here, $\{-\cos\alpha_n, -\cos\beta_n, -\cos\gamma_n\}$ is the direction of the incident beam with respect to the coordinate system with its origin at the point y_{n+1}^*, $k_1^{(n)}$ and $k_2^{(n)}$ ($n = 1, 2, 3, \ldots, N$) being the principal curvatures of the surface at the point y_n^*.

It is worth noting that the estimate of many-dimensional diffraction integral (16) is not reduced to the sequential asymptotic analysis of double integrals, since the structure of the phase function is represented by a rather complicated combination depending on all points in the vicinities $S_1, S_2, \ldots, S_N$ that take part in the beam reflection.

4. The explicit expressions (10), (14), and (18) obtained above show that the pressure $p(x)$ in the reflected wave is determined by the principal curvatures, by the Gaussian curvature of the surface at the points of mirror reflection, by distances between the mirror-reflection points, by their removal from both the wave source and the point of reception of the reflected wave, as well as by the directions of incident waves.

The theoretical significance of formula (18) consists in the following. The pressure in a reflected acoustic wave for an arbitrary number of its repeated reflections is obtained in the closed form. The practical importance of formula (18) consists in the fact that estimation of pressure in the repeatedly (*N* times) reflected wave is reduced to calculation of the determinant of the symmetric band-shaped matrix on the order of *N* and with the bandwidth equal to 7. This determinant can be calculated using modern computers in the real-time scale mode.

The developed method is also applicable in the case of acoustic waves repeatedly reflected on systems of obstacles of a complicated shape.

ACKNOWLEDGMENTS

The work was supported by the Grant NSh 2113-2003.1 of the President of Russian Federation for Supporting Leading Scientific Schools.

REFERENCES

1. V. M. Babich and V. S. Buldyrev, *Asymptotic Methods in Short-Wave Diffraction Problems* (Nauka, Moscow, 1972).
2. I. D. Druzhinina and M. A. Sumbatyan, Akust. Zh. **38**, 470 (1992) [Sov. Phys. Acoust. **38**, 257 (1992)].
3. M. A. Sumbatyan and N. V. Boyev, J. Acoust. Soc. Am. **5**, 2347 (1995).
4. D. A. M. McNamara, C. W. I. Pistorius, and J. A. G. Malherbe, *Introduction to the Uniform Geometric Theory of Diffraction* (Artech House, Norwood, 1990).
5. E. L. Shenderov, *Wave Problems of Hydroacoustics* (Sudostroenie, Leningrad, 1972).
6. M. V. Fedoryuk, *Steepest Descend Method* (Nauka, Moscow, 1977).

Translated by G. Merzon

Doklady Physics, Vol. 48, No. 10, 2003, pp. 545–548. Translated from Doklady Akademii Nauk, Vol. 392, No. 5, 2003, pp. 618–622.
Original Russian Text Copyright © 2003 by Kandaurova, Rusinov, Osadchenko.

PHYSICS

Formation and Destruction of Dynamic Spiral Domains in the Anger State of a Ferrite–Garnet Film

G. S. Kandaurova*, A. A. Rusinov, and V. Kh. Osadchenko**

Presented by Academician V.V. Osiko June 21, 2003

Received April 22, 2003

It is known [1–4] that thin ferrite–garnet films with perpendicular anisotropy and original maze domain structure can transit to a certain excited state, or anger state, in varying spatially uniform magnetic fields of low frequencies (10^2–10^4 Hz). In this state, processes of self-organization occur in an ensemble of chaotically moving interacting domains; i.e., ordered stable dynamic domain structures of various geometry (spiral, ring, etc.) arise. It is specific to the anger state that a spiral domain formed in the observed section of the film exists during the time T_l and then disappears. After a certain time (waiting time T_w), one or several new spiral domains arise in this section. Spiral dynamic domains can have different forms in different films [1].

In this work, we analyze the “life” of individual spiral domains in a thin highly anisotropic ferrite–garnet film with the focus on both the first stage in the life of spiral domains, i.e., origin and formation of a multiturn spiral domain, and the last stage, i.e., aging and destruction.

We studied a (111) ferrite–garnet film with induced uniaxial perpendicular anisotropy, $(\mathrm{YLuBi})_3(\mathrm{FeGa})_5\mathrm{O}_{12}$ composition, thickness $L = 9.5$ μm, and 4 × 4 mm in section at a temperature of 25°C. A sample in the initial demagnetized state had the ordinary maze structure with the period $P_0 = 33$ μm of the strip domains. The static saturation field determined by the collapse of cylinder domains was equal to 50 Oe. The quality factor of the film was equal to $Q = \dfrac{K}{2\pi J_s^2} = 96$, where K is the constant of induced uniaxial anisotropy and J_s is the saturation magnetization. The spatially uniform, continuously acting magnetic field $H = H_0\sin 2\pi ft$ was oriented along the normal to the sample. Dynamic domain structures were observed through a microscope by the Faraday magneto-optic effect. Microvideography of dynamic domain structures was carried out with an exposure time of 10^{-4} s. The time between two sequential frames (gate time) was equal to 4×10^{-2} s.

In the above regimes of videography, various life stages of a spiral domain from its appearance to disappearance can rarely be fixed. In this case, other spiral domains do not arise in the vicinity (it is a random process), and spirals do not interact with each other, which can strongly change the behavior and parameters of the observed spiral domain. Figure 1 shows such a successful series of video frames obtained with the frequency $f = 2.56$ kHz and amplitude $H_0 = 45.7$ Oe. These field parameters correspond to the amplitude–frequency domain *AC*, where large, multiturn, spiral domains are formed [5].

Let us analyze the patterns of the dynamic domain structure in more detail. Only disordered dynamic domain structure is seen on the frame in Fig. 1a. This structure consists of complexly bent strip domains, where kinks are more or less noticeable. The ends of the strip domains curling clockwise and counterclockwise form half, one, and one-and-a-half turn spirals. They disappear, new spirals appear, and so forth. The entire domain system is in continuous motion, and the velocities of domain boundaries are different. This conclusion is corroborated by indistinct contours of domains and the presence of three contrasts in the image of the dynamic domain structure [4]. We also emphasize that a certain average scale parameter $\lambda \approx 100$–200 μm that approximately characterizes this inhomogeneity can be seen in Fig. 1a. The state of the multidomain medium presented in Fig. 1a is called *magnetic, dynamic, space–time domain chaos* or *chaos* for short.

In the following frame after chaos, which was taken after 0.04 s (Fig. 1b), a contrasting, clearly outlined, two-turn spiral domain is seen. From this spiral domain, a multiturn spiral domain with ten turns (for definiteness, it is the number of “black” turns) is formed after 0.04 s (Fig. 1c).

The time between frames 1a, 1b, and 1c is equal to 0.04 s, which corresponds to 100 periods of the oscillating magnetic field $H = H_0\sin 2ft$. What are the mechanisms of the appearance of the two-turn spiral domain in Fig. 1b and the ten-turn spiral domain in Fig. 1c? Direct experimental data are absent. Only plausible scenarios can be proposed. According to [6], a dynamic spiral domain arises at a place where favorable condi-

---

Ural State University, Yekaterinburg, 620083 Russia
** e-mail: Gerta.Kandaurova@usu.ru*
*** e-mail: Alexander.Rusinov@usu.ru*

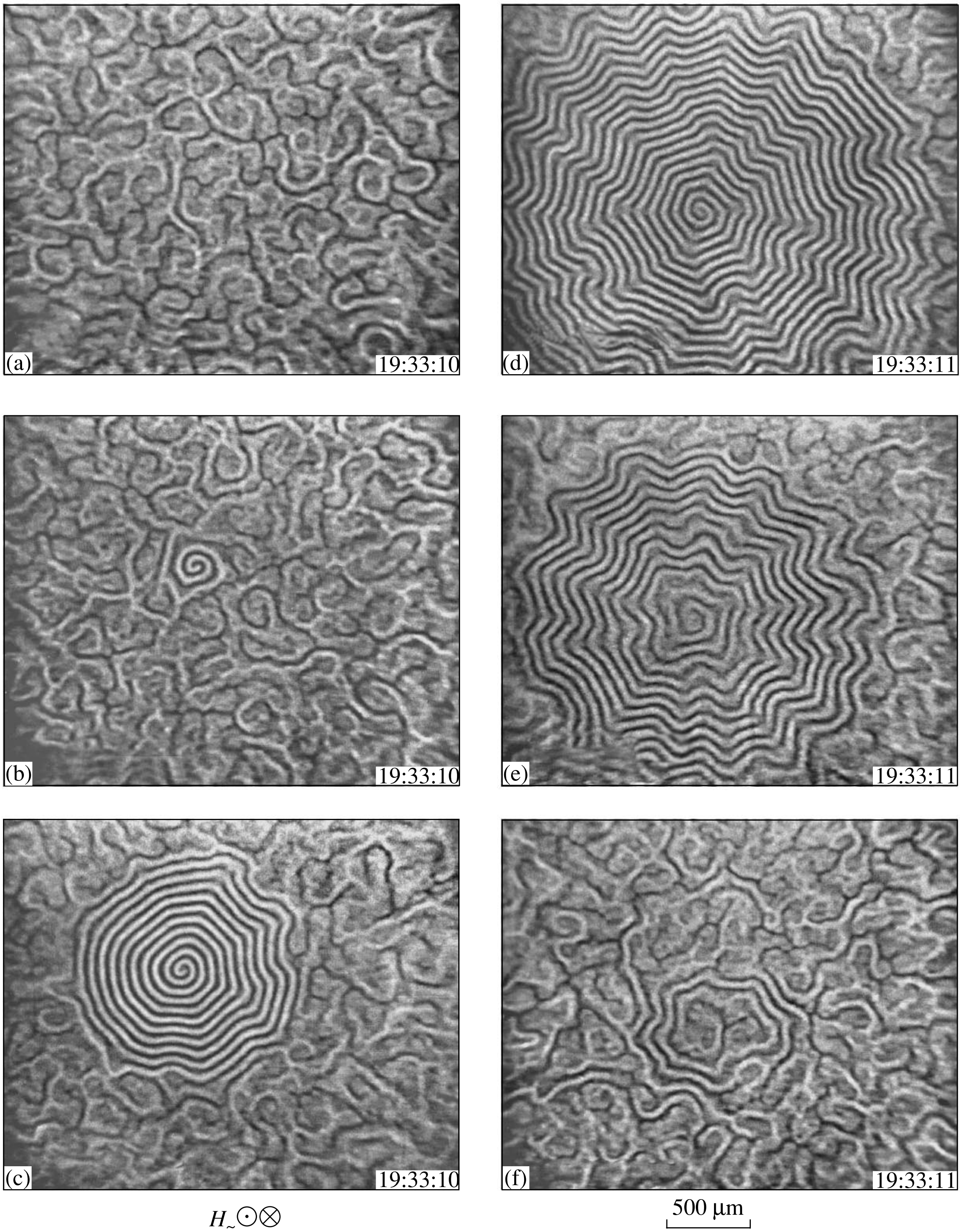

Fig. 1. (a–c) Appearance and formation, as well as (d–f) destruction of the dynamic spiral domain for a varying-field frequency of 2.56 kHz and a field amplitude of 45.7 Oe. Magnetization in domains is perpendicular to the plane of the figure.

tions—the minimum local density of a dynamic domain structure and a very high speed of the end of the strip domain curling to a spiral by the gyrotropic force—are formed in the disordered dynamic domain structure.

Detailed analysis of the shape and behavior of the spiral domain in a static field [7] showed that the behavior of the spiral domain depends on which end of the spiral, inner or outer, is attached. The behavior of dynamic spiral domains is expected to be no less diverse. In the film under investigation, the growth of one of the retained "rigid" cylinder domains to an S-shaped strip domain with a decrease in the static field from the saturation value and further dominant advance of one of the ends of the domain and its curling to a single-arm multiturn spiral was observed [6]. We can think that such a mechanism is also realized for dynamic spiral domains (see Figs. 1b, 1c), the more so as the curling–uncurling mechanism of spiral domains through motion of the end of the outer turn of the spiral domain was theoretically justified in [8]. Estimating the speed of this motion by the value $V = 12$ m/s given in [9] for the translation of a cylindrical domain in a ferrite–garnet film of similar composition, we find that the number of turns increases from two to ten in 0.01 s, i.e., in 25 field periods. This estimate remarkably coincides with the value obtained from the time dependence of the outer radius of the dynamic spiral domain given in [8]. As an example, it was shown in [8] that, for certain parameters of the film and varying field, the spiral domain with a size less than the dynamically equilibrium size relaxes to the equilibrium state in 20–30 field periods.

In actual conditions, few-turn spiral domains (Fig. 1b) are possibly formed through curling of the free end of an extended strip domain bonded to the surrounding disordered dynamic domain structure by the other end. Further, this bond breaks, the outer end of the spiral domain is formed, and the number of turns increases according to the above scheme.

After the frame shown in Fig. 1c, the microvideo film presents all the life of the spiral domain under consideration. During $T_l = 1.12$ s (29 frames of the video film, i.e., 3000 field periods), the spiral domain randomly moves in domain chaos as a Brownian particle [5] and increases or decreases its sizes due to an increase or decrease in the number of turns N. This behavior is clearly seen in Fig. 2. The basic lifetime $T_L \approx 0.8$ s, when $N = 17$–21 (i.e., it deviates from the average value $N \approx 19$ by approximately 10%) can be conventionally identified in the $N(t)$ curve. This N value is reasonably considered as the corresponding dynamically equilibrium state of this spiral domain [8].

During all the time T_l, the spiral domain has a contrast form and holds an unchanged topological charge (the direction of turn curling), the period $P \approx 40$ μm of the structure in turns is virtually constant, the size of the nucleus of the spiral domain and the diameter of the first turn vary only slightly, and P is almost independent of the turn number ν in the spiral domain. The situation changes fundamentally at the final stage of the life of the spiral domain. Frames 1d–1f show sequential stages of the aging and destruction of the spiral domain. This process begins with an increase in P at the center of the spiral domain (Fig. 1d). Further, “loosening” covers the entire spiral domain, particularly the region of the nucleus. The number of turns in the spiral domain decreases sharply (Figs. 1e, 2). 0.04 s after the frame shown in Fig. 1e, the spiral domain almost completely breaks down (Fig. 1f). Only a two-turn spiral domain with a large nucleus, inside which the same chaotic dynamic domain structure as around the spiral domain is observed, remains. In the next frame after the frame shown in Fig. 1f, the spiral domain is not observed, and only domain chaos is observed. The described mechanism of the destruction of the spiral domain both from the inside and from the outside is observed for many spiral domains. Therefore, it is likely general.

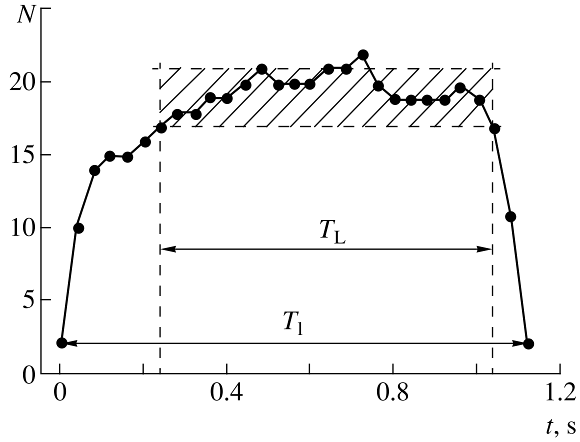

Fig. 2. Time dependence of the number of turns in the dynamic spiral domain.

The series of the dynamic domain structure patters in Fig. 1 provides the unique possibility of comparing the configuration of the spiral domain with an approximately identical number of turns at the beginning and end of its “life”: Figs. 1b and 1f show two-turn spiral domains, while Figs. 1c and 1e show spirals with 10 and 11 turns, respectively. As is seen, the patterns of the comparable structures are qualitatively different for the development of the spiral domain and its destruction. At the stage of the formation of the spiral domain, turns are closely packed and weakly distorted, so that the spiral domain is an Archimedes spiral in the first approximation (Fig. 1c). It is possible that domain boundaries in such a spiral domain undergo similar in-phase oscillations with the acting field.

At the stage of the aging and destruction of the spiral domain (Figs. 1e, 1f), turns are strongly deformed and bent. The entire structure of the spiral domain loses compactness and is loosened, particularly the center of the spiral. In Fig. 1c, the period of the strip domains in turns of the spiral domain is equal to $P \approx 40$ μm and is almost independent of the turn number. In Fig. 1e, the period P increases from about 50 μm at the periphery to about 70 μm at the center of the spiral domain.

Previously [4, 10], three-contrast patterns of strongly distorted spiral domains showed that the speed of the oscillations of boundaries in the sections of spiral domains with the maximum period P can be higher than the speed of boundaries in the region of densely packed turns (minimum P) by more than one order of magnitude. Therefore, the case of deformed spiral domains (Figs. 1d–1f) can also have complex dynamics of boundaries in different sections of the spiral domain.

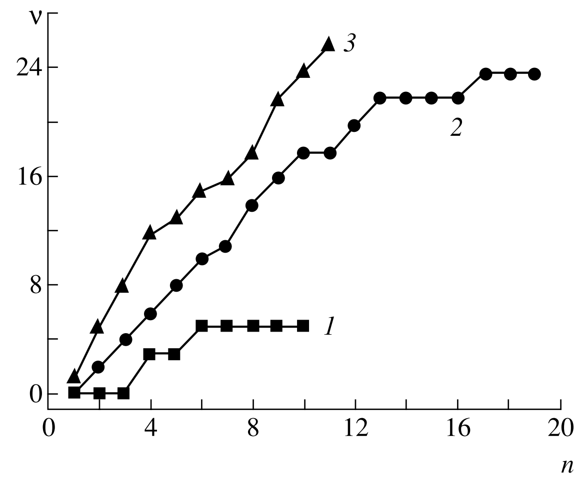

Fig. 3. Number of kinks ν in the turns of the spiral domain vs. the turn number *n*. Lines *1–3* correspond to spiral domains in Figs. 1c–1e, respectively.

We point to kinks in turns of the spiral domain. Lines *1–3* in Fig. 3 show the relation between the number of kinks ν and turn number *n* for spiral domains in Figs. 1c–1e, respectively. As is seen, the number of kinks in all cases increases with the number, i.e., when approaching the outer turn of the spiral domain. The average distance between kinks in the outer turn is equal to 100–200 μm; i.e., it is of the same order of magnitude as the inhomogeneity scale λ introduced above for the surrounding domain chaos. Turns of the spiral domain are apparently deformed due both to the continuous interaction of the spiral domain with the disordered dynamic domain structure and to the appearance of various defects, such as Bloch loops, lines, and points in the micromagnetic structure of the domain boundaries of the spiral domain. The number of defects, as well as the number of kinks in turns, increases with time (cf. lines *1* and *3* in Fig. 3). With the accumulation of defects in walls and, accordingly, with an increase in the boundary energy, with a change in the configuration of the spiral domain and complication of the dynamics of oscillations of boundaries in turns of the spiral domain, the conditions of the dynamic equilibrium of the spiral domain [8] are violated, and the spiral domain breaks and transforms to the chaotic dynamic domain structure.

Experimental results similar to the above results were also obtained in the analysis of the behavior of dynamic spiral domains in the anger state of the ferrite–garnet film being studied.

The results of this work are as follows.

(i) By the example of a single spiral domain, it has been shown that the spiral domain passes through several significant stages: appearance of a stable two-turn domain; formation of a multiturn spiral domain; the basic period of the existence of the spiral domain, during which the state of the spiral domain can be considered as a dynamically equilibrium state; and the aging and destruction of the spiral domain.

(ii) It has been found that the parameters of the spiral domain at the first stage differ from those at the last stage both qualitatively and quantitatively.

(iii) It has been shown that the spiral domain breaks down through an increase in the bending of turns and loosening of the spiral domain, as well as through the transformation of the inner and outer turns to a disorder structure.

(iv) The aging and destruction of the spiral domain have been assumed to be associated with the accumulation of defects in the internal structure of domain walls and complication of their nonlinear local dynamics due to the continuous interaction of the spiral domain with the surrounding space–time domain chaos.

ACKNOWLEDGMENTS

This work was supported by the Program "Basic Research in Natural Sciences," Ministry of Education of the Russian Federation (project no. E02-3.4-393); the US Civilian Research and Development Foundation for the Independent States of the Former Soviet Union (grant no. REC-005); the Program "Universities of Russia" (project no. UR.01.01.027); and the Russian Foundation for Basic Research (project no. 02-02-96410).

REFERENCES

1. G. S. Kandaurova, Usp. Fiz. Nauk **172**, 1165 (2002).
2. G. S. Kandaurova and A. É. Sviderskiĭ, Pis'ma Zh. Éksp. Teor. Fiz. **47**, 410 (1988) [JETP Lett. **47**, 490 (1988)].
3. G. S. Kandaurova, A. Ya. Chervonenkis, and A. É. Sviderskiĭ, Fiz. Tverd. Tela (Leningrad) **31**, 238 (1989) [Sov. Phys. Solid State **31**, 1049 (1989)].
4. G. S. Kandaurova and A. É. Sviderskiĭ, Zh. Éksp. Teor. Fiz. **97**, 1218 (1990) [Sov. Phys. JETP **70**, 684 (1990)].
5. G. S. Kandaurova, V. Kh. Osadchenko, A. A. Rusinov, and E. A. Rusinova, Pis'ma Zh. Éksp. Teor. Fiz. **63**, 453 (1996) [JETP Lett. **63**, 478 (1996)].
6. G. S. Kandaurova and A. A. Rusinov, Fiz. Tverd. Tela **40**, 1865 (1998) [Phys. Solid State **40**, 1691 (1998)].
7. K. V. Lamonova, Yu. A. Mamaluĭ, and Yu. A. Siryuk, Fiz. Tekh. Vys. Davleniĭ **1**, 33 (1996).
8. V. N. Mal'tsev, G. S. Kandaurova, and L. N. Kartagulov, Fiz. Tverd. Tela **45**, 658 (2003) [Phys. Solid State **45**, 691 (2003)].
9. V. V. Randoshkin, Tr. Inst. Obshch. Fiz., Ross. Akad. Nauk **35**, 49 (1992).
10. G. S. Kandaurova and Yu. V. Ivanov, Fiz. Met. Metalloved. **76**, 49 (1993).

Translated by R. Tyapaev

Doklady Physics, Vol. 48, No. 10, 2003, pp. 549–552. Translated from Doklady Akademii Nauk, Vol. 392, No. 5, 2003, pp. 623–626.
Original Russian Text Copyright © 2003 by Ptitsin.

PHYSICS

Phenomenological Model of the Initial Stage of Electron Ablation in Metals

V. É. Ptitsin

Presented by Academician A.V. Elyutin April 22, 2003

Received April 22, 2003

INTRODUCTION

It is known that ablation (i.e., removal or discharge of a substance) occurs when condensed matter interacts with concentrated energy fluxes that can be carried by flows of various particles (including photons). The physical mechanism of this phenomenon remains unclear in many aspects and has not yet received an unambiguous interpretation.

The ablation process can be conventionally divided into two stages. The first stage is characterized by the formation of a plasma plume that expands to the free (of the substance) space. This stage is primarily governed by the interaction of the substance with incident radiation, because “secondary” processes (such as the absorption of radiation energy by plasma and the interaction of dense plasma with the substance) can be ignored. With an increase in the concentration and linear dimensions of the plasma plume (the next stage of ablation), the secondary processes cannot be ignored in the overall energy balance. In particular, recombination processes proceeding in plasma at this (second) stage produce clusters and droplet fractions of the substance.

The quantitative description of processes occurring at the second stage of ablation is a very difficult problem. For this reason, only the first stage of ablation is analyzed in this work. The model of processes proceeding at this stage includes the interaction of intense electron beams with metals. These carriers of the concentrated energy flux, as well as this “object” of energy action, are considered because a number of laws have been reliably established for this case [1].

(i) Electron ablation has a threshold; i.e., it appears only when the beam intensity or the power density P of the electron flux exceeds the threshold value P_l characteristic for a given substance. Experiments show that $P_l \sim 50$ MW/cm^2 for many condensed media.

(ii) The onset of the exposure of the substance to a concentrated energy flux and the moment of the phase transition of the substance to the plasma are separated by a finite time Δt, which depends strongly on P and can vary from $\sim 10^{-8}$ s (at $P \sim P_l$ ($P \geq P_l$)) to $\sim 10^{-13}$ s (at $P \gg P_1$).

(iii) The charge content during electron ablation in the dense plasma also depends substantially on P. At the initial stage of plasma formation (at P close to P_l ($P > P_l$)), most excited atoms (molecules) of the substance remain neutral when transiting from bound to free states. At high levels of P ($P \gg P_l$), the average charge number of plasma ions can be $Z \gg 1$.

In view of the above laws, ablation is treated here as a fast phase transition from bound to free ionized states of structural elements (atoms, molecules) of condensed matter (metal) exposed to intense electron fluxes. This work aims to study the physical mechanism of ablation and to develop a phenomenological model of electron ablation in metals at the initial stage of the process.

HEAT CONDUCTION AS A LIMITING FACTOR FOR THE RATE OF ENERGY ABSORPTION BY CONDENSED MATTER

In accordance with the formulation of the problem, to calculate the rate of the absorption of incident radiation energy by a condensed substance (measured in W/m^2), the condensed substance (e.g., metal) is considered as a set of two interconnected subsystems of electrons and phonons.

It is known [2] that, when the substance’s surface is exposed to electromagnetic radiation or electron flux, the incident flux energy is mainly absorbed by the electron subsystem and then, due to electron–phonon interaction, is transferred to the phonon subsystem. The energy absorbed in the phonon subsystem propagates in the substance through the phonon–phonon interaction, i.e., due to the heat conduction mechanism.

Based on the above scheme of the absorption of the radiation energy by the substance, one can estimate the power density Θ of the heat flux in the substance. In the one-dimensional approximation, for heat flux propagat-

Institute for Analytical Instrumentation,
Russian Academy of Sciences,
Rizhskiĭ pr. 26, St. Petersburg, 198103 Russia
e-mail: ptitsin@iai.rssi.ru

ing from the surface into the bulk of the substance, Θ can be expressed as [3]

$$\Theta \approx \frac{1}{3} n_{\text{ph}} V_{\text{s}} \varepsilon, \qquad (1)$$

where n_{ph} is the phonon concentration, V_{s} is the velocity of sound, and ε is the average energy transferred by a phonon when it transits from the area with a local temperature $T + \Delta T$ to the area with the temperature T. In the Debye approximation, the average phonon energy is determined by the expression [3]

$$\varepsilon \simeq 9 \frac{N}{n_{\text{ph}}} k \theta \xi^4 \int_0^{1/\xi} dx \frac{x^2}{e^x - 1}, \qquad (2)$$

where N is the concentration of atoms in the substance, k is Boltzmann's constant, θ is the Debye temperature, and $\xi = \frac{T}{\theta}$. Integration of Eq. (2) in view of Eq. (1) yields

$$\Theta \simeq Nk\theta V_{\text{s}} \xi \left[1 - \frac{3}{8\xi} + 3 \sum_{n=1}^{\infty} \frac{(-1)^{n+1} B_n \xi^{-2n}}{(2n)!(2n+3)} \right], \qquad (3)$$

where B_n are Bernoulli numbers. The series in Eq. (3) converges rapidly, so, if $\xi \geq 1$, Eq. (3) reduces to

$$\Theta \approx \gamma Nk\theta V_{\text{s}}, \qquad (4)$$

where $\gamma = \gamma(\xi)$ is a dimensionless parameter close to $\gamma \approx 0.5$ at $\xi \approx 1$. Equation (4) shows that Θ depends only weakly on the nature of the substance, because the substance's characteristics appearing in Eq. (4) are close for different substances. Substitution of the parameter values into Eq. (4) gives $\Theta \approx (50 \pm 20)$ MW/cm^2, which is close to experimental values of the electron ablation threshold P_1.

Thus, the estimates of Θ suggest that the threshold of electron ablation exists because the dissipation rate of the radiation energy absorbed by the substance is finite in the phonon subsystem. According to Eq. (4) and the law of energy conservation, if the rate of the supply of the incident-radiation energy to a condensed substance exceeds Θ, the energy of the incident radiation (or electron flux) is somehow "reflected" by the substance. A flow of excited neutrals and ions of condensed matter is evidently the physical "carrier" of the reflected energy flux during ablation.

Below, expressions for the ablation threshold P_1 and delay time $\Delta t = \Delta t \frac{(P_1)}{P}$ will be derived by the example of the interaction of an intense electron flux with metals. It will also be shown that, for $P > P_1$, the "reflection" of the concentrated energy flux by the substance can be attributed to the fast phase transition of atoms (molecules) from bound to free excited and ionized states in the condensed substance.

SIMULATION OF ABLATION IN A METAL EXPOSED TO A CONCENTRATED ENERGY FLUX CARRIED BY A HIGH-POWER ELECTRON BEAM

To develop a model of ablation, it is natural to assume that the phase transition of surface atoms of the metal from bound to free excited (or ionized) states is caused by a significant decrease in the binding (or cohesion) energy of the atoms due to the excitation of the electron subsystem in the metal surface layer by external radiation or a high-intensity corpuscular flux. To describe the mechanism of processes occurring in the substance when the beam power density exceeds Θ, we consider the interaction of an intense electron flux with the metal surface.

The interaction between the electron and phonon subsystems is described in the well-known relaxation time approximation [3, 4].

The absolute value of the binding energy for the excitation of the electron subsystem in a metal (Λ^*) can be defined as [3–5]

$$\Lambda^* \approx \Lambda - r\left(\mu - \frac{3}{5} E_{\text{F}}\right), \qquad (5)$$

where Λ is the absolute value of the binding energy of a surface atom in the absence of the excitation of the electron subsystem, $r \approx 0.6$–0.7 is a dimensionless coefficient equal (in the absence of the excitation of the electron subsystem) to the ratio of the average binding energy of a surface atom to the cohesion energy, μ is the average kinetic energy of the conduction electron, and E_{F} is the Fermi energy.

In the model of free electrons in metals, the balance equation for the kinetic energy μ of a conduction electron in the metal exposed to an electron flux in the one-dimensional approximation can be written as [6, 7]

$$\frac{d\mu}{dt} = \frac{(1-\eta) P \varphi(E)}{nE} - \frac{\varepsilon}{2\tau} \frac{k(T_e - T_{\text{p}})}{E_{\text{F}}}. \qquad (6)$$

Here, η is a dimensionless coefficient characterizing both the elastic reflection of electrons from the metal surface and nonzero probability of emissive recombination of excited electrons (according to [2], $\eta < 0.1$), E is the energy of electrons incident on the metal surface, $\varphi(E)$ is the specific loss function of an electron injected into the metal surface layer [$\varphi(E)$ for metal "surface" points should be calculated from the known Bethe formula for inelastic energy losses; moreover, since the Bethe formula is approximate, in quantitative calculations, the theoretical value of this function must be corrected by using available experimental data], n is the electron concentration in the metal conduction band, P is the power density of the electron flux, τ is the characteristic time of the electron–phonon interaction, and T_e and T_{p} are the absolute temperatures of electrons and lattice, respectively.

Generally, to integrate Eq. (6), it is necessary to specify (or to determine) the function $T_\mathrm{p} = T_\mathrm{p}(t)$. However, as was shown in [1], when a metal is exposed to intense electron fluxes, the lattice temperature increases only slightly during the delay time (about ~10 ns) and, e.g., for Cu, it does not exceed ~800 K. In view of this circumstance and taking into account that the heat capacity of the lattice of the metal is much greater than that of the electron gas, Eq. (6) can be integrated under the assumption that $T_e \gg T_\mathrm{p}$ = const. The relationship between T_e and μ has the form [5]

$$kT_e \approx \left[\mu^2 - \left(\frac{3}{5}E_\mathrm{F}\right)^2\right]^{1/2}. \tag{7}$$

Using the approximation

$$kT_e \approx 3\left(\mu - \frac{3}{5}E_\mathrm{F}\right) \tag{8}$$

(with a maximum error of 20% in the interval $\frac{3}{5}E_\mathrm{F} \le \mu \le E_\mathrm{F}$) for Eq. (7) and Eqs. (5)–(8) with the initial condition $\mu(0) = \frac{3}{5}E_\mathrm{F}$, we obtain

$$\Lambda^*(P, t) \approx \Lambda - \frac{2r(1-\eta)\tau E_\mathrm{F}\varphi P}{3\varepsilon n E}\left[1 - \exp\left(-\frac{3\varepsilon}{2E_\mathrm{F}}\frac{t}{\tau}\right)\right]. \tag{9}$$

Equating expression (9) to zero in the limit $t \gg \tau$, one can obtain an expression for the minimum (or threshold) value P_1 of the power density of the electron flux at which the excitation of the metal electron subsystem begins and, as a result, the binding energy of surface atoms decreases (down to zero). In other words, the conditions $\Lambda^*(P, t) = 0$, $t \gg \tau$ physically mean that, for $P \ge P_1$, after a certain time interval (delay time), "pumping" of the electron subsystem leads the transition of excited and (or) ionized atoms of the metal surface from bound to free states.

According to Eq. (9), the threshold power density can be expressed as

$$P_1 \approx \frac{3\varepsilon n E \Lambda}{2r(1-\eta)\tau E_\mathrm{F}\varphi}. \tag{10}$$

Numerical estimates of P_1 by Eq. (10) for Cu provide

$$P_1 \approx \Theta. \tag{11}$$

The delay time Δt (for $P > P_1$) can also be calculated from Eq. (9). After some rearrangements, Eq. (9) provides

$$\Delta t \approx -\frac{2}{3}\frac{E_\mathrm{F}}{\varepsilon}\tau \ln\left(1 - \frac{P_1}{P}\right). \tag{12}$$

Calculations by Eq. (12) show that, in agreement with the experimental data [1], Δt depends strongly on P and (for currently realized P values) can vary from $\sim(10^{-7}–10^{-8})$ s to $\sim10^{-13}$ s.

Finally, we estimate the velocity ν of the condensed substance–plasma interface at the initial stage of ablation. In the framework of the proposed model of ablation, the activation energy for the transition of an atom from the bound to free state can be assumed zero. Based on the known Arrhenius–Frenkel concepts about the probabilistic character of thermally activated bound–free transitions of surface atoms, the interface velocity during ablation can be expressed in the form

$$\nu \approx \lim_{\Lambda^* \to 0}\left[af\exp\left(\frac{\Lambda^*}{kT_\mathrm{p}}\right)\right] = a\frac{kT_\mathrm{p}}{h}, \tag{13}$$

where a is the lattice parameter and $f \approx \frac{kT_\mathrm{p}}{h}$ is the oscillation frequency of a surface atom. For example, for Cu, it is easy to find from Eq. (13) that $\nu \sim V_\mathrm{s}$ even at temperature T_p close to ≈600 K. The estimates of ν and T_p are in quite satisfactory quantitative agreement with the data from [1]. Equation (13) also shows that the phonon subsystem of the substance cannot be substantially heated at the initial stage of ablation, because the thermal front velocity in the Debye approximation does not exceed V_s. Moreover, since ν is proportional to T_p and the thermal front velocity is finite, the velocities ν and V_s must be consistent with each other and, hence, equalize to each other during ablation.

The above conclusion that the temperature of the phonon subsystem is relatively low in this case does not contradict the known fact that ablation results in erosion markings and surface-scarred craters formed at the substance surface [1].

According to the proposed ablation model, considerable heating and melting of the substance can occur when $\nu < V_\mathrm{s}$ and, hence, the power density of the concentrated energy flux at the substance surface is less than P_1. First, such a decrease in the power density always happens at the trailing edge of the energy pulse because relatively short (down to 10 ns or less) high-power pulses are usually bell-shaped. Second, if the energy pulse is relatively long, the power density absorbed by the substance can decrease to $P < P_1$ in a substantially shorter time than the pulse duration due to an increase in the plasma plume thickness and density with time and, hence, in the efficiency of energy absorption in the plasma.

Finally, the termination of the energy pulse (independently of the pulse shape and width) and a decrease in P to $P < P_1$ are always accompanied by the increase in the temperature of the phonon subsystem as compared to that at the initial stage of ablation. This is because the phonon subsystem of the surface layer at $P < P_1$ is additionally heated due to both subsurface recombination of the plume and inertial absorption of the electron excitation energy by the phonon subsystem of the substance.

CONCLUSIONS

A phenomenological model for the initial stage of electron ablation in metals has been proposed. It has been shown that the interaction of intense electron fluxes with metals leads to the phase transition of condensed matter (metal) to a dense plasma if the rate of injection of the electron flux energy is $P > \Theta$. The analytical expressions agreeing with the experimental data are obtained for (i) threshold power density of the electron flux; (ii) time delay between the onset of the exposure of the metal surface to the electron flux and the moment when the binding energy of surface atoms becomes close to zero; and (iii) interface velocity at the initial stage of election ablation.

ACKNOWLEDGMENTS

This work was supported by the Russian Foundation for Basic Research (project no. 02-02-17268) and by St. Petersburg Scientific Center, Russian Academy of Sciences.

REFERENCES

1. G. A. Mesyats, *Ectons in Vacuum Discharge: Breakdown, Spark, Arc* (Nauka, Moscow, 2000).
2. K. A. Valiev, *Physics of Submicron Lithography* (Nauka, Moscow, 1990).
3. J. M. Ziman, *Electrons and Phonons* (Clarendon Press, Oxford, 1960; Inostrannaya Literatura, Moscow, 1962).
4. M. I. Kaganov, I. M. Lifshits, and L. V. Tanatarov, Zh. Éksp. Teor. Fiz. **31**, 232 (1956) [Sov. Phys. JETP **4**, 173 (1956)].
5. Yu. V. Martynenko and Yu. N. Yavlinskiĭ, Preprint No. 4084/11 (Ross. Nauchn. Tsentr “Kurchatovskiĭ Inst.,” Moscow, 1985).
6. V. É. Ptitsin, Doctoral Dissertation (Inst. Analytich. Priborostroeniya, Ross. Akad. Nauk, St. Petersburg, 1996).
7. V. E. Ptitsin, Rev. Sci. Instrum. **65**, 1476 (1994).

Translated by V. Ptitsin

Doklady Physics, Vol. 48, No. 10, 2003, pp. 553–555. Translated from Doklady Akademii Nauk, Vol. 392, No. 6, 2003, pp. 755–757.
Original Russian Text Copyright © 2003 by Boriskov, Bykov, Il'kaev, Selemir, Simakov, Trunin, Urlin, Fortov, Shuĭkin.

PHYSICS

Shock-Wave Compression of Solid Deuterium at a Pressure of 120 GPa

G. V. Boriskov, A. I. Bykov, Academician **R. I. Il'kaev, V. D. Selemir, G. V. Simakov,**
R. F. Trunin, V. D. Urlin, Academician **V. E. Fortov, and A. N. Shuĭkin**

Received May 21, 2003

In [1], a sharp increase in the density of shock-wave-compressed deuterium was observed at pressures exceeding 50 GPa. The shock waves were generated by intense laser radiation at the NOVA facility. For a number of investigators, the reliability of the results obtained in [1] seemed to be doubtful, which stimulated the studies described below.

Verification of the data of [1] was begun in [2, 3]. A facility was employed that was capable of generating shock waves to produce the required pressures in the deuterium samples under study. These shock waves arose as a result of the detonation of an explosive charge having a hemispheric shape. In contrast to [1], we used deuterium in a solid, not liquid, initial state. In our opinion, this difference is not decisive, since an anomaly in the deuterium compression, if it exists, must be equally manifested in the adiabats of the both initial states.

The results of [2, 3] did not exhibit a sharp increase in the density of shock-wave-compressed deuterium at P = 60 GPa. However, the pressures used in these experiments only slightly exceeded those for which a sharp density increase was observed in [1]. In addition, there were different initial states in [1] and in [2, 3]. Thus, there remained a possibility of qualitative change in the behavior of compressed deuterium at higher pressures (see [3]). Therefore, it seemed to be both reasonable and necessary to study compression of solid deuterium at pressures twice as large as those attained in [2, 3].

In order to prepare solid deuterium samples, we employed a cryogenic setup developed in [2, 3] in which condensation of solid deuterium from the initial gas phase took place. The transformation into the solid phase proceeded via two stages. At the first stage, the smooth transformation of gas state into the liquid state occurred. Deuterium was held in this state for 5–10 min. Furthermore, the deuterium temperature was lowered to 10–15 K (deuterium solid state), and in 15–30 min, the explosive was detonated. The deuterium temperature was measured by two precision thermal sensors. A hemispherical explosive charge more intense than that used in [2, 3] (with a weight higher by a factor of 2.5) was employed to produce gigabar pressures. The schematic diagram for the measuring unit of the experimental device is shown in Fig. 1. A steel shell 3 mm thick is accelerated by the explosion products of the converging detonation wave up to a velocity of 20 km s^{-1}. At the radius $r = 0.07R_{\text{expl}}$, the shell strikes

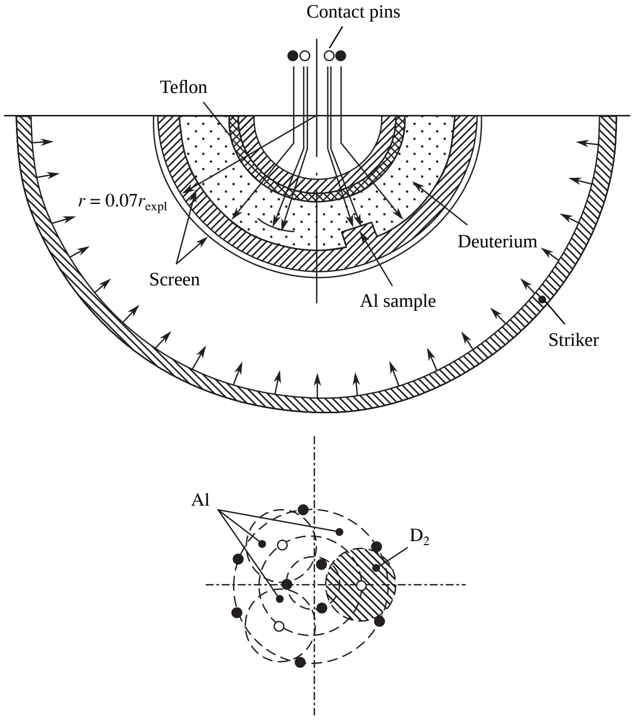

Fig. 1. Schematic diagram of the measuring device and disposition of samples under investigation and of electrocontact sensors. At the upper and lower parts of the figure, the vertical cut and positions of the sensors and samples are indicated. (●) and (○) correspond to the sensors of the lower and upper levels, respectively.

Russian Federal Nuclear Center—All-Russia Research Institute of Experimental Physics,
pr. Mira 37, Sarov, Nizhegorodskaya oblast,
607200 Russia
e-mail: root@gdd.vnief.ru

1028-3358/03/4810-0553$24.00 © 2003 MAIK "Nauka/Interperiodica"

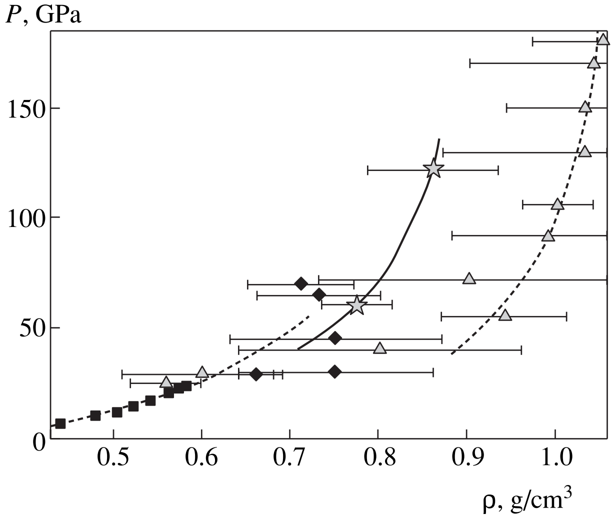

Fig. 2. P–ρ diagrams for the shock-wave compression of deuterium. Experimental points ★ and (▲, ■, ◆) correspond to this experiment and to the results of [1, 4, 5], respectively. Solid and dashed lines are the Hugoniot curve for solid (in the initial state) and liquid deuterium.

an aluminum screen producing in it a shock wave with an amplitude of 720 GPa. This shock wave is transmitted to the deuterium sample under investigation, in which required states are realized. The thicknesses of the screen and sample are chosen to be 6.5 and 4 mm, respectively. We note that in [1], the sample thickness corresponded to tenths of a millimeter. If we admit that nonequilibrium states are realized at the interface, then measurements under the conditions of these small thicknesses can result in noticeable errors while interpreting the results. In addition, at such sample sizes, the mutual tuning of the incident laser beam producing the shock wave and an X-ray beam allowing the shock wave velocity to be measured becomes extremely important. Any deviation from the rigorous geometry of the experiment can result in measurement errors. These problems do not arise in our experiment.

As is seen from Fig. 1, we used the standard disposition of plug-shaped samples, which was the same as in [2, 3]. In the experiments, the number of aluminum and deuterium samples alternated but was not less than three in each run. The time of penetration of the samples by the shock wave was registered using electrocontact sensors. To that end, insulated copper wires 150 μm in diameter were used. To ensure their stability, the wires were installed in thin-walled nickel tubes. The first (over the wave motion) sensors located at the aluminum–deuterium interface were not screened (because their screen is aluminum in itself). The other sensors were covered by thin screening aluminum foils that ensured reliable closure. A voltage of 300 V was applied to the sensors. The schematic diagram of sensor positioning is shown in the lower part of Fig. 1. Registration of wave processes was performed by HP54645 and TDS 784A recorders providing a time measurement error at the level of 2.5 and 1.0 ns, respectively.

The measured time of the shock-wave passage through the sample and its known thickness determine the average wave velocity for the given measurement base. It is worth noting that the process being registered is unsteady. Therefore, in the interpretation of the results obtained, we should allow for a number of corrections to the measured velocities. These corrections are introduced on the basis of numerical calculations of parameters of converging spherical shock waves in both deuterium and aluminum for the particular design of the explosion device.

(i) A correction associated with the passage from experimental velocities $\frac{\Delta r}{\Delta t} = D_{\mathrm{av}}$ to instantaneous velocities D_{in}, which correspond to average radii of sample positioning.

(ii) A correction associated with the fictitious shifting of the aluminum–deuterium interface to the average measurement radius. This correction is stipulated by the fact that the comparison of parameters in the screen and in the substance under investigation must necessarily be performed at the interface, since the pressures and mass rates for both substances are equal there. In our experimental conditions, the initial position of this interface differs by 2 mm from the average radius of the samples. Shifting the interface to the average radius results in a small decrease in the parameters of the deuterium sample under study.

(iii) A correction for the difference in wave velocities in deuterium and in the protective aluminum foil screen standing near the upper contacts in deuterium.

(iv) A correction associated with the difference in aluminum properties at normal temperature and for cold aluminum at $T = 10$–15 K. The correction is determined by the accepted equation of state and is taken into account in constructing the Hugoniot curve for cold aluminum and, correspondingly, the isentrope of its expansion, while calculating the mass rate in deuterium by the reflection method.

All the corrections listed above (although their total value did not exceed 1–1.5%) were taken into account in determination of deuterium compression parameters.

After averaging the data obtained in independent experiments (7 measurements in deuterium and 7 in aluminum), we have arrived at the following conclusions.

According to the equation of state for aluminum, which was used by us, the average shock-wave velocity for aluminum is $D = 21.2 \pm 0.3$ km s^{-1}. This corresponds to the mass rate $U = 12.50$ km s^{-1} ($\rho_0 = 2.737$ g cm^{-3}).

For deuterium, $D = 28.2 \pm 0.6$ km s^{-1} ($\rho_0 = 0.199$ g cm^{-3}), $U = 21.6$ km s^{-1}, $P = 121$ GPa, $\rho_0 = 0.85$ g cm^{-3}).

The new experimental point is shown in Fig. 2. The point is compared to the data related to the shock-wave compression of liquid deuterium, which were obtained by American investigators using a light-gas gun [4] of the NOVA laser facility [1] and in the case of acceleration of a striker by superstrong magnetic field [5]. This figure also demonstrates our experimental point taken from [2, 3] for solid deuterium ($P = 60$ GPa). As is seen, there is satisfactory mutual consistency in the positions of two of our experimental points and in the data obtained in [4]. For all the experiments, the anomalous density increase found in [1] was not observed.

Possible errors in interpreting the measurement results of [1] were indicated previously. The data obtained by investigators from Sunday's National Laboratory [5] also testify to this fact. However, the general character of disposition of the points obtained does not allow us to make a definite conclusion due to spreading of the experimental data.

Thus, in the present study, experimental data are obtained on the shock-wave compression of solid deuterium in the region of gigabar pressures. These data show the erroneous character of the measurement results of [1] obtained at the NOVA facility.

REFERENCES

1. L. Da Silva, P. Celliers, G. W. Collins, *et al.*, Phys. Rev. Lett. **78**, 483 (1997).
2. S. I. Belov, G. V. Boriskov, A. I. Bykov, *et al.*, in *Shock-Wave Compression of Solid Deuterium. VI Zababakhinskie Chteniya* (Snezhinsk, 2001).
3. S. I. Belov, G. V. Boriskov, G. V. Bykov, *et al.*, Pis'ma Zh. Éksp. Teor. Fiz. **76**, 508 (2002) [JETP Lett. **76**, 433 (2002)].
4. N. C. Holms, M. Ross, and W. J. Nellis, Phys. Rev. B: Condens. Matter **52**, 15835 (1995).
5. M. D. Knudson, D. L. Hanson, J. E. Bailey, *et al.*, Phys. Rev. Lett. **87**, 25501 (2001).

Translated by G. Merzon

Doklady Physics, Vol. 48, No. 10, 2003, pp. 556–558. Translated from Doklady Akademii Nauk, Vol. 392, No. 6, 2003, pp. 758–760.
Original Russian Text Copyright © 2003 by Vedenyapin, Batisheva, Melikhov, Gorbatchevski.

PHYSICS

On the Motion of Solids in a Chemically Active Gas

V. V. Vedenyapin*, J. G. Batisheva*,
Corresponding Member of the RAS I. V. Melikhov, and A. Ya. Gorbatchevski****

Received June 23, 2003

In this paper, equations of motion for a solid moving in a chemically active medium are developed and analyzed by kinetic-theory methods [1–3]. The solutions obtained exhibit spiral-shaped trajectories, which is confirmed by the experimental data of [4, 5].

Here we describe gas by the distribution function $f = f(\mathbf{r}, \mathbf{p})$ depending on spatial coordinates $\mathbf{r}$ and momenta $\mathbf{p}$. We describe the state of the solid by the following variables: radius vector $\mathbf{R}$ of the body's center of mass, momentum $\mathbf{Q}$, angular momentum $\mathbf{K}$, and the unit vector $\mathbf{S}$ directed from the center of mass to the center of the active zone. The portion of gas molecules is assumed to be elastically reflected from the surface of the solid, while the other portion adheres to the surface (in this case, the adherence models chemical interaction). The momenta transferred by an adhering molecule and by an elastically reflected molecule are different. In the case of inhomogeneous adherence, a force arises causing motion called chemoreactive motion [4]. Here we analyze the simplest case of a spherical body (ball). We assume that the fraction of adhering particles at a point of the ball with the internal normal $\mathbf{n}$ is $\beta = \beta(\mathbf{n})$, $0 \le \beta \le 1$. The vector $\mathbf{S}$ is determined by the relationship

$$\mathbf{S} = -\frac{\mathbf{A}}{|\mathbf{A}|}, \quad \mathbf{A} = \int\limits_{S_2} \mathbf{n}\beta(\mathbf{n})d\mathbf{n}.$$

When the active zone is axisymmetric, the function β may be represented in the form

$$\beta = \beta(\zeta), \quad \zeta = (\mathbf{n}, \mathbf{S}).$$

The force and the moment that act on the body can be described by the following integrals taken over the entire surface and for all collisions:

$$\mathcal{F} = \int \Delta\mathbf{Q}_{sorp}\beta d\Omega + \int \Delta\mathbf{Q}_{elast}(1-\beta)d\Omega,$$

$$\mathcal{M} = \int \Delta\mathbf{K}_{sorp}\beta d\Omega + \int \Delta\mathbf{K}_{elast}(1-\beta)d\Omega.$$

Here, $d\Omega$ is the differential frequency for collisions of molecules with an element of the surface:

$$d\Omega = (\mathbf{u}, \mathbf{n})\theta((\mathbf{u}, \mathbf{n}))f(\mathbf{R} - \rho\mathbf{n}, \mathbf{p})d\mathbf{n}d\mathbf{p}.$$

In this formula, $\mathbf{u} = \frac{\mathbf{p}}{m} - \frac{\mathbf{Q}}{M}$ is the relative velocity; $(\mathbf{u}, \mathbf{n})$ is the scalar product of the relative velocity $\mathbf{u}$ and the normal $\mathbf{n}$; ρ is the ball radius; and $\theta((\mathbf{u}, \mathbf{n}))$ is the Heaviside function. This function is either 0 or 1 for positive and negative values of its argument, respectively. The appearance of the Heaviside function is associated with the fact that the ball's surface undergoes impacts of only those particles for which $(\mathbf{u}, \mathbf{n}) > 0$.

Furthermore, $\Delta\mathbf{Q}_{elast}$, $\Delta\mathbf{K}_{elast}$ are the variations of both the ball's momentum and moment in elastic collisions:

$$\Delta\mathbf{Q}_{elast} = \mu(\mathbf{u}, \mathbf{n})\mathbf{n}, \quad \Delta\mathbf{K}_{elast} = 0.$$

Here, $\mu = \frac{2mM}{M + m}$ is the reduced mass of the system consisting of the ball and a molecule. In the case of the sorption of the molecule, we have

$$\Delta\mathbf{Q}_{sorp} = \mathbf{p}, \quad \Delta\mathbf{K}_{sorp} = \frac{\mu}{2}[\mathbf{r} - \mathbf{R}, \mathbf{u}].$$

Below, we use the following assumptions.

1. The distribution function for gas molecules is Maxwellian:

$$f(t, \mathbf{r}, \mathbf{p}) = n_0(2\pi mkT)^{-3/2}\exp\left(-\frac{|\mathbf{p}|^2}{2mkT}\right),$$

where n_0 is the gas density, m is the mass of a molecule, T is gas temperature, and k is the Boltzmann constant (the proportionality factor between the temperature and energy).

2. In the course of the process under study, the variation of the ball's mass is negligibly small. This can be admitted since the ratio of the masses of a molecule and

---

* *Keldysh Institute of Applied Mathematics,*
Russian Academy of Sciences,
Miusskaya pl. 4, Moscow, 125047 Russia

** *Moscow State University,*
Vorob'evy gory, Moscow, 119899 Russia

e-mail: vicveden@keldysh.ru; batisheva@keldysh.ru;
melikhov@radiochem.msu.ru;
gorba@radiochem.msu.ru

1028-3358/03/4810-0556$24.00 © 2003 MAIK “Nauka/Interperiodica”

the body in the experiments of [4, 5], as well as in numerous chemical reactions, is much lower than unity: $\varepsilon = \dfrac{m}{M} \ll 1$.

3. The ratio of the ball velocity and the mean square velocity of gas molecules is small:

$$\mathbf{v} = \frac{\mathbf{Q}}{M}\sqrt{\frac{m}{kT}} \ll 1.$$

In the experiments of [3, 4], as well as in numerous other reactions, this is true because the average thermal velocity of molecules is $\sqrt{\dfrac{kT}{m}} \approx 200$ m s^{-1}, whereas the body velocity is on the order of 1–10 m s^{-1}.

Under the assumptions indicated above, upon calculating the integrals for the forces and the moment, we arrive at the following set of equations:

$$\begin{aligned}\frac{d\mathbf{R}}{dt} &= \frac{\mathbf{Q}}{M},\\ \frac{d\mathbf{Q}}{dt} &= (\chi_0 + \chi_1(\mathbf{Q}, \mathbf{S}))\mathbf{S} - \lambda\mathbf{Q},\\ \frac{d\mathbf{S}}{dt} &= \frac{1}{J}[\mathbf{K}, \mathbf{S}],\\ \frac{d\mathbf{K}}{dt} &= \gamma[\mathbf{Q}, \mathbf{S}].\end{aligned} \tag{1}$$

Here, the first equation corresponds to the definition of the velocity. The second equation corresponds to Newton’s second law, in which the term on the right-hand side is the force. The third equation is an analogue of the Euler equation for a solid: the body rotates at an angular velocity $\dfrac{\mathbf{K}}{J}$, where J is the ball’s moment of inertia. (for a ball, all three principal moments of inertia coincide). Finally, the fourth equation corresponds to the angular-moment variation.

For the coefficients, we have the following expressions:

$$\begin{aligned}\chi_0 &= -\frac{1-\varepsilon}{1+\varepsilon}\pi\rho^2 n_0 kT\int_{-1}^{1}\beta(\zeta)\zeta d\zeta,\\ \chi_1 &= \frac{\rho^2 n_0\sqrt{2\pi mkT}}{2M}\frac{(3-\varepsilon)}{(1+\varepsilon)}\int_{-1}^{1}\beta(\zeta)(3\zeta^2-1)d\zeta,\\ \lambda &= \frac{\rho^2 n_0\sqrt{2\pi mkT}}{M(1+\varepsilon)}\left(\frac{8}{3} - \frac{3-\varepsilon}{2}\int_{-1}^{1}\beta(\zeta)(1-\zeta^2)d\zeta\right),\\ \gamma &= -\frac{\rho^3 n_0\sqrt{2\pi mkT}}{M(1+\varepsilon)}\int_{-1}^{1}\beta(\zeta)\zeta d\zeta.\end{aligned}$$

These coefficients correspond to the case of an axisymmetric active zone.

We now analyze the situation when the characteristic time for the variation of the angular momentum $\mathbf{K}$ substantially exceeds the corresponding times for both the momentum $\mathbf{Q}$ and orientation vector $\mathbf{S}$. Then, we can consider the moment $\mathbf{K}$ to be approximately constant and can replace the last equation by $\dfrac{d\mathbf{K}}{dt} = 0$. After this replacement, we are able to solve the penultimate equation: $\mathbf{S}(t) = \exp(\Omega t)\mathbf{S}(0)$, where

$$\Omega = \begin{pmatrix} 0 & \omega_3 & -\omega_2 \\ -\omega_3 & 0 & \omega_1 \\ \omega_2 & -\omega_1 & 0 \end{pmatrix}.$$

Performing the substitution $\mathbf{Q}(t) = \exp(\Omega t)\mathbf{P}(t)$ in the second equation of the set (which implies the passage to a rotating coordinate system), we arrive at a linear set of equations with constant coefficients:

$$\frac{d\mathbf{P}}{dt} = -\lambda\mathbf{P} - \Omega\mathbf{P} + \chi_1(\mathbf{P}, \mathbf{S}(0))\mathbf{S}(0) + x_0\mathbf{S}(0). \tag{2}$$

Each solution to this set of three equations tends to a limiting point $\mathbf{P}(t) \to \mathbf{P}_\infty$ unambiguous for each initial $\mathbf{K}(0)$ and $\mathbf{S}(0)$ but independent of the initial value of the momentum $\mathbf{Q}(0)$.

Thus, we arrive at the knowledge of the asymptotic behavior for the set of equations (1) under the above-mentioned assumptions. The solution for vector $\mathbf{Q}$ tends to the uniform circular rotation about the same axis about which the orientation vector $\mathbf{S}$ rotates at the same frequency $\omega = \dfrac{\mathbf{K}}{J}$ but with a phase delay depending on magnitudes of the quantities λ and $|\omega|$. Therefore, the coordinate trajectory becomes a cylindrical spiral with a constant step L and diameter D:

$$L = \frac{2\pi(\mathbf{P}_\infty, \omega)}{M\omega^2}, \quad D = \frac{2\sqrt{\mathbf{P}_\infty^2\omega^2 - (\mathbf{P}_\infty, \omega)^2}}{M\omega^2}.$$

We can conclude that, in the present study, the equations of motion for a solid moving in an active medium are derived in the simplest case of a spherical body. In finding an analytical solution, we arrive at spiral-shaped trajectories. Qualitatively, this result corresponds to the experimental data of [5], in which such spirals were observed with a very sensitive photographic camera. In order to arrive at quantitative consistencies, we should apparently reject certain simplifications, in particular, the assumption that the solid under consideration is a ball.

ACKNOWLEDGMENTS

We are grateful to M.V. Maslennikov and participants of the seminar on mathematical physics at the Keldysh Institute of Applied Mathematics, Russian Academy of Sciences, for fruitful discussions.

The work was supported by the Russian Foundation for Basic Research., project nos. 01-01-00407 and 02-03-33176.

REFERENCES

1. C. Cercignani, *Theory and Application of Boltzmann Equation* (American Elsevier, New York, 1975; Mir, Moscow, 1978).
2. V. V. Vedenyapin, *Boltzmann and Vlasov Kinetic Equations* (Fizmatlit, Moscow, 2001).
3. N. N. Beletskiĭ and A. M. Yanshin, *An Effect of Aerodynamic Forces on Rotation of Satellites* (Naukova Dumka, Kiev, 1984).
4. I. V. Melikhov, E. F. Simonov, A. A. Vedernikov, *et al.*, Khim. Fiz. **41** (3), 5 (1997).
5. J. Willneff and H.-G. Maas, Int. Arch. Photogramm. Remote Sens. **33**, 894 (2000).

Translated by G. Merzon

Doklady Physics, Vol. 48, No. 10, 2003, pp. 559–564. Translated from Doklady Akademii Nauk, Vol. 392, No. 6, 2003, pp. 761–766.
Original Russian Text Copyright © 2003 by Krishenik, Shkadinskiĭ.

PHYSICS

High-Temperature Thermal Front in a Medium with Nonlinear Thermal Conductivity

P. M. Krishenik* and K. G. Shkadinskiĭ**

Presented by Academician V.E. Fortov March 29, 2003

Received April 23, 2003

Media with constant (or piecewise constant) thermal conductivity are traditionally considered in the classical theory of thermal waves. In this case, the developed technique of mathematical physics can be applied, and the temperature field can be analytically represented in the exponential description. The structure of a high-temperature field in a medium with a power temperature dependence of thermal conductivity was first determined in [1]. As was shown, there is a distinct boundary separating the heated area from the cold area, where thermal perturbation has not yet penetrated. This boundary propagates with a finite velocity, in contrast to the case of linear thermal conductivity, where heat propagates instantaneously over the entire space. Nonlinear thermal conductivity is characteristic for high-power processes with the radiative mechanism of heat exchange.

In this work, problems of the stability of a nonlinear high-energy thermal front in the presence of a chemical power source are analyzed for the first time. The stability of the propagation of such a front is determined both by the macrokinetics of chemical heat release and by the enthalpy excess in the heated area of the thermal front. In turn, this excess depends on the mechanism of nonlinear heat conduction.

MATHEMATICAL MODEL

We consider the propagation of a thermal front in a chemically active medium with thermal conductivity nonlinear depending on temperature. This process is sustained by high-energy exothermal chemical interaction and is described by the equations

$$c\rho\frac{\partial T}{\partial t} = \frac{\partial}{\partial x}\left(\lambda(T)\frac{\partial T}{\partial x}\right) + \rho Q\frac{\partial \eta}{\partial t}, \qquad (1)$$

$$\frac{\partial \eta}{\partial t} = (1-\eta)k\exp\left(-\frac{E}{RT}\right). \qquad (2)$$

Here, T is the temperature, η is the transformation depth, c is the heat capacity of the medium, ρ is its density, Q is the latent heat, k is the pre-exponential factor, E is the activation energy, R is the universal gas constant, t is time, and x is the spatial coordinate. The thermal conductivity $\lambda(T)$, which is a complex function of temperature, is usually approximated by either the effective constant λ_{com} or an empirical function.

The mathematical model specified by Eqs. (1) and (2) is substantially nonlinear and cannot be solved analytically. For this reason, we simplify it by taking into account the physical and chemical properties of the process. First, we approximate $\lambda(T)$ as $\lambda_{\text{com}} = \left(\frac{T}{T_{\text{com}}}\right)^n$, where $T_{\text{com}} = T_0 + \frac{Q}{c}$ is the combustion temperature, T_0 is the initial temperature, λ_{com} is the effective thermal conductivity for the combustion temperature, and n is the exponent of the temperature dependence. The power function $\left(\frac{T}{T_{\text{com}}}\right)^n$ presents a decrease in the thermal conductivity with a decrease in temperature. Second, we assume that (i) the chemical interaction is strongly activated $\left(\beta = \frac{RT_{\text{com}}}{E} \ll 1\right)$ and (ii) the exothermal transformation proceeds with high energy release $\left(\frac{T_0}{T_{\text{com}}} \ll 1\right)$. Under these assumptions, approximate analytical solutions characterizing the structure and dynamics of the thermal front can be obtained.

---

* *Institute of Structural Macrokinetics and Materials Science, Russian Academy of Sciences, Chernogolovka, Moscow oblast, 142432 Russia*
e-mail: petr@ism.ax.ru

** *Institute of Problems of Chemical Physics, Russian Academy of Sciences, Chernogolovka, Moscow oblast, 142432 Russia*
e-mail: shkad@icp.ac.ru, shcad@ism.ac.ru

STRUCTURE OF THE STATIONARY FRONT

The stationary combustion front is described by the traveling wave solution

$$T(x, t) = T(x + ut), \quad \eta(x, t) = \eta(x + ut)$$

of the model specified by Eqs. (1) and (2). Here, u is the velocity of the front with respect to the fixed original medium. The rate of the chemical transformation is negligibly low near the initial temperature, where it is taken zero. Using asymptotic methods of combustion theory [2] and taking into account that the parameters β and $\frac{T_0}{T_{\text{com}}}$ are small, we pass to the (T, p) phase plane, where $p = \lambda(T)\frac{dT}{dx}$, and construct an approximate analytical solution of Eqs. (1) and (2). We separate two qualitatively different subareas of the front: the heated area, where chemical heat release is immaterial, and the temperature-narrow reaction area, where

$$\lambda(T) \approx \lambda_{\text{com}}, \quad 1 - \eta \approx \lambda(T)\frac{c}{Qu}\frac{dT}{dx}.$$

Then, in the reaction area,

$$\frac{p}{\lambda_{\text{com}}}\left(\frac{T_{\text{com}}}{T}\right)^n \frac{dp}{dT} + \rho cpk\exp\left(-\frac{E}{RT}\right) \approx 0. \tag{3}$$

Solving this equation using the Frank–Kamenetskiĭ expansion of the exponential near the combustion temperature and satisfying the requirements of continuity of temperature and heat flux at the boundaries of the areas, we arrive at the following expression for the squared front velocity in the zero approximation:

$$u^2 \approx \frac{\lambda_{\text{com}}}{\rho}\frac{RT_{\text{com}}^2}{QE}k\exp\left(-\frac{E}{RT_{\text{com}}}\right), \tag{4}$$

which is well known in combustion theory. It is seen that, although the thermal conductivity depends on temperature, the front velocity continues to depend exponentially on combustion temperature and is determined by the effective value of the coefficient λ_{com}. The front structure described in the phase space almost completely corresponds to the case $\lambda(T) \approx \lambda_{\text{com}}$. Substantial changes arise when determining the spatial front structure expressed as

$$\lambda(T)\frac{dT}{dx} = p(T) \tag{5}$$

in terms of the front structure $p(T)$ in the phase space. In the heated area, $p(T) = c\rho uT$. Therefore, for the power dependence $\lambda(T) = \lambda_{\text{com}}\left(\frac{T}{T_{\text{com}}}\right)^n$, we obtain (for $n > 0$) the temperature distribution

$$\left(\frac{T(x)}{T_{\text{com}}}\right)^n = \frac{nc\rho u}{\lambda_{\text{com}}}(x + x_{\text{fr}}) \text{ for } 0 > x \geq -x_{\text{fr}}, \tag{6}$$
$$T(x) = 0 \text{ for } x < -x_{\text{fr}},$$

which was described by Zel’dovich and Kompaneets for temperature waves [1]. We emphasize that a self-similar solution such as a traveling wave is determined up to a shift. According to combustion theory, the position of the relatively narrow reaction area (more precisely, the maximum of the chemical interaction rate) is taken as the origin of the moving (connected with the front) coordinate system.

For the adiabatic case, temperature in the reaction area and in products can be taken as T_{com}. Therefore, the width of the heated area beyond which thermal perturbation does not penetrate is equal to

$$x_{\text{fr}} = \frac{\lambda_{\text{com}}}{nc\rho u}. \tag{7}$$

The temperature distribution in the heated area for constant thermal conductivity ($n = 0$, Michelson profile)

$$T = T_{\text{com}}\exp\frac{c\rho ux}{\lambda_{\text{com}}} \tag{8}$$

has the infinite area of the thermal action. According to combustion theory, the characteristic width of heated area (8) corresponds to formula (7) with $n = 1$. In the first approximation, the sizes of the relatively narrow area of the effective chemical interaction (reaction area h_{r}) are independent of the temperature-dependence exponent n. The width of the reaction area is equal to the combustion rate multiplied by the characteristic time of the chemical process:

$$h_{\text{r}} = u/k\exp\left(-\frac{E}{RT_{\text{com}}}\right) \approx \frac{\lambda_{\text{com}}}{c\rho u}\frac{RT_{\text{com}}}{E}. \tag{9}$$

According to combustion theory, the reaction area is strongly narrowed due to the strong activation of the chemical interaction ($\beta \ll 1$). Enthalpy excess at the front

$$\Delta H(n) = \int_{-\infty}^{\infty} \rho[c(T - T_0) - Q\eta]dx \tag{10}$$

decreases considerably with an increase in n, because it is accumulated in the heated area. For $n = 0$, $\Delta H(0) \approx \frac{\lambda_{\text{com}}T_{\text{com}}}{u}$, while $\Delta H(n) = \frac{\Delta H(0)}{n+1}$ for a nonlinear temperature dependence of λ. It is theoretically known [3] that the stability of the combustion front depends on the enthalpy excess at the front.

ANALYSIS OF FRONT STABILITY

Assuming that $\frac{RT_{\text{com}}}{E} \ll 1$ and $\frac{T_0}{T_{\text{com}}} \approx o(1)$ for $n > 0$, the temperature distribution $T^0(x)$ in the stationary self-similar thermal front with a narrow reaction area has the form

$$\frac{T^0(x)}{T_{\text{com}}} \approx 0$$

in the original-composition area ($x < -x_{\text{fr}}$), area I,

$$\frac{T^0(x)}{T_{\text{com}}} \approx \left[\frac{nc\rho u}{\lambda_{\text{com}}}(x + x_{\text{fr}})\right]^{1/n} \qquad (11)$$

in the heated area ($-x_{\text{fr}} \le x \le 0$), area II,

$$\frac{T^0(x)}{T_{\text{com}}} \approx 1$$

in the product area ($x > 0$), area III.

Using approaches developed in [4, 5], we specify perturbations of the temperature of the stationary front in the form

$$T(x, t) = T^0(x) + X(x)\exp(\omega t). \qquad (12)$$

Here, $X(x)$ are small perturbations of the temperature of the stationary front and the complex quantity ω characterizes both the damping factor of perturbations and the frequency of arising oscillations. Substituting Eq. (12) into Eq. (11), we obtain

$$-\frac{c\rho\omega}{\lambda}X - \frac{c\rho}{\lambda}uX'_x + X''_{xx} = 0; \qquad (13)$$

$$-\frac{\omega}{un}X + \left(2 - \frac{1}{n}\right)X'_x + (x + x_{\text{fr}})X''_{xx} = 0; \qquad (14)$$

$$\frac{\omega}{u}X + X'_x = 0 \qquad (15)$$

for regions III, II, and I, respectively.

Further, it is necessary to obtain the general solution for perturbation in all three areas. Satisfying the matching conditions (heat balance, temperature continuity, and conditions of the complete expenditure of the substance in the reaction area), we arrive at the condition of nontrivial solvability of the arising homogeneous system with respect to undetermined coefficients. It is the dispersion relation that determines the region of determining parameters, where the damping factor is positive and perturbations increase exponentially in time (the region of instability of the front with respect to this class of perturbations). It is easy to obtain the analytical expression for the general solution of Eqs. (13) and (15) with constant coefficients. The analytical description is restricted to Eq. (14) with variable coefficients. According to [6], an analytical solution is possible only for $n = 1$ and 2. For $n = 2$, it has the form

$$X = C_1\frac{d}{dx}\cosh\left(2\sqrt{\frac{\omega}{2u}(x + x_{\text{fr}})}\right) + C_2\sinh\left(2\sqrt{\frac{\omega}{2u}(x + x_{\text{fr}})}\right).$$

For $n = 1$, Eq. (14) reduces to the Bessel differential equation, whose solution has the form

$$X = C_1J_0\left(2\sqrt{\frac{\omega}{u}(x + x_{\text{fr}})}\right) + C_2K_0\left(2\sqrt{\frac{\omega}{u}(x + x_{\text{fr}})}\right),$$

where C_1 and C_2 are undetermined coefficients of the general solution in the second area. Omitting cumbersome intermediate manipulations, we immediately present the dispersion equation characterizing the nontrivial solvability of the homogeneous system with respect to undetermined coefficients:

$$\frac{\Omega}{2}\sqrt{1 + 4\Omega} = \Omega(Ze - 0.5) - \sqrt{\Omega}(Ze + \Omega)J^s, \qquad (16)$$

where $\Omega = \frac{\lambda}{c\rho}\frac{\omega}{u^2}$, $Ze = \frac{(T_{\text{com}} - T_0)E}{2RT_{\text{com}}^2}$ is the Zel'dovich number, and J^s is the complex function. For $n = 1$, $J^s = \frac{J_0(2\sqrt{\Omega})}{J_1(2\sqrt{\Omega})}$ is the ratio of the modified Bessel function of the first kind. For $n = 2$, $J^s = \coth\sqrt{\Omega}$.

We take $\Omega = i\Psi$ and find the boundary of the "oscillation" stability by substituting the corresponding expressions into Eq. (16). Separating the real and imaginary parts of Eq. (16), we arrive at the set of the two transcendental equations

$$F_1(Ze, \Psi) = 0 \text{ and } F_2(Ze, \Psi) = 0. \qquad (17)$$

By numerical analysis, we determine the frequency Ψ at the stability boundary and the critical Ze value characterizing the stability boundary of the stationary combustion front. The following table presents the critical parameter values for three n values (the Ψ and Ze values for $n = 0$ are taken from [5], where they were obtained when analyzing gasless combustion).

n	0	1	2
Ψ	1.06	1.45	1.82
Ze	4.24	4.52	4.98

It is seen that, with an increase in n, the instability region with respect to one-dimensional perturbations is

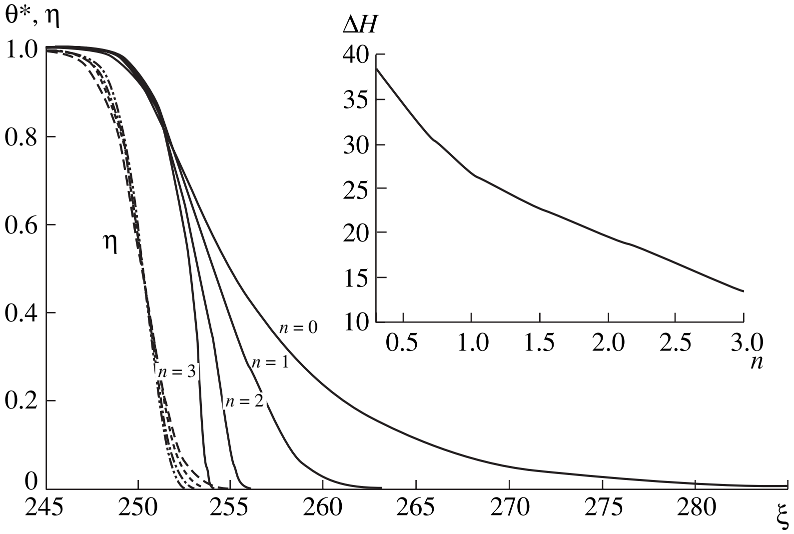

Fig. 1. Steady structure of the stationary combustion front and enthalpy excess ΔH for different n values for a heterogeneous system with the parameters $\theta_0 = -7.180$, $\gamma = 0.139$, $\beta = 0.121$, $\theta^* = \dfrac{\theta_0 - \theta}{\theta_0}$.

shifted to large *Ze* values, the oscillation frequency at the stability boundary increases, and, therefore, the wavelength decreases. According to the Stefan–Boltzmann law, the flux density of equilibrium radiation is $S \sim T^4$. For the model with nonlinear thermal conductivity specified by Eqs. (1) and (2), this law corresponds to $n = 3$. Extrapolating the results of analysis of the stability of the stationary thermal front, one can expect that, with an increase in n, the boundary of stability with respect to the *Ze* parameter expands, and the wavelength of the pulsing mode arising in the stationary front region decreases. It is seen that a decrease in enthalpy at the front with an increase in n stabilizes the thermal front and affects the frequency characteristics of periodic regimes of the front propagation.

The stability of the stationary front is analyzed by taking into account the features of its structure. According to Eqs. (7) and (9), the ratio of the reaction-area width to the heated-area width (the latter is considered as small due to strong activation, $E \longrightarrow \infty$) is equal to

$$\frac{h_{\mathrm{r}}}{x_{\mathrm{fr}}} = \frac{nRT_{\mathrm{com}}}{E}. \qquad (18)$$

Since the process has large energy release and the temperature in the products behind the thermal front is high, we have

$$\frac{RT_{\mathrm{com}}}{E} = \frac{1}{2Ze}.$$

According to the above data, $Ze \sim 5$ in the region of the existence of the stable stationary front. Therefore, the ratio of the widths of the reaction area and heated area is equal to 0.1–0.3 for real n values. The reaction area becomes narrower with an increase in the activation energy. However, the stationary thermal front loses stability for high energies. Information that is more reliable is acquired by numerically analyzing the total nonlinear problem specified by Eqs. (1) and (2).

NUMERICAL ANALYSIS OF THE DYNAMICS OF THE PROPAGATION OF THE THERMAL FRONT

The steady mode of the thermal-front propagation, which is sustained by the energy of the exothermal chemical transformation, is an intermediate asymptotic mode, where the process has already “forgotten” the substantially unsteady stage of its initiation, but chemical-interaction processes in the original low-temperature medium are frozen. The front structure, as well as the dynamics of its motion, is determined by the determining parameters of the medium. If the stationary front is unstable, the stable self-oscillating frontal regime is realized. The structure and velocity of such a front are periodic functions of time. We consider the steady mode of the propagation of the thermal front initiated by a high-temperature source with constant temperature. The process is analyzed by numerically solving the problem specified by Eqs. (1) and (2) in the dimensionless form. Scale quantities and dimensionless parameters are as follows:

$$t_* = RT_*^2 k^{-1}\left(\exp\frac{E}{RT_*}\right)\frac{c}{QE}$$

is the time scale; the length scale x_*^2 is determined by

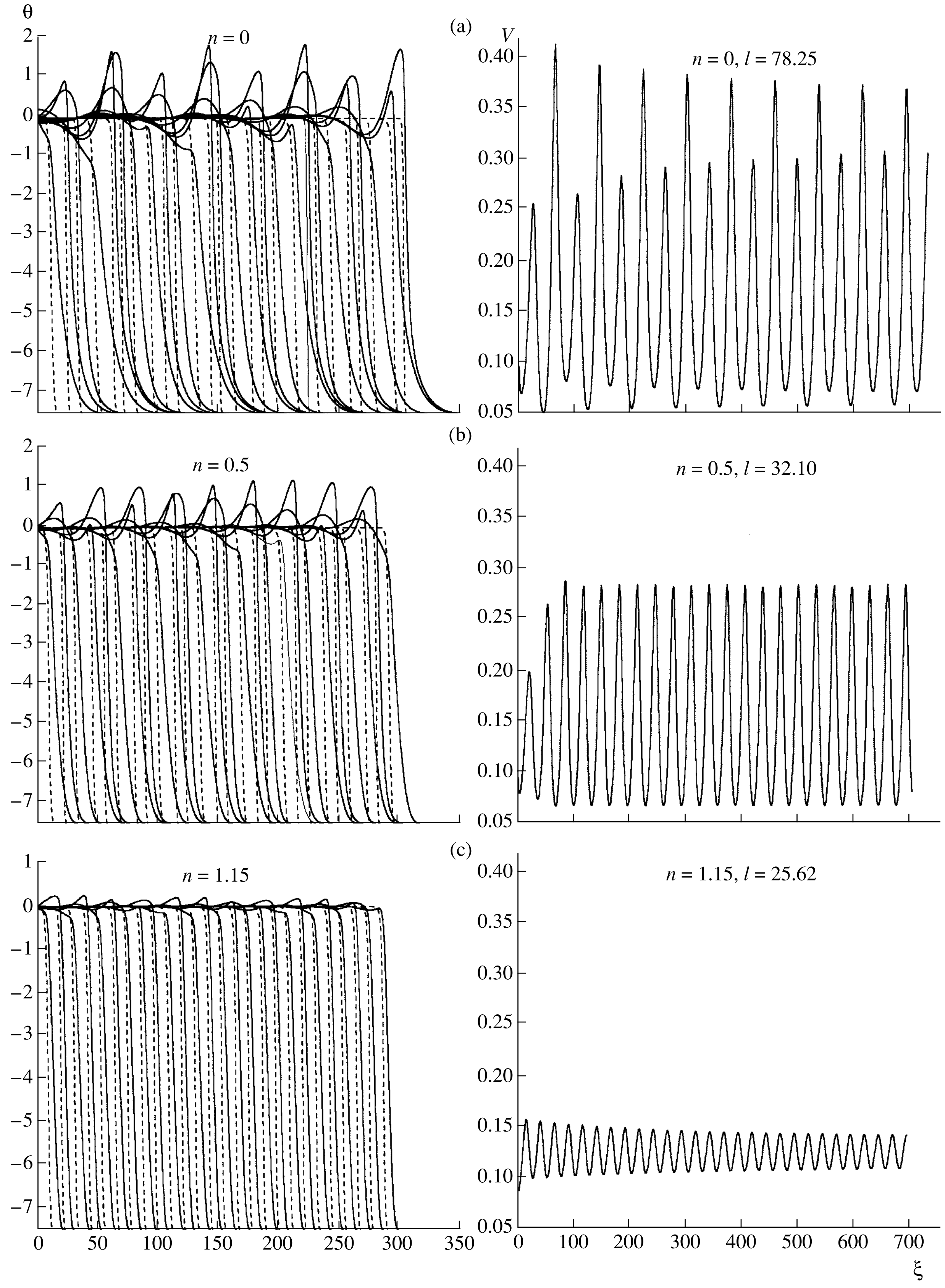

Fig. 2. Spatial–time distribution of (solid lines) temperature θ, (dashed lines) normalized transformation depth $\theta_0(1 - \eta)$, and front dimensionless velocity V for different n values, $\theta_0 = -7.550$, $\gamma = 0.132$, and $\beta = 0.115$.

the relation

$$x_*^2 = \frac{\lambda_{\mathrm{com}} t_*}{c\rho};$$

$$\theta = \frac{(T - T_*)E}{RT_*^2},$$

$\tau = \frac{t}{t_*}$, $\xi = \frac{x}{x_*}$ are the dimensionless temperature, time, and length, respectively; and $T_* = T_0 + \frac{Q}{c}$ is the characteristic temperature. The dimensionless set of Eqs. (1) and (2) is complemented by the initial data

$$\tau = 0, \quad \xi > 0, \quad \theta = \theta_0, \quad \eta = 0$$

and the conditions of initiation

$$\tau > 0, \quad \xi = 0, \quad \theta = \theta_{in} = 0.$$

Nonlinear thermal conductivity corresponds to the sum of the small conductive mechanism of heat conduction and the dominant temperature-nonlinear power mechanism. For brevity, we here present only the results of mathematical simulation that refer to the above approximate analysis.

Figure 1 shows the numerical results for the steady structure of the stationary combustion front near the stability boundary for different n values. For constant thermal conductivity ($n = 0$), the front structure is classical with an exponential temperature distribution in the heated area. The high-temperature reaction area is narrow. According to the approximate analytical analysis, the front velocity and reaction-area width change slightly with variation in n. At the same time, the width of the heated area decreases with an increase in n. Temperature in the heated area is close to a linear function for $n = 1$ and behaves as $(\xi + \xi_{\mathrm{fr}})^{1/n}$ for large n values. The area between the curves of the normalized dimensionless temperature and transformation depth (dimensionless enthalpy excess at the front) decreases with an increase in n (upper right part of Fig. 1).

Figure 2 shows the numerical results for the dynamics of establishing the temperature field and front velocity for different n values when parameters are near the boundary of the stability of the stationary front. Figure 2a corresponds to the constant effective thermal conductivity ($n = 0$). In this case, the stationary front is unstable, and the stable "two-frequency" periodic mode of front propagation is realized. With a change in thermal conductivity (increase in n, Figs. 2b, 2c), the frontal process is stabilized, the oscillations of the front velocity first become single-frequency, then the oscillation amplitude decreases, and finally, for $n = 2$, the front propagates in the stable stationary regime. The wavelength of oscillations l decreases with an increase in n. Thus, the approximate analytical analysis of stability is consistent with the numerical analysis of the dynamics of front propagation.

CONCLUSIONS

A wide temperature range at the front for high-energy compositions requires a more adequate description of the heat transfer. Since thermal conductivity depends nonlinearly on temperature and since the properties and chemical composition of the medium vary, the spatial structure of the front differs from that accepted in combustion theory. The relation between the spatially wide heated area and reaction area that is characteristic for combustion changes. This change is responsible both for the change in enthalpy excess at the front and for the change in the boundary of the stability of the stationary front with respect to small perturbations. The stationary mode that became unstable changes to the periodic dynamic propagation regime.

ACKNOWLEDGMENTS

This work was supported by the Russian Foundation of Basic Research, project no. 02-03-33186.

REFERENCES

1. Ya. B. Zel'dovich and A. S. Kompaneets, in *Collection of Works Dedicated to the 70th Anniversary of A. F. Ioffe* (Izd. Akad. Nauk SSSR, Moscow, 1950).
2. B. V. Novozhilov, Dokl. Akad. Nauk SSSR **141**, 151 (1961).
3. K. G. Shkadinskiĭ, B. I. Khaĭkin, and A. G. Merzhanov, Fiz. Goreniya Vzryva **7** (1), 19 (1971).
4. G. I. Barenblatt, Ya. B. Zel'dovich, and A. G. Istratov, Prikl. Mekh. Tekh. Fiz., No. 4, 21 (1962).
5. G. M. Makhviladze and B. V. Novozhilov, Prikl. Mekh. Tekh. Fiz., No. 5, 51 (1971).
6. E. Kamke, *Handbook of Ordinary Differential Equations* (Acad. Verlag, Leipzig, 1959; Nauka, Moscow, 1976).

Translated by R. Tyapaev

Doklady Physics, Vol. 48, No. 10, 2003, pp. 565–567. Translated from Doklady Akademii Nauk, Vol. 392, No. 4, 2003, pp. 470–472.
Original Russian Text Copyright © 2003 by Kichigin.

ASTRONOMY, ASTROPHYSICS, COSMOLOGY

Model of the Origin of Cosmic Rays in the Galaxy

G. N. Kichigin

Presented by Academician G.A. Zherebtsov March 13, 2003

Received March 23, 2003

The origin of cosmic rays (CRs) is a key problem in astrophysics. As follows from the wide list of literature devoted to CR (see, e.g., reviews and monographs [1–3] and references to original studies therein), considerable progress has been achieved in understanding CR physics, although at present the process of CR generation is not completely understood. Therefore, constructing a model in which available experimental data are consistent with a reasonable theoretical substantiation of basic CR characteristics is rather urgent.

Presently, a model of CR origin based on the Fermi acceleration mechanism of the first kind is widely used. The principles of this model are described in [4, 5], where a mechanism was proposed for acceleration of particles in the vicinity of fronts of collisionless shock waves. This model is associated with the concept that the main fraction of observed CRs is generated in supernovas. The concept was developed by Berezhko *et al.* in [6], in which the process of CR acceleration in supernova remnants was thoroughly analyzed.

In the present paper, after performing a theoretical analysis of the problem of CR origin in the Galaxy, we make an attempt to construct a new alternative model. In order to be consistent, the model must explain at least the following important problems of CR physics: CR sources, particle acceleration mechanisms, injection problems, and energy loss during the traversal of space by CR particles. In the development of the model, these problems are analyzed especially thoroughly.

To a great extent, the model proposed is a result of detailed analysis of CR acceleration in the solar and galactic plasma, which was performed by the author in [7–10]. Allowing for the concept of feeding the total CR energy in the Galaxy by supernova explosions, we discuss one of the basic aspects of the problem of CR origin, namely, the mechanism of acceleration of the charged particles composing CRs. As is well known, the most efficient acceleration occurs in electric fields whose origin is associated with either variations of magnetic field or plasma motion in magnetic field. Particle acceleration by statistical mechanisms or particle acceleration by turbulent motion are less efficient. In our opinion, the most promising is the so-called surfatron mechanism (surfing) [9–12]. Even first estimates of the energy that can be acquired by particles in large-amplitude longitudinal waves propagating in galactic plasma have shown the high efficiency of this acceleration mechanism. In particular, if this mechanism acts on the galactic scale, atomic nuclei can accumulate maximum energies up to 10^{20} eV [13]. The most detailed analysis of the surfatron mechanism of CR acceleration in the Galaxy was performed in [10]. This is the basis employed below for constructing the model under consideration.

The surfatron acceleration mechanism used in the proposed model exists in weakly magnetized plasmas. In this mechanism, charged particles are captured in a potential wave propagating in a plasma with a weak transverse magnetic field. Under certain conditions, these particles can be confined by the wave for a rather long time and can be accelerated at the wave front. The moving positive and negative potential jumps are capable of accelerating ions and electrons, respectively. We analyze the two most widely propagated types of wave perturbations of the potential in the collisionless plasma: a longitudinal plasma wave [14, 15] and a quasitransverse magnetoacoustic shock wave [11]. Since a periodic plasma wave contains positive and negative potential jumps, it is capable of accelerating both ions and electrons. The magnetoacoustic shock wave is characterized by the positive potential jump. Therefore, only ions can be accelerated at the front of this wave.

It is worth noting that the longitudinal plasma waves and quasitransverse magnetoacoustic shock wave are the most propagated in collisionless space plasma. This is because these waves are both easily excited in the case of sharp variations in parameters of weakly magnetized plasma and attenuate relatively weakly. We now discuss possible variants of excitation of waves of the types under consideration with the solar plasma taken as an example. In the magnetosphere plasma, steady-state magnetoacoustic shock waves are produced as a result of interaction of the solar wind with planetary magnetic fields. Take for example the near-terrestrial shock wave. The dominant fraction of the waves are

---

Institute of Solar and Terrestrial Physics,
Siberian Division, Russian Academy of Sciences,
Post Office Box 21, Irkutsk, 664082 Russia
e-mail: king@iszf.irk.ru

excited in the solar atmosphere (photosphere, chromosphere, solar corona). These waves propagate away from the Sun. In this case, the most intense waves, such as plasma waves and magnetoacoustic shock waves (e.g., interplanetary shock waves), arise in chromosphere flares and other similar explosive processes on the Sun. Large-amplitude plasma waves can be generated in various nonlinear plasma processes. However, basically, they are produced by means of either transformation of strong electromagnetic waves into plasma waves or as a result of the development of plasma instabilities while fast charged-particle beams move in the galactic plasma.

In the case of surfing, the acceleration takes place in a regular electric field E_y (in the wave reference frame) always present at the wave front. If we assume that, in the laboratory reference frame, a wave propagates in the direction opposite to the x axis at a velocity u transverse to the magnetic field with the induction B_0,which is directed along the z axis, then in the wave reference frame the field E_y is directed along the y axis and is equal to

$$E_y = \frac{\gamma u B_0}{c}, \quad \gamma = \left(1 - \frac{u^2}{c^2}\right)^{-1/2},$$

where c is the speed of light.

In the case of surfing, in order to provide long-term (perpetual) acceleration of particles captured by a wave, the validity of the condition $R > 1$ is necessary for the parameter $R = \frac{E_0}{B}$. (Here, E_0 is the maximum value (amplitude) of longitudinal (i.e., directed along the x axis) components of the wave electric field, and $B = \gamma B_0$ is the magnetic field in the wave reference system at a point at which the electric field is maximal [9–10, 12]. In space plasma, this condition for waves of the type under consideration is valid in the majority of cases.

It is assumed in our model that epithermal particles corresponding to the tail of the plasma particle distribution function are captured into a wave. In this method of involving particles in the acceleration process, their number is sufficient to ensure the observed CR concentration in the Galaxy. In the case of surfing, the acceleration rate determined by the relationship $W = \gamma u B_0$ per charge unit is so high that we can ignore both the energy loss due to interaction of CRs with the medium and the basic processes of radiation of the particles being accelerated. Thus, at low particle energies, i.e., at the initial stage of acceleration, when ionization energy loss and collision loss play the constitutive role, the so-called injection problem is absent [1]. The energy loss of ultrarelativistic particles turns out to be negligibly low compared to W for the most dangerous radiation types, namely, in the cases of particle acceleration in the wave electric field E_y, of CR interaction with charged plasma particles, and of CR collisions with photons (Compton energy loss). The energy loss is also low in the case of allowance for the process of wave attenuation due to the wave energy consumed for the acceleration of captured particles. However, the principal fact is that, in the case of surfing, when a particle is captured by a wave, synchrotron radiation (magnetic bremsstrahlung) is absent. In other words, this most intense channel of CR radiation loss, which is especially dangerous for electrons, does not exist.

The maximum energies that can be obtained by CRs in the Galaxy turn out to be determined by the maximum size of galactic domains having quasihomogeneous magnetic fields in which nonlinear waves can propagate. The following scenario of sequentially increasing particle energies is intrinsic to the model proposed. Initially, particles are captured from plasma into nonrelativistic shock waves and into nonlinear plasma waves. In this case, the maximum possible energy attains values on the order of 10^{15} eV nucleon^{-1} provided that the particle acceleration is considered in atmospheres (chromosphere, corona, and vicinities (heliosphere)) of stars, as well as in the interstellar medium. Furthermore, ultrarelativistic particles confined by the magnetic field within the Galaxy can continue the acceleration process in relativistic plasma waves. Over distances comparable with the galactic-disk thickness (~100 pc), they can acquire an energy on the order of 10^{20} eV.

Nonlinear waves in the galaxy may be assumed to arise without interruption, and, apparently, their propagation directions are isotropic, their velocity distribution being rather wide. In this case, particles escaping capture by one wave can be subjected to resonance capture by another nonlinear wave that moves in the necessary direction and possesses a velocity corresponding to the capture condition. Then, the acceleration process for the given particles can be repeated many times, as in a relay race. It is worth noting that, in escaping capture by a wave, particles are confined in the galactic magnetic field in a certain domain bounded by their Larmor radius. Furthermore, they either are captured by a proper relativistic plasma wave and continue accumulation of energy or lose, for various reasons, the energy acquired at the first stage. It is clear that, in pauses between the acceleration stages, relativistic and ultrarelativistic electrons lose their energy relatively rapidly. These are electrons whose energy in the process of their motion through the galactic magnetic field intensely decreases due to the loss of synchrotron radiation.

The results of studies of the surfatron-acceleration mechanism as applied to charged particles in the Galaxy testify to the indisputable advantages of the given acceleration method. We may state without doubt that the solution of the majority of problems related to CR acceleration in the Galaxy is possible within the framework of the surfatron mechanism. First, particles are captured into waves directly from the galactic plasma, so that their number is sufficient to ensure the observed

CR concentration in the Galaxy. Second, within the framework of the same injection-free mechanism, particles are accelerated to high energies from those close to thermal energies in plasma. Third, there is no difference in the acceleration of various types of particles: electrons and atomic nuclei are accelerated by the same manner and up to the same maximum energies (per unit charge). Finally, since in the case of surfing the capture of particles occurs in a resonance manner and the acceleration rate is constant, there is no danger of nuclear decomposition in the process of their acceleration. It is worth mentioning the conclusion obtained in [13]: the CR differential power energy spectrum obtained as a result of surfing turns out to be close to the observed spectrum (the exponent is close to 3).

We now formulate the most significant conclusions following from the model proposed.

1. The main source of CRs is space plasma. In other words, either near-stellar or interstellar plasma is a reservoir from which particles composing CRs originate. In particular, this conclusion testifies to the fact that the problem of primary or secondary origin of the CR electron component [1, 2] is solved within the framework of our model in favor of the primary origin of electrons.

2. The formation of the high-energy part of the CR spectrum proceeds in two stages. At the first stage, a small fraction of the epithermal part of the energy distribution for charged particles from galactic plasma is captured into nonrelativistic nonlinear waves and is accelerated by the surfatron mechanism up to an energy of 10^{13} eV nucleon^{-1} in stellar atmospheres and up to an energy of 10^{15} eV nucleon^{-1} in the galactic disk. At the second stage, these particles can acquire energies of 10^{16}–10^{20} eV nucleon^{-1} by the surfatron mechanism in relativistic plasma waves propagating in the magnetized galactic plasma.

It is of interest to note that the energy demarcating these two stages lies in the break region of the CR spectrum curve [2].

3. The ultimate particle energy obtained according to the surfatron mechanism in nonlinear waves is bounded mainly by the dimensions of a wave's propagation domain. It is established that, in the case of the surfatron mechanism, the energy loss of relativistic particles, which is associated with well-known types of radiation and with the attenuation of nonlinear waves due to their energy loss for particle acceleration, may be ignored in the first approximation.

4. It is necessary to note that, for surfatron acceleration, the most dangerous channel of energy loss by relativistic particles, namely, synchrotron radiation, is absent. In particular, owing to this fact, electrons and atomic nuclei can be accelerated in the Galaxy by the surfing mechanism up to energies of 10^{20} eV.

Thus, the model proposed has a number of significant advantages. They are the anomalously high particle-acceleration rate; the CR acceleration up to maximum energies on the order of 10^{20} eV (only up to 10^{15} eV in the existing model); the possibility of accelerating electrons interchangeably with ions (in the existing model, the acceleration of electrons is doubtful); and the absence of the most dangerous channel of radiation energy loss, namely, of the synchrotron radiation channel.

REFERENCES

1. V. L. Ginzburg and S. I. Syrovatskiĭ, *The Origin of Cosmic Rays* (Izd. Akad. Nauk SSSR, Moscow, 1963; Gordon and Breach, New York, 1969).
2. V. S. Berezinsky, S. V. Bulanov, V. A. Dogiel, V. L. Ginzburg, and V. S. Ptuskin, *Astrophysics of Cosmic Rays*, Ed. by V. L. Ginzburg (Nauka, Moscow, 1984; Elsevier, North-Holland, 1990).
3. E. G. Berezhko and G. F. Krymskiĭ, Usp. Fiz. Nauk **154**, 49 (1988) [Sov. Phys. Usp. **31**, 27 (1988)].
4. G. F. Krymskiĭ, Dokl. Akad. Nauk SSSR **234**, 1306 (1977) [Sov. Phys. Dokl. **22**, 327 (1977)].
5. W. I. Axford, E. Leer, and G. Skadron, in *Proceedings of the XV International Cosmic-Ray Conference, Plovdiv, 1977*, Vol. 11, p. 132.
6. E. G. Berezhko and L. T. Ksenofontov, Zh. Éksp. Teor. Fiz. **116**, 737 (1999) [JETP **89**, 391 (1999)].
7. G. N. Kichigin, Zh. Éksp. Teor. Fiz. **101**, 1487 (1992) [Sov. Phys. JETP **74**, 793 (1992)].
8. G. N. Kichigin, Pis'ma Astron. Zh. **19**, 547 (1993) [Astron. Lett. **19**, 216 (1993)].
9. G. N. Kichigin, Zh. Éksp. Teor. Fiz. **108**, 1342 (1995) [JETP **81**, 736 (1995)].
10. G. N. Kichigin, Zh. Éksp. Teor. Fiz. **119**, 1038 (2001) [JETP **92**, 895 (2001)].
11. R. Z. Sagdeev, in *Problems of Plasma Theory* (Atomizdat, Moscow, 1964), Vol. 4, p. 20.
12. J. M. Dawson and T. Katsouleas, Phys. Rev. Lett. **51**, 392 (1983).
13. N. S. Erokhin, S. S. Moiseev, and R. Z. Sagdeev, Pis'ma Astron. Zh. **15**, 3 (1989) [Sov. Astron. Lett. **15**, 1 (1989)].
14. A. I. Akhiezer and R. V. Polovin, Dokl. Akad. Nauk SSSR **102**, 919 (1955).
15. G. N. Kichigin, Fiz. Plazmy **29**, 172 (2003) [Plasma Phys. Rep. **29**, 151 (2003)].

Translated by G. Merzon

Doklady Physics, Vol. 48, No. 10, 2003, pp. 568–571. Translated from Doklady Akademii Nauk, Vol. 392, No. 5, 2003, pp. 627–630.

Principle of Temperature–Time Superposition for Composites with a Highly Elastic Matrix

V. É. Zgaevskiĭ and Yu. G. Yanovskiĭ

Presented by Academician I.F. Obraztsov May 27, 2003

Received June 5, 2003

The viscoelastic properties of composites with a highly elastic matrix and hard particles of a filler (rubber) depend strongly on temperature. The temperature effect on the mechanical properties of such a material is similar to the time factor of the deformation effect.

A quite complete set of the mechanical properties of a composite can be obtained in mechanical tests either for long times or in wide frequency bands under cyclic variations of strain or stress. Such tests are associated with difficult technical problems. However, the viscoelastic behavior of polymers corresponds to large times or low frequencies for high temperatures and to short times or high frequencies for low temperatures. This fact shows that the effects of time and temperature are equivalent to each other. Therefore, the same mechanical characteristics of a sample can be obtained by varying the temperature and time regimes of action on the sample. Thus, this property provides a unique possibility of carrying out tests in limited time or frequency ranges for various temperatures with recalculation of the results to wide time or frequency ranges for a given temperature. This approach is called the principle of temperature–time reduction and is based on the principle of the temperature–time superposition, which was first formulated by Aleksandrov and Lazurkin [1, 10] and then was experimentally checked in [2, 3].

The method of temperature–time reduction was developed earlier than theories where it was justified. Simple phenomenological methods of viscoelastic bodies (Maxwell, Voigt) are often used to theoretically justify this method [4, 5]. However, we consider works based on molecular approaches [6] as most interesting, because they can not only justify the physical essence of the phenomenon but also provide the molecular interpretation of a number of the material constants of the reduction. Molecular approaches and theories can also predict and describe a number of new effects and relations.

In this work, the applicability of the principle of temperature–time superposition for composites with a highly elastic matrix and hard filler particles (rubber, polymer matrix composites, etc.) is justified on the basis of the molecular model in the framework of the scaling concept.

We consider the composite as identical spherical particles that are uniformly distributed in space and are located between polymer chains [7–9]. The segments of these chains are adsorbed on the surfaces of the particles (Fig. 1). For quantitative estimates, we consider a model element consisting of two particles that have diameter D and are coupled through a macromolecule having N segments of size a. The surface layer of each particle contains n segments.

We consider that both N and n are the same for all macromolecules. The distance between the surfaces of neighboring particles is equal to l_0. Each particle is surrounded with a potential well with thickness $\delta \sim a$. A macromolecule unit falling into this well has negative energy $-\varepsilon$. Each particle is surrounded by an adsorption layer of thickness $\Delta \ll D$. The fraction $\delta\Delta^{-1}$ of n segments in the adsorption layer is in the potential well.

In [7–9] based on scaling theory, the free energy F of the model element was represented as a sum of the energy of segments in potential wells, the energy of n segments in the adsorption layer, the energy of the volume interaction between segments in the adsorption layer, and the energy of $N - 2n$ segments of the polymer chain with the distance l_0 between the ends.

Expressions for n and Δ were obtained in [7] by minimizing the free energy of the model element via variation in n and Δ for given l_0 and T (temperature in energy units) and for the following ranges of molecular and structure parameters: $N > n$, $D \le 30$ nm, $N \ge 5000$, $a \sim \delta \sim 1$ nm, $\varepsilon \sim 1$ kcal/mol, and the volume fraction of the filler in the interval $0.1 \le \varphi \le 0.5$. This provided an expression for the free energy of the deformed sample as a function of the molecular and structural parameters of the composite. By using the expression for the free energy density, the high-elasticity properties of the composite were described in dependence on the above-listed molecular and structure parameters of the model.

---

*Institute of Applied Mechanics,
Russian Academy of Sciences,
Leninskiĭ pr. 32a, Moscow, 117334 Russia*

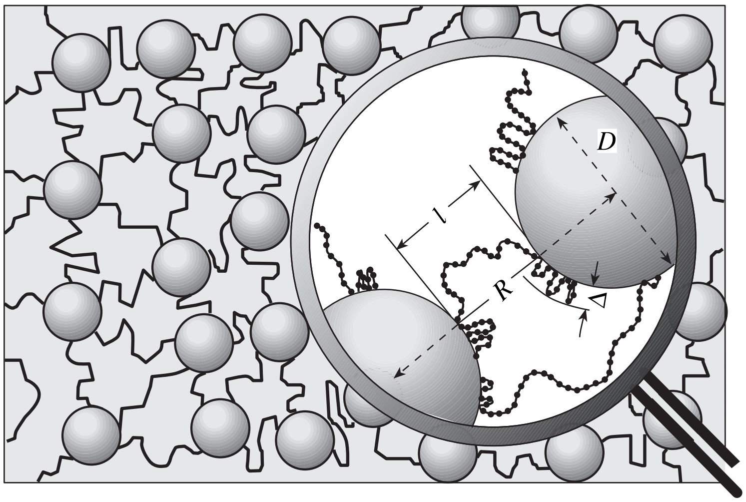

Model of a composite with a highly elastic matrix.

The comparison of the results with the experimental data corroborated that the theoretical approach proposed in [7] is justified.

With further development of this approach [8], the mechanical relaxation properties of such a composite were described. Three components of the internal viscosity of the composite, which are associated with different mechanisms of molecular motions, are taken into account [8, 9]. The first component η_1 is associated with the displacement of the chain section in the surface layer due to migration of chain segments in the potential wells of active centers of the surface of filler particles. This component is described in the Frenkel–Airing theory. The second component η_2 is associated with motion of segments of the chain section in the surface layer as in a tube. This component is calculated in the scaling approach for the dynamics of the macromolecule in the medium with spatial boundaries. The third component η_3 is the viscosity of the chain section containing $N - 2n$ segments connecting the surfaces of two neighboring particles.

The relations obtained in [8, 9] provide the following expression for the relaxation time of the composite in the above-listed ranges of the molecular and structure parameters (where $\eta_3 < \eta_2$):

$$\xi = 10N^{\frac{3}{2}}a^3\frac{\eta_s}{T}\left(1 - \frac{3D^2\varepsilon\delta}{Na^3T}\right), \tag{1}$$

where η_s is the solvent viscosity.

For the case $\eta_3 > \eta_2$, which can be achieved due either to an increase in N or to a decrease in D, we obtain

$$\xi = \frac{10D^2\delta^2\varepsilon^{\frac{3}{2}}\eta_s}{aT^{\frac{3}{2}}}\left(1 - \frac{2\varepsilon\delta D^2}{Na^3T}\right). \tag{2}$$

In this case, as was shown in [9], the deformation behavior of the composite can be approximated in the Kelvin–Voigt–Meir model. For stepwise loading ($\sigma = \sigma_0$ for $t = 0$), the time dependence of strain has the form

$$u(t) = \frac{\sigma_0}{G}\left(1 - e^{-\frac{t}{\xi}}\right), \tag{3}$$

where

$$G = \frac{18aT_0^2T}{\pi D\varepsilon^2\delta^3N}\left(1 + \frac{2\pi\varepsilon\delta D^2}{3Na^3T}\right)\Psi(\varphi),$$
$$\Psi(\varphi) = \left(\frac{\pi}{6}\right)^{\frac{2}{3}}\varphi^{\frac{1}{3}}; \tag{4}$$

T_0 is the temperature at which potential wells on the surface of each particle (see model) are completely filled with segments of macromolecules [7–9].

When loading changes exponentially as $\sigma = \sigma_0 e^{i\omega t}$, strain varies as

$$u(t) = \frac{\sigma_0}{G}\frac{1}{1 + i\omega\xi}e^{i\omega t}. \tag{5}$$

The relaxation time ξ in Eqs. (3) and (5) is specified by Eqs. (1) and (2). As follows from Eqs. (3) and (5), the relaxation time appears in combination either with current time [Eq. (3)] or with frequency [Eq. (5)]. The relaxation time ξ and shear modulus G are functions of the current temperature (temperature of the experiment). Therefore, the same mechanical reaction of the material to an external action can be obtained by varying the temperature of the experiment or correspondingly selecting the test time in Eq. (3) or frequency in Eq. (5). This corresponds to the principle of temperature–time superposition.

Contrary to the known relations predicting temperature–time superposition for polymer media on the basis of phenomenological models, the explicit functional expressions of ξ and G in this case are obtained as functions of not only temperature but also the molecular and microstructure parameters of the composite medium. The latter dependence makes it possible to point out a number of interesting features of the mechanical behavior of such composites.

We analyze the frequency dependence of the strain-to-stress ratio $C_T(\omega)$ with cyclic variations of stress (compliance) for a certain temperature under periodic small-amplitude deformation (dynamic tests). According to Eq. (5),

$$C_1(\omega) = \frac{f[\omega\xi(T_1)]}{G(T_1)} \tag{6}$$

for $T = T_1$, where $f(X)$ is the given function. For $T = T_2$, we have

$$C_2(\omega) = \frac{f[\omega\xi(T_2)]}{G(T_2)} = \frac{f\left[\omega\xi(T_1)\frac{\xi(T_2)}{\xi(T_1)}\right]}{G(T_1)}\frac{G(T_1)}{G(T_2)}. \tag{7}$$

Let us obtain the common logarithm of expression (7) as a function of the common logarithm of the argument of the function f:

$$\log C_2(\omega) = \log\frac{f\left[\log\omega\xi(T_1) + \log\frac{\xi(T_2)}{\xi(T_1)}\right]}{G(T_1)} + \log\frac{G(T_1)}{G(T_2)}. \tag{8}$$

Comparison of Eqs. (8) and (6) provides easy rules for recalculation of test results obtained for certain temperature to different temperature. The curve of $\log C_2(\omega)$ as a function of $\log\omega\xi(T_2)$ is obtained by shifting the curve of $\log C_1(\omega)$ as a function of $\log\omega\xi(T_1)$ by $\log\frac{\xi(T_2)}{\xi(T_1)}$ and $\log\frac{G(T_1)}{G(T_2)}$ along the abscissa and ordinate axes, respectively. Thus, the standard reduction principle has been obtained. Explicit expressions (2) and (4) for ξ and G as functions of the molecular and microstructure parameters of the model provide predictions of a number of the features of the mechanical behavior of such materials. In particular, for the case $\eta_2 > \eta_3$ (the viscosity of the composite is primarily determined by motion of sections of polymer chains connecting the surfaces of two neighboring particles of the filler), using Eq. (1), we arrive at the expression

$$a_T = \frac{\xi(T_2)}{\xi(T_1)} \simeq \frac{\eta_s(T_2)T_1}{\eta_s(T_1)T_2} \tag{9}$$

for the frequency shift factor under the assumption of a weak temperature dependence of the segment size. In this case, expression (9) coincides with the known result obtained in the molecular approach for unfilled polymer media [2]. The difference is in the displacement along the ordinate axis, where, according to Eqs. (4) and (8), the different coefficients of thermal expansion of particles of the filler and matrix must be taken into account, and temperature change in D and $\Psi(\varphi)$ must be estimated. For the case $\eta_3 > \eta_2$ (the viscosity of the composite is determined by outflow of sections of chains from the surface layer), the frequency shift factor depends more strongly on T according to Eq. (2):

$$a_T \simeq \frac{\eta_s(T_2)T_1^{\frac{5}{2}}}{\eta_s(T_1)T_2^{\frac{5}{2}}}. \tag{10}$$

We emphasize that expressions (1) and (2) representing the relaxation time of the composite as a function of the molecular and microstructure parameters can provide estimates of change in the shift factor with the size of particles of the filler and molecular mass of the polymer (sizes of macromolecules). According to Eqs. (1) and (2), the frequency shift factor varies as

$$a_D \simeq \begin{cases} 1 \quad \text{for} \quad \eta_2 > \eta_3 \\ \left(\frac{D_2}{D_1}\right)^2 \quad \text{for} \quad \eta_3 > \eta_2 \end{cases} \tag{11}$$

and

$$a_N \simeq \begin{cases} \left(\frac{N_2}{N_1}\right)^{\frac{3}{2}} \quad \text{for} \quad \eta_2 > \eta_3 \\ 1 \quad \text{for} \quad \eta_3 > \eta_2 \end{cases} \tag{12}$$

with the particle size D and molecular mass of the polymer (or polymerization degree of macromolecules), respectively.

The shift factor along the ordinate axis for these two cases is easily calculated by using Eq. (4). A thorough experimental test of the relations obtained above will provide both more clear representations about the viscoelastic properties of composites (e.g., rubber) and a number of useful practical procedures for control of the mechanical properties of such materials.

ACKNOWLEDGMENTS

This work was supported by the International Science and Technology Center, grant no. 2154p.

REFERENCES

1. A. P. Aleksandrov and Yu. S. Lazurkin, Zh. Tekh. Fiz. **9**, 1249 (1939); Zh. Tekh. Fiz. **9**, 1261 (1939).
2. J. D. Ferry, *Viscoelastic Properties of Polymers* (Wiley, New York, 1980).
3. A. V. Tobolsky, *Properties and Structure of Polymers* (Wiley, New York, 1960; Khimiya, Moscow, 1964).
4. A. I. Lukomskaya and V. F. Evstratov, *Fundamentals of Predicting the Mechanical Behavior of Caoutchoucs and Rubbers* (Khimiya, Moscow, 1975).
5. I. K. Senchenkov and V. G. Karnaukhov, Prikl. Mekh. **37** (11), 33 (1981).
6. Yu. G. Yanovsky, *Polymer Rheology: Theory and Practice* (Chapman and Hall, London, 1993).
7. V. É. Zgaevskiĭ, Dokl. Akad. Nauk **341**, 758 (1995) [Phys. Dokl. **40**, 179 (1995)].
8. V. É. Zgaevskiĭ, Dokl. Akad. Nauk **363**, 42 (1998) [Dokl. Phys. **43**, 685 (1998)].
9. V. É. Zgaevskiĭ and Yu. G. Yanovskiĭ, Mekh. Kompoz. Mater. **4** (3), 106 (1998).
10. A. P. Aleksandrov and Yu. S. Lazurkin, Kauchuk i Rezina, No. 10, 34 (1939).

Translated by R. Tyapaev

Doklady Physics, Vol. 48, No. 10, 2003, pp. 572–575. Translated from Doklady Akademii Nauk, Vol. 392, No. 4, 2003, pp. 473–476.
Original Russian Text Copyright © 2003 by Zelepugin, Grigoryan, Dorokhov, Zhbankov.

MECHANICS

Failure of a Long-Rod Projectile Perforating a Target with a Middle Elastomer Layer

S. A. Zelepugin*, V. A. Grigoryan, N. S. Dorokhov**, and Yu. P. Zhbankov****

Presented by Academician V.M. Titov April 16, 2003

Received May 7, 2003

Wide application of various long-rod projectiles in ballistics supports continuous interest in investigation of the features of their interaction with targets in high-velocity impacts [1–4]. Although there are many experimental and theoretical works in this field, the problem is far from a complete solution. In this paper, we report experimental and numerical investigations of the interaction of a tungsten-alloy long-rod projectile with a three-layer target consisting of the front and rear steel layers and middle elastomer layer. An impact occurs at an angle of 60° with a velocity of 1600 m/s.

Figure 1 shows the sequential X-ray patterns of the penetration of the long-rod projectile with diameter d_0 and length $l_0 = 20d_0$ through the three-layer target with front, middle, and rear layers of thicknesses $0.34d_0$, $1.82d_0$, and $0.34d_0$, respectively. Figure 1a shows the failure of the projectile part immediately after the projectile penetrates though the target and reaches its rear surface. The characteristic feature of the asymmetric high-velocity impact of the long-rod projectile with the finite-thickness target is the formation of two bulges on the rear surface of the target. The first of them arises opposite the point where the projectile touches the front layer of the target and is due to the arrival of the shock wave at the rear surface of the target. The second bulge is due to the deformation factor and arises in the process of the projectile's penetration. The projectile perforates the target in this region. Further, these two regions are united, forming a fragment debris behind the target. Analysis of the experimental data shows that, when the projectile moves behind the target at later stages of the process, its front part bends (Fig. 1b) and fails (Fig. 1c), which is accompanied by the separation of the projectile part from the basic reminder.

Numerical investigations were carried out to analyze in detail the features of the interaction of long-rod projectiles with the three-layer target with various thicknesses of the layers. The set of equations for describing unsteady adiabatic motions of an elastoplastic medium, including nucleation and accumulation of microdamages and temperature effects, consists of the equations of continuity, motion, and energy [5]. To numerically simulate the failure of the material in high-velocity impact, we applied the active-type kinetic model determining the growth of microdamages, which continuously change the properties of the material and induce the relaxation of stresses [6]. The strength characteristics of the medium (shear modulus and dynamic yield strength) depended on temperature and the current level of damages [7]. The critical specific energy of shear deformations was used as a criterion of the erosion failure of the material that occurs in the region of intense interaction and deformation of contacting bodies [8]. The constants for the elastomer were taken from [9]. Calculations were carried out by the finite-element method [10]. Moreover, sliding conditions were realized between the projectile and target, as well as between the layers of the target.

Calculations were carried out for thicknesses $0.34d_0$ and $0.68d_0$ of the front layer, thicknesses $0.34d_0$, $0.68d_0$, and $1.02d_0$ of the rear layer, and various materials of the middle layer whose thickness was equal to $2.05d_0$. The table presents the parameters of six calculation variants.

Figure 2 shows the calculated chronograms of the process for basic variant *a*. Figure 2a illustrates the onset of the interaction of the projectile with the rear layer of the three-layer target, while Fig. 2b corresponds to the motion of the projectile reminder behind the target, which is accompanied by the bending of the front part of the projectile.

Calculations for the basic variant show that, despite a considerable impact angle of 60°, the ricocheting fragment of the front projectile part formed at the initial interaction stage is small due to the geometric parameters of the problem and characteristics of the materials of interacting bodies.

---

* *Department of Structural Macrokinetics,*
Tomsk Scientific Center, Siberian Division,
Russian Academy of Sciences, pr. Akademicheskiĭ 10/3,
Tomsk, 634021 Russia
e-mail: szel@tbism.tomsk.ru

** *Research Institute of Steel OAO NII Stali,*
ul. Dubninskaya 81a, Moscow, 127411 Russia

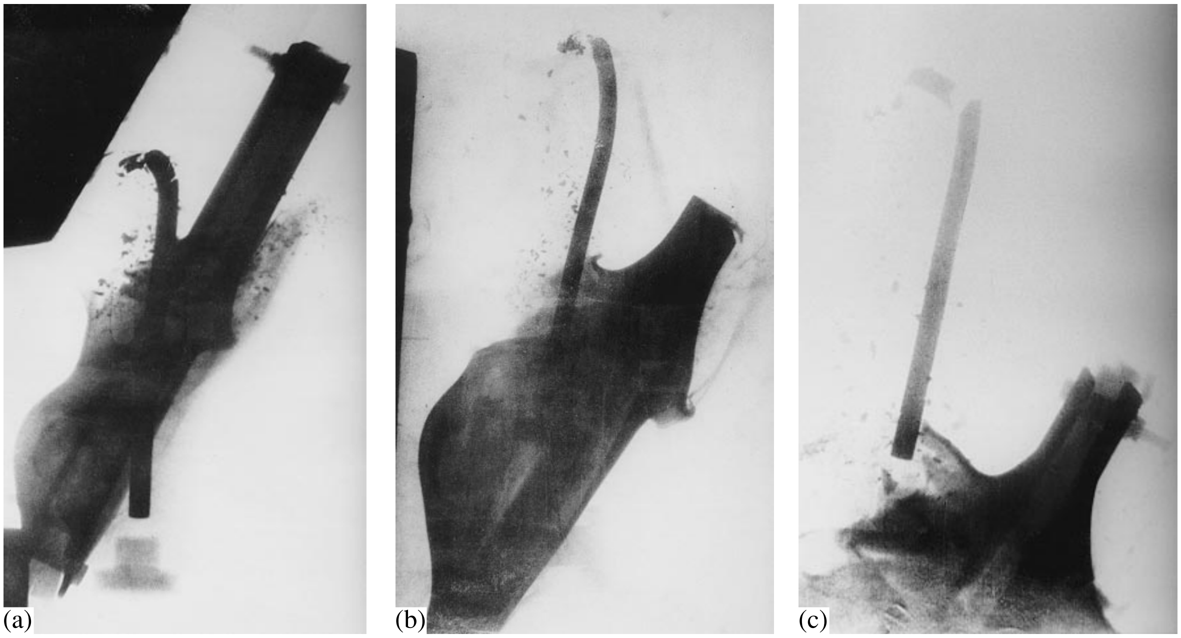

Fig. 1. X-ray patterns for interacting bodies at times (a) 90, (b) 160, and (c) 200 μs.

At the main stage of the interaction process, i.e., at the penetration stage, the shape of contacting bodies changes under the continuous effect of the erosion failure processes (wear) accompanied by the separation of the failed material. We list several characteristic stages of the process. When the shock wave reaches the rear surface of the target, the rear bulge is formed. The front cavity is simultaneously formed with the failure of the front layer of the target and front part of the projectile. With the further penetration of the projectile into the target, the additional rear bulge is formed (Fig. 2a). When the projectile reaches the rear layer of the target, the projectile begins to destroy this layer and a hole is formed through the target. Further, the rear layer of the target near the impact region fails into fragments.

Calculations show that the projectile directly interacts with a region of the rear layer of the target with low mobility (particularly in the horizontal direction). After interaction with this region, the front part of the projectile begins to bend towards the normal to the target surface, which is observed at a time of 120 μs (Fig. 2b).

For the cases under consideration, Fig. 3 shows the configurations of projectile fragments moving behind the target after the penetration through the target (t = 300 μs). Common features are the bending of the front part of the projectile for thicknesses $0.34d_0$ and $0.68d_0$ of the rear layer of the target (variants *a*, *b*, *d*) and prevailing failure of the front part in other cases. A certain bending of the front part is also observed for variants *c* and *f*, which is additionally caused by the effect of the free rear surface on the oblique motion of the projectile in the target.

Analysis of calculations shows that the result of interaction depends qualitatively on the thickness of the rear plate. With an increase in the thickness of the rear layer to a value close to d_0 (Fig. 3, variant *c*), the failure

Parameters of calculation variants

Variant	Thickness of the front steel layer	Thickness of the rear steel layer	Thickness of the middle layer	Material of the middle layer
a	$0.34d_0$	$0.34d_0$	$2.05d_0$	Elastomer
b	$0.34d_0$	$0.68d_0$	Same	″
c	$0.34d_0$	$1.02d_0$	″	″
d	$0.68d_0$	$0.34d_0$	″	″
e	$0.34d_0$	$0.34d_0$	″	Air
f	$0.34d_0$	$0.34d_0$	″	Steel

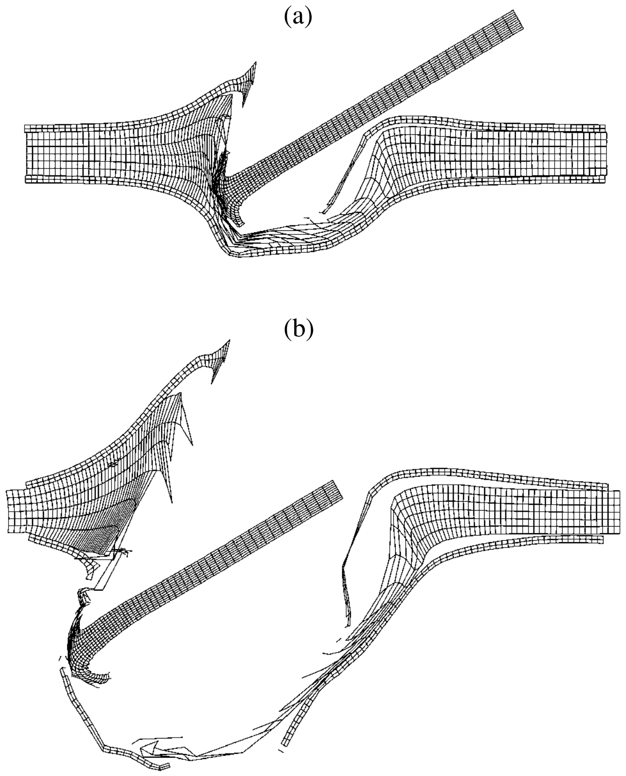

Fig. 2. Calculated configurations of the projectile and three-layer target at times (a) 60 and (b) 120 μs.

(erosion) of the front part of the projectile, as well as the reduction of its length, becomes prevailing.

The middle layer also noticeably affects the interaction character. Calculations for the separated target (without the middle layer) show that the bending of the projectile is virtually unobserved for the thickness of the layers $0.34d_0$ (Fig. 3, variant *e*). In fact, the projectile sequentially interacts with two quite thin targets. As a result, the front part of the projectile deforms and partially fails. For comparison, we consider the case of a steel layer instead of the elastomer (variant *f*). Calculations show that the ricochet effect at the initial stage of the process becomes stronger, and plastic deformations at the penetration stage increase, which is accompanied by the erosion of the material of the interacting bodies. In this case, the final length of the projectile is minimal among all variants of the target composition, but the bending of the front part of the projectile, as well as the further fracture and separation of a part of the projectile, is not observed.

When the thickness of the front layer is doubled (variant *d*), the mass of the ricocheting part, as well as the duration of the phenomenon, increases. However, this does not qualitatively affect the dynamics of the penetration process.

Thus, complex experimental–theoretical investigations of the interaction of the long-rod projectile with the three-layer target containing the middle elastomer layer reveal the dynamics of the penetration, erosion,

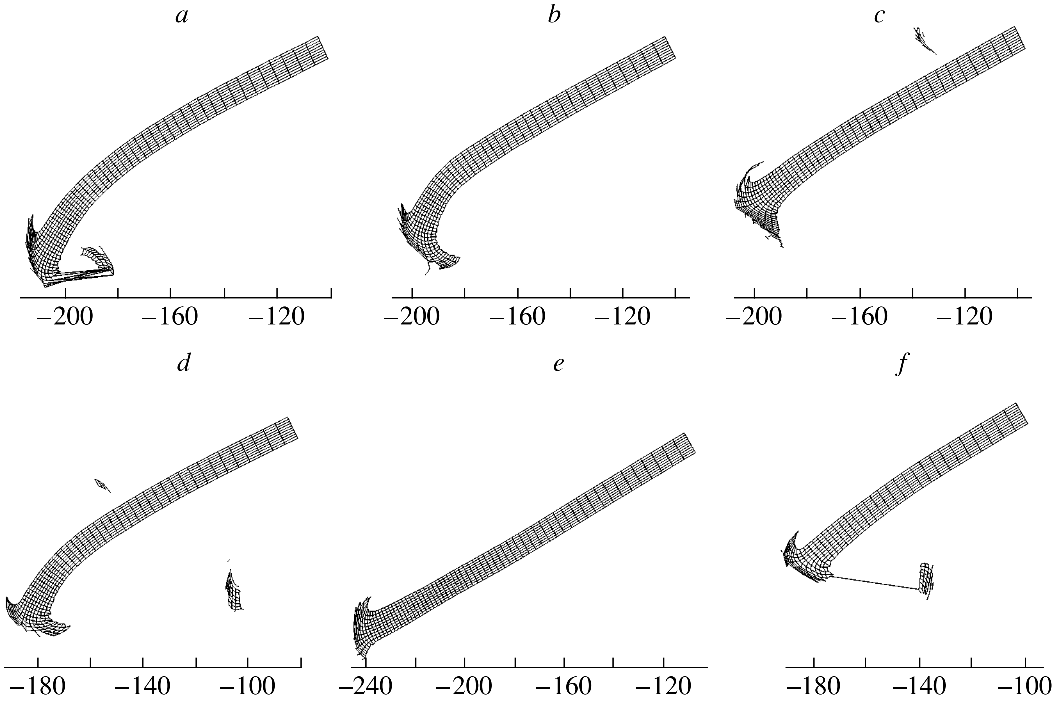

Fig. 3. Projectile shape after interaction with the target for target variants *a*–*f* from the table.

bending, and further failure of the projectile. The character of the failure of the front part of the projectile was found to depend significantly on the thickness of the rear layer of the target. The protective properties of such a target can be improved by properly choosing the material of the middle layer and the thicknesses of middle and rear layers with a fixed thickness of the front layer of the three-layer construction.

ACKNOWLEDGMENTS

This work was supported in part by the Russian Foundation for Basic Research (project no. 03-01-00122).

REFERENCES

1. V. A. Grigoryan, N. S. Dorokhov, I. F. Kobylkin, *et al.*, Oboronnaya Tekhn., Nos. 1–2, 20 (2002).
2. B. V. Voĭtsekhovskiĭ and V. A. Istomin, Fiz. Goreniya Vzryva **36** (6), 87 (2000).
3. S. A. Afanas'eva, N. N. Belov, V. A. Grigoryan, *et al.*, Dokl. Ross. Akad. Nauk **362**, 759 (1998) [Dokl. Phys. **43**, 641 (1998)].
4. V. M. Fomin, A. I. Gulidov, G. A. Sapozhnikov, *et al.*, *High-Velocity Interaction of Bodies*, Ed. by V. M. Fomin (Izd. Sib. Otd. Ross. Akad. Nauk, Novosibirsk, 1999).
5. *Physics of Explosion*, Ed. by L. P. Orlenko (Fizmatlit, Moscow, 2002), Vol. 2.
6. G. I. Kanel', S. V. Razorenov, A. V. Utkin, and V. E. Fortov, *Impact-Shock-Wave Phenomena in Condensed Matter* (Yanus-K, Moscow, 1996).
7. S. A. Zelepugin and V. B. Nikulichev, Fiz. Goreniya Vzryva **36** (6), 186 (2000).
8. I. E. Khorev, S. A. Zelepugin, A. A. Konyaev, *et al.*, Dokl. Ross. Akad. Nauk **369**, 481 (1999) [Dokl. Phys. **44**, 818 (1999)].
9. Yu. B. Kalmykov, G. I. Kanel', I. P. Parkhomenko, *et al.*, Prikl. Mekh. Tekh. Fiz., No. 1, 126 (1990).
10. G. R. Johnson, J. Appl. Mech. **44** (3), 95 (1977).

Translated by R. Tyapaev

Doklady Physics, Vol. 48, No. 10, 2003, pp. 576–579. Translated from Doklady Akademii Nauk, Vol. 392, No. 4, 2003, pp. 477–480.
Original Russian Text Copyright © 2003 by Inogamov, Oparin.

MECHANICS

Wedge and Conic Singularities on the Free Surface of a Fluid: The Dynamics of Rayleigh–Taylor Bubbles and Bubbles near the Wall of an Inclined Tube

N. A. Inogamov* and A. M. Oparin**

Presented by Academician O.M. Belotserkovskiĭ May 26, 2003

Received May 23, 2003

The Rayleigh–Taylor instability is studied in applications to astrophysics, inertial confinement fusion, etc. [1, 2]. The problem of bubbles arises in combustion (flames in channels [3]), the power industry (hydraulics of heat-transfer systems [4, 5]), geophysics (intrusion of salt flows along a bottom, “gravity flows” [6, 7]), and in analysis of the pipeline transport of energy carriers (motion of gas–oil flows [4, 5, 8–12]). A solution with bubbles is important for insight into the physics of slug regimes [4–6, 8–12] of a two-phase flow in pipelines and wells. In addition to the applied aspect, there is a fundamental aspect associated with nonlinear boundary value problems of hydrodynamics (dynamics of a heavy fluid, gravitational waves on water, etc. [1, 2]).

1. FORMULATION OF THE PROBLEM

Figure 1a shows a gas bubble floating in a fluid in a pipe inclined to the horizon at angle α. The bubble moves near the upper wall of the pipe, and the fluid forms a jet j running down under the gravitational acceleration $\mathbf{g}$ along the lower wall. Let the density of the gas, viscosity of the fluid, and surface tension be small. The bubble vertex is at the point B, and BT is the tangent to the free boundary G at the vertex. In the steady state, the angle θ_c (Fig. 1a) between the x axis and tangent BT in 2D geometry is equal to 120°. In the laboratory coordinate system associated with the pipe walls, the fluid is at rest at infinity $x = +\infty$ (the pipe is closed on top), because the fluid is supported by gas pressure. During the motion, the gas ascends and the fluid descends (opposing flows). Vorticity is localized at the boundary G. The flow is potential in the bulk of the fluid and gas. The gas is at rest near the vertex in the coordinate system associated with the bubble vertex B. In this case, the fluid arrives from infinity with the velocity $U(\alpha)$. The velocity of the fluid in the jet j either increases infinitely ($\alpha > 0$) or tends to a constant $U_j > U(0)$ ($\alpha = 0$, horizontal pipe).

The angle θ_c between the wall and boundary G is independent of the slope α. Therefore, a solution with a wedge $\theta_c = 120°$ also exists for $\alpha = 90°$ (Fig. 1b). A bubble with a round vertex $\theta_c = 90°$ (Fig. 1c) has been analyzed in connection with the Rayleigh–Taylor instability [1, 2, 12–14]. Thus, the problem of the Rayleigh–Taylor instability has two steady solutions with $\theta_c = 90°$ and $\theta_c = 120°$ (2D). The solution with the right angle $\theta_c = 90°$ is possible only for $\alpha = 90°$; i.e., only the solution with the wedge $\theta_c = 120°$ exists for $\alpha < 90°$.

2. CONFORMAL MAPPING AND VELOCITY HODOGRAPH

We derive an approximate analytical formula for the velocity of bubbles with an edge (Fig. 1a) by the

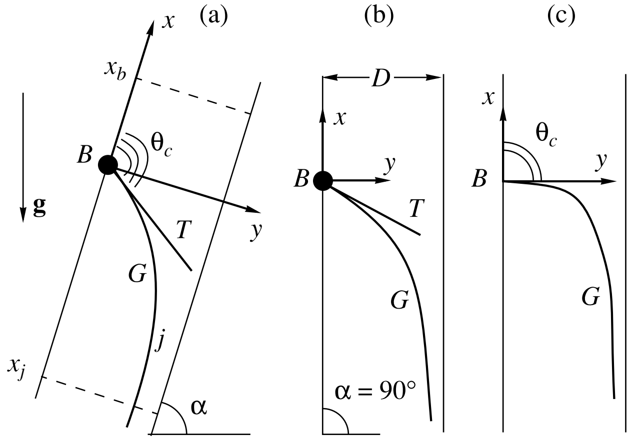

Fig. 1. Bubbles with (a, b) wedge $\theta_c = 120°$ and (c) round $\theta_c = 90°$ vertices.

---

* *Landau Institute for Theoretical Physics, Russian Academy of Sciences, Chernogolovka, Moscow oblast, 142432 Russia*
e-mail: nail@landau.ac.ru

** *Institute for Computer Aided Design, Russian Academy of Sciences, Vtoraya Brestskaya ul. 19/18, Moscow, 123056 Russia*
e-mail: a.oparin@icad.org.tu

1028-3358/03/4810-0576$24.00 © 2003 MAIK “Nauka/Interperiodica”

hodograph method. We write

$$f = U\ln\left(1+\frac{\zeta}{U}\right) - \zeta + \frac{\zeta^2}{2U} \approx \frac{\zeta^3}{3U^2}, \qquad (1)$$

where $\zeta = \frac{df}{dz} = u + iv$ is the velocity hodograph, $z = x + iy$, $f = \varphi + i\psi$ is the complex potential, and $u = \varphi_x$ and $v = \varphi_y$ are the velocity components. The logarithm in Eq. (1) represents the source $(-U, 0)$ on the plane ζ. The power terms substantial near the vertex ($z = 0$, $\zeta = 0$) are chosen specifically. First, the deceleration (stagnation) point must be at the center $\zeta = 0$. Second, the expansion must begin with the cubic term (compensation of the quadratic term), because the zero flow line $\psi(\mathrm{Re}\,\zeta, \mathrm{Im}\,\zeta) = 0$ must leave the center $\zeta = 0$ at an angle of $-120°$ to the $\mathrm{Re}\,\zeta$ axis.

Let us calculate U in Eq. (1). We take the first nonvanishing term in the expansion of the logarithm. Using the formula $\zeta = \frac{df}{dz}$, we obtain $dz = \frac{\zeta}{U^2}d\zeta$. Therefore, $z = \frac{\zeta^2}{2U^2}$ or $\zeta = \frac{df}{dz} = -\sqrt{2}\,U\sqrt{z}$. Integrating the last equation, we obtain the complex potential in terms of the physical variables near the vertex $f = -\frac{2\sqrt{2U}}{3}z^{3/2}$. Separating the imaginary part $\psi(x, y) = \mathrm{Im}f = 0$, we arrive at the equation for the zero flow line $y|_{\psi=0} = -\sqrt{3}\,x$ near the $z = 0$ point (kinematic condition). The squared velocity modulus is equal to $\zeta\zeta^* = 2U^2\sqrt{x^2+y^2}$. On the zero flow line ψ_0, we obtain

$$(\zeta\zeta^*)|_{\psi=0} = 2U^2\sqrt{x^2 + [y(x)|_{\psi=0}]^2} = 4U^2(-x). \qquad (2)$$

We now use the dynamical boundary condition. From the Bernoulli integral at the boundary G (on ψ_0), we have

$$\frac{v^2}{2} = \frac{\zeta\zeta^*}{2} = (\mathbf{g}\cdot\mathbf{r}) = g(y\cos\alpha - x\sin\alpha). \qquad (3)$$

Substituting $y(x)|_{\psi=0} \approx -\sqrt{3}\,x$ into Eq. (3) and transforming Eqs. (2) and (3), we obtain

$$U(\alpha) = \sqrt{\frac{\cos(\pi/6-\alpha)}{\pi}}\sqrt{gD}. \qquad (4)$$

This expression is the desired approximate analytical expression describing the rise of wedge bubbles in inclined pipes for arbitrary angles α. For $\alpha = 90°$, we obtain $\frac{U}{\sqrt{gD}} = \frac{1}{\sqrt{2\pi}}$. As is seen, a wedge bubble floats faster than a round bubble by a factor of $\sqrt{3/2} \approx 1.225$, because $\frac{U}{\sqrt{gD}} \approx \frac{1}{\sqrt{3\pi}}$ for the round bubble [2, 3, 12–14].

3. CONIC SINGULARITY

A singularity at the free boundary appears due to the stop of the flow at the singularity point and the linear coordinate dependence of the gravitational potential. As a result, a 120° wedge is formed in 2D geometry. For the 3D case, the equation $\Delta\varphi = 0$ has the form

$$\frac{(r^2\varphi_r)_r}{r^2} + \frac{(S\varphi_\theta)_\theta}{r^2 S} = 0,$$

where $S \equiv \sin\theta$, in the spherical coordinates r and θ. Let us consider the vicinity of the deceleration point $r = 0$. In view of the homogeneity of gravity and the Bernoulli integral, we have $v \propto \sqrt{r}$. Therefore, $\varphi = r^{3/2}\Phi(\theta)$. The equation for Φ has the form

$$\frac{4(S\Phi_\theta)_\theta}{S} + 15\Phi = 0,$$

which is a 3/2-degree Legendre equation [15]. Its solution regular on the vertical polar axis $\theta = 0$ is the 3/2-degree Legendre function $P_{3/2}(C)$ ($C \equiv \cos\theta$).

We now determine the angle θ_c. The polar component of the velocity is equal to

$$v^{(\theta)} = \sqrt{r}\Phi_\theta = -\frac{\sqrt{r}\,dP_{3/2}}{dC}\sin\theta.$$

It vanishes at the polar axis $\theta = 0$ due to symmetry. Moreover, the $v^{(\theta)}$ component vanishes on the surface of the θ_c cone. The generatrices of the cone compose the angle θ_c with the polar axis. The quantity $C_c = \cos\theta_c$ is the root of the equation $\frac{dP_{3/2}(C)}{dC} = 0$. Numerically solving this equation, we obtain

$$\theta_c = 114.8°. \qquad (5)$$

4. CONSERVATION LAWS

Let us determine the velocity of conic bubbles in a vertical circular pipe. The solution is symmetric about its axis. Let us write the law of conservation of the momentum of the fluid between sections x_j and x_b (Fig. 1a) and the laws of conservation of mass and energy (Bernoulli integral). We approximate the boundary η by the formula

$$y = \eta(x) = x\tan\theta_c - \frac{x^2}{2r}, \qquad (6)$$

where the angle θ_c is given by Eq. (5). Approximation (6) involves the shape of the boundary G near the vertex. It

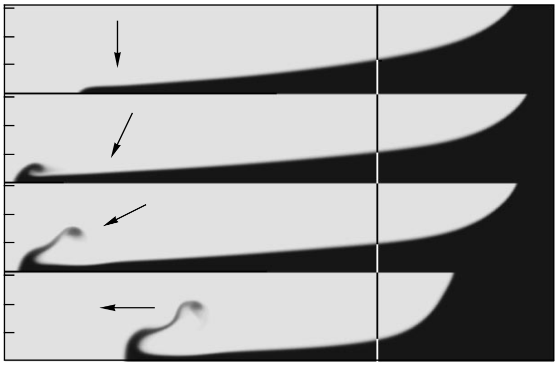

Fig. 2. Bubble–jet flow for the angles $\alpha = 0°, 30°, 60°$, and $90°$. The arrow is the **g** vector. The vertical straight line is the boundary η for $t = 0$.

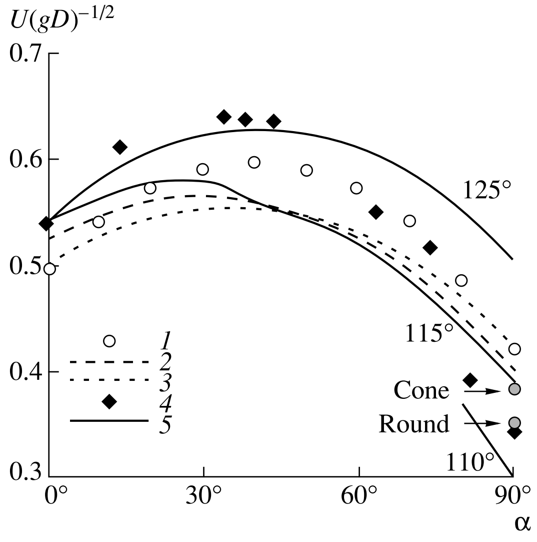

Fig. 3. Bubble velocity U vs. the pipe slope α.

includes one unknown parameter r, which is determined from the laws of conservation of mass, momentum, and energy. Solving the corresponding set of algebraic equations, we determine the following expression for the velocity of the conic bubble in the vertical pipe of the radius $R = \frac{D}{2}$:

$$U \approx 0.54\sqrt{gR} \approx 0.38\sqrt{gD}. \qquad (7)$$

A similar calculation in plane geometry (in this case, $\theta_c = 120°$) provides

$$U \approx 0.42\sqrt{g\left(\frac{\lambda}{2}\right)} \approx 0.3\sqrt{g\lambda}, \qquad (8)$$

where $\frac{\lambda}{2} = D$, see Fig. 1b.

The method is generalized for an arbitrary slope α. The solution in an inclined circular pipe is not axisymmetric, because the bubble moves in the upper part of the pipe. The joining angle θ_c of the boundary of the bubble to the wall is unknown ($\theta_c \sim 120°$). For this reason, it is chosen so that results in the model with conservation laws agree with experiment. In this respect, the 3D solution in the inclined pipe differs from the axisymmetric (in fact, 2D) solution in the vertical circular pipe, when the vertex moves along the axis. The angle θ_c in Eq. (6) is a varying parameter and definite number given by Eq. (5) in the former and latter cases, respectively.

5. CONCLUSIONS CONCERNING SIMULATION AND EXPERIMENT

We now compare analytical results with direct numerical simulation and experiment. Although simulation is extensively used in analysis of the Rayleigh–Taylor instability [1, 2, 14], it has been generalized for the first time to the case of inclined pipes, which is important for technology and close in physical meaning. This generalization opens new prospects for investigations of two-phase flows in such pipes as compared to the traditional purely experimental approach [4, 5, 8, 9].

We describe the basic results. Figure 2 illustrates the role of the slope of the 2D pipe. The arrow is the direction of the gravitational acceleration **g**. The thin vertical straight line is the initial position of the free boundary $\eta(x, t = 0)$ separating the gas and fluid. The gas-to-fluid density ratio is equal to 1 : 20 (gas inertia is small). The gas and fluid are in the white and black regions in Fig. 2, respectively. The position of the boundary η in Fig. 2 is shown for the time $t = 5$. The units $D = \pi$ (width of the 2D channel, Fig. 1) and $g = 1$ were used. Calculations were carried out up to the time $t = 10$. The pipe is long ($15D$) so that the end effects are absent. The mushroom-shaped structure at the ends of the jets increases with α. Comparison of frames in Fig. 2 shows that the velocity $U(\alpha)$ is maximal for angles intermediate between horizontal and vertical. This is also valid for jets. Figure 3 shows the function $U(\alpha)$ for bubbles.

Solid lines *5* (3D model) and *3* (2D model) in Fig. 3 are calculated from the conservation laws (Section 4). The numbers 125, 115, and 110 near the lines are the values of the angle θ_c in Eq. (6) for the 3D case ($\theta_c = 120°$ in the 2D case). According to the experiment [9], it is considered that the boundary of the bubble adjoins the upper wall at the angle $\theta_c \neq 90°$. In this connection, our calculations based on approximation (6) differ from works [11], where η was replaced with a quarter ellipsis (in this case, $\theta_c = 90°$), which is inconsistent with the experiment [9] for low surface tensions. The dashed line is calculated by formula (4). For large slopes ($\alpha = 80°–90°$), 3D data [9] (rhombi) are below the 2D velocity! Thus, the commonly accepted representation that 3D bubbles move much faster than 2D bubbles is invalid for almost vertical pipes.

For the horizontal case ($\alpha = 0$), the exact values 0.5 and 0.54213 of the velocity U follow from the conservation laws for the 2D and 3D cases, respectively. In this case, the shape of η vanishes and calculation is similar to the calculation of the shock adiabatic curve from the conservation laws. The $\alpha = 0$ case was described in [6]. The calculation made in [3] noticeably underestimates the velocity U (0.5/0.43) (our calculations are much more accurate). Circles in Fig. 3 are the 2D simulation (sample in Fig. 2). All 2D lines $U(\alpha)$ obtained by formula (4), calculation by conservation laws (Section 4), and direct numerical simulation (Section 5) are in good agreement. Arrows to the points CONE and ROUND in Fig. 3 correspond to conic (7) and round axisymmetric bubbles, respectively, in the circular vertical pipe.

ACKNOWLEDGMENTS

This work was supported by the Russian Foundation for Basic Research (project nos. 02-02-17499 and 03-01-00700) and the Council for Support of the Leading Scientific Schools of the Russian Federation (project nos. NSh-2045.2003.2 and NSh-70.2003.1).

REFERENCES

1. O. M. Belotserkovskiĭ, *Numerical Simulation in Mechanics of Continuous Media* (Fizmatlit, Moscow, 1994).
2. N. A. Inogamov, A. Yu. Dem'yanov, and É. E. Son, *Hydrodynamics of Mixing* (Izd. Mosk. Fiz.-Tekh. Inst., Moscow, 1999).
3. V. V. Bychkov, Phys. Rev. E **55**, 6898 (1997).
4. G. B. Wallis, *One-Dimensional Two-Phase Flow* (McGraw-Hill, New York, 1969).
5. R. I. Nigmatulin, *Dynamics of Multiphase Media* (Nauka, Moscow, 1987).
6. T. B. Benjamin, J. Fluid Mech. **31**, 209 (1968).
7. C.-S. Yih, *Stratified Flows* (Academic, New York, 1980).
8. G. E. Odishariya and A. A. Tochigin, *Applied Hydrodynamics of Gas–Fluid Mixtures* (Vseros. NII Prirod. Gazov Gaz. Tekhnol., Ivanovsk. Gos. Énerg. Univ., Moscow, 1998).
9. E. E. Zukoski, J. Fluid Mech. **25**, 821 (1966).
10. R. H. Bonnecaze, W. Eriskine, Jr., and E. J. Greskovich, Am. Inst. Chem. Eng. J. **17**, 1109 (1971).
11. I. N. Alves, O. Shoham, and Y. Taitel, Chem. Eng. Sci. **48**, 3063 (1993).
12. K. H. Bendiksen, Int. J. Multiphase Flow **11**, 797 (1985).
13. D. Layzer, Astrophys. J. **122**, 1 (1955).
14. N. A. Inogamov and A. Yu. Dem'yanov, Prikl. Mekh. Tekh. Fiz. **37** (5), 93 (1996).
15. H. Bateman and A. Erdelyi, *Higher Transcendental Functions* (McGraw-Hill, New York, 1953).

Translated by R. Tyapaev

Doklady Physics, Vol. 48, No. 10, 2003, pp. 580–582. Translated from Doklady Akademii Nauk, Vol. 392, No. 4, 2003, pp. 481–483.
Original Russian Text Copyright © 2003 by Loskutov, Dzhanoev.

MECHANICS

Stabilization of the Chaotic Behavior of Dynamical Systems

A. Yu. Loskutov and A. R. Dzhanoev

Presented by Academician V.V. Kozlov May 14, 2003

Received May 20, 2003

Based on the Melnikov criterion, the explicit analytical form of external parametric perturbations leading to stabilization of the chaotic and/or unstable behavior of dissipative dynamical systems is obtained. As an example, analytical results are complemented by numerical analysis of the Duffing–Holmes system.

Stabilization of the unstable or chaotic behavior of a dynamical system is usually meant as the artificial creation in the system of stable (as a rule, periodic) oscillations on the basis of external multiplicative or additive perturbations [1–4]. In other words, in order to realize stabilization, it is necessary to find external perturbations capable of leading the system from the chaotic regime to a regular one. Although the formulation of the problem seems rather simple, its solution for a number of dynamical systems turns out to be a rather complicated task.

We consider the stabilization problem on the basis of analysis of systems with a separatrix loop. As is well-known, in the majority of cases, chaos arises by means of the homoclynic-structure destruction [5]. We perform our analysis for two-dimensional autonomous systems with a single hyperbolic point, which are subject to the action of a periodic perturbation

$$\dot{x} = f_0(x) + \varepsilon f_1(x, t).$$

The basic tool for the analysis of similar systems is the Melnikov method. This method makes it possible to determine the size of the gap $D(t, t_0)$ between stable and unstable branches of the separatrix as (see [6–8])

$$D(t, t_0) = -\int_{-\infty}^{\infty} dt(f_0 \times f_1)\Bigg|_{\Gamma^{(0)}(t-t_0)},$$

where the integral is calculated along the unperturbed separatrix $\Gamma^{(0)}(\tau)$. If $D(t, t_0)$ is an alternating function, then the separatrices intersect each other, and the dynamics in this domain becomes chaotic.

Let the initial set of equations be of the form

$$\begin{aligned} \dot{x} &= P(x, y), \\ \dot{y} &= Q(x, y) + \varepsilon[f(\omega, t) + \alpha F(x, y)]. \end{aligned} \tag{1}$$

Here, $f(\omega, t)$ is a periodic perturbation; $P(x, y)$, $Q(x, y)$, and $F(x, y)$ are smooth functions; and α is dissipation.

Let $x_0(t)$ be the solution on the separatrix. For system (1), in the presence of a perturbation, the Melnikov distance $D(t, t_0)$ can be written as

$$\begin{aligned} D(t, t_0) &= -\int_{-\infty}^{\infty} y_0(t-t_0)[f(\omega, t) + \alpha F(x_0, y_0)]dt \\ &\equiv I[g(\omega, \alpha)], \end{aligned} \tag{2}$$

where $y_0(t) = \dot{x}_0(t)$. We assume that, for system (1), quantity (2) is alternating, i.e., that the separatrices intersect each other. We now find an external perturbation $f^*(\omega, t)$ whose application to the system results in a situation such that the separatrices cannot intersect, i.e., such that the system dynamics is stabilized:[1]

$$\begin{aligned} \dot{x} &= P(x, y), \\ \dot{y} &= Q(x, y) + \varepsilon[f(\omega, t) + \alpha F(x, y) + f^*(\omega, t)]. \end{aligned} \tag{3}$$

It is worth noting that, since system (1) depends on the parameter α, such a stabilization must be performed for each fixed value of this parameter.

We denote the segment in which the function $D(t, t_0)$ changes its sign as $[s_1, s_2]$. After the external perturbation $f^*(\omega, t)$ has been applied, two variants are possible: $D^*(t, t_0) > s_2$ or $D^*(t, t_0) < s_1$, where $D^*(t, t_0)$ is the Melnikov distance for system (3). We analyze the first variant. The second one can be studied in the same manner. In this case,

$$I[g(\omega)] + I[g^*(\omega)] > s_2, \tag{4}$$

Moscow State University,
Vorob’evy gory, Moscow, 119992 Russia
e-mail: Loskutov@moldyn.phys.msu.ru

---

[1] We conditionally call this perturbation f^* “regularizing,” or stabilizing.

where

$$I[g^*(\omega)] = -\int_{-\infty}^{+\infty} y_0(t-t_0) f^*(\omega, t)dt.$$

Expression (4) is true for all values of the left-hand side of the inequality, which exceed s_2. Therefore, we can always find χ such that

$$I[g(\omega)] + I[g^*(\omega)] = s_2 + \chi = \text{const},$$

where $\chi, s_2 \in \mathbb{R}^+$. Hence,

$$I[g^*(\omega)] = \text{const} - I[g(\omega)].$$

On the other hand,

$$I[g^*(\omega)] = -\int_{-\infty}^{\infty} y_0(t-t_0) f^*(\omega, t)dt.$$

We choose $f^*(\omega, t)$ from the class of functions absolutely integrable within an infinite segment and expandable into a Fourier series. We write $f^*(\omega, t)$ in the form

$$f^*(\omega, t) = \text{Re}\{A(t)e^{-i\omega t}\}.$$

Therefore,

$$-\int_{-\infty}^{\infty} e^{-i\omega t}A(t)y_0(t-t_0)dt = \text{const} - I[g(\omega)].$$

The inverse Fourier transformation yields

$$A(t)y_0(t-t_0) = \int_{-\infty}^{\infty} (I[g(\omega)] - \text{const})e^{i\omega t}d\omega.$$

Hence,

$$A(t) = \frac{1}{y_0(t-t_0)}\int_{-\infty}^{\infty} (I[g(\omega)] - \text{const})e^{i\omega t}d\omega.$$

The quantity $A(t)$ may be interpreted as the amplitude of the regularizing perturbation.

Thus, for systems representable in form (1), the external stabilizing perturbation is

$$f^*(\omega, t) = \text{Re}\left[\frac{e^{-i\omega t}}{y_0(t-t_0)}\int_{-\infty}^{\infty} (I[g(\omega)] - \text{const})e^{i\omega t}d\omega\right].$$

In systems for which a displacement from the critical value of the Melnikov function $D(t, t_0)$ is possible by the *additive* shift, we can obtain the stabilizing perturbation in the explicit form:

$$f^*(\omega, t) = -\frac{4\pi a\delta(t)}{y_0(t-t_0)}\cos(\omega t). \quad (5)$$

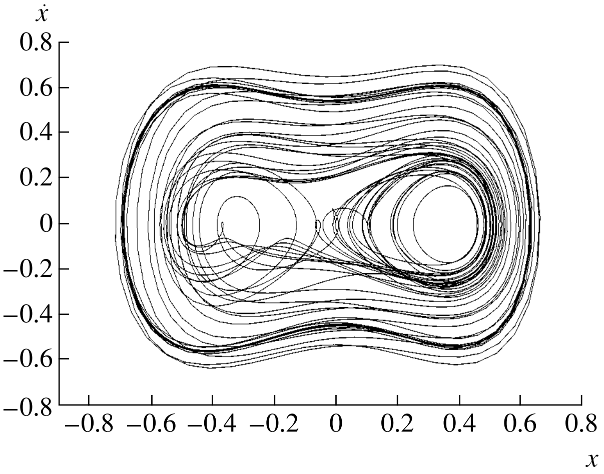

Fig. 1. Phase portrait of Duffing–Holmes system (6) for $\alpha = 0.145$, $\beta = 8$, $\eta = 0.01$, $\gamma = 0.14$, and $\Omega = \omega = 1.1$ (chaotic regime).

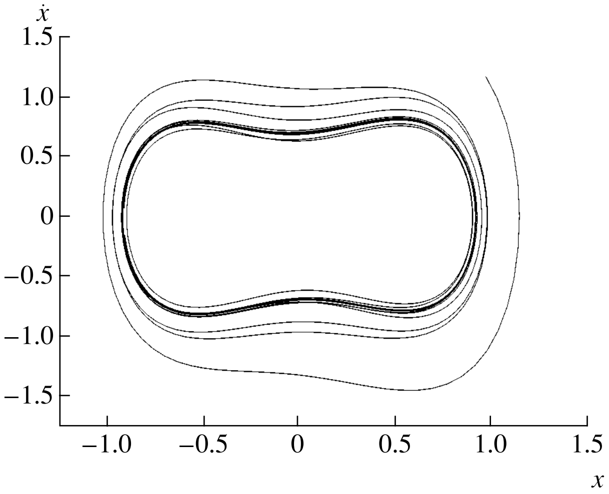

Fig. 2. Phase portrait of Duffing–Holmes system (8) for $\alpha = 0.145$, $\beta = 8$, $\eta = 0.01$, $\gamma = 0.14$, $\Omega = \omega = 1.1$; and $a = 2$ (stabilized behavior).

We now employ this method for the Duffing–Holmes equation. This equation with the parametric perturbation of the cubic term is of the form [8, 9]

$$\ddot{x} - x + \beta[1 + \eta\cos(\Omega t)]x^3 = \varepsilon[\gamma\cos(\omega t) - \alpha\dot{x}], \quad (6)$$

where $\eta \ll 1$ (η and Ω are the amplitude and frequency of the parametric perturbation).

Using the above analysis, it is easy to obtain the explicit form for the external stabilizing perturbation $f^*(\omega, t)$ for system (6). In accordance with relationship (5), we have

$$f^*(\Omega, t) = 2\pi\sqrt{2\beta}\frac{\cosh^2(t-t_0)}{\sinh(t-t_0)}a\delta(t)\cos(\Omega t). \quad (7)$$

Next, we perform the numerical analysis of the system of Duffing–Holmes equations (6). In this system, chaos is developed by means of decomposing of the separatrix contour of the eight-shaped type. The typical structure of a chaotic set is shown in Fig. 1. When perturbation (7) is added to this system, Eq. (6) is written as

$$\begin{aligned}&\ddot{x}-x+\beta[1+\eta\cos\Omega t]x^3\\&=\varepsilon[\gamma\cos\omega t-\alpha\dot{x}+f^*(\Omega,t)].\end{aligned}\tag{8}$$

The numerical solution to this equation is shown in Fig. 2. As is clearly seen, the dynamics of the system becomes completely periodic with time, and the phase curve rapidly tends to a stabilized periodic regime (Fig. 2).

Thus, the numerical analysis is consistent with the analytical calculations.

REFERENCES

1. V. V. Alekseev and A. Yu. Loskutov, Dokl. Akad. Nauk SSSR **293**, 1346 (1987) [Sov. Phys. Dokl. **32**, 270 (1987)].
2. A. Yu. Loskutov, *Nonlinear Dynamics and Control,* Ed. by S. V. Emel'yanov and S. K. Korovin (Fizmatlit, Moscow, 2001), pp. 163–216.
3. A. Loskutov and S. D. Rybalko, in *Proceedings of the V International Conference on Difference Equations and Applications (ICDEA'2000), Temuco, 2000* (Taylor and Francis, London, 2002), pp. 207–230.
4. S. Boccaletti, C. Grebogi, Y.-C. Lai, *et al.*, Phys. Rep. **329**, 103 (2000).
5. L. Shilnikov, in *Proceedings of the International Conference on Nonlinear Dynamics, Chaotic and Complex Systems, Zakopane, 1995*, Ed. by E. Infeld, R. Zelazny, and A. Galkowski (Cambridge Univ. Press, Cambridge, 1997), Vol. 363, pp. 39–63.
6. V. K. Mel'nikov, Tr. Mosk. Mat. Obshchestva **12** (1), 3 (1963).
7. V. G. Gel'freĭkh and V. F. Lazutkin, Usp. Mat. Nauk **56** (3), 79 (2001).
8. J. Guckenheimer and P. J. Holmes, *Nonlinear Oscillations, Dynamical Systems, and Bifurcation of Vector Fields* (Springer, Berlin, 1990).
9. R. Lima and M. Pettini, Phys. Rev. A **41**, 726 (1990).

Translated by G. Merzon

Doklady Physics, Vol. 48, No. 10, 2003, pp. 583–586. Translated from Doklady Akademii Nauk, Vol. 392, No. 4, 2003, pp. 484–488.

MECHANICS

On the Viscosity of Rarefied Gas Suspensions Containing Nanoparticles

V. Ya. Rudyak* and S. L. Krasnolutskiĭ**

Presented by Academician A.K. Rebrov May 14, 2003

Received May 29, 2003

The presence of dispersed solid particles in a continuum radically changes its properties, including viscosity. The viscosity of suspensions for a low particle volume fraction is usually calculated by formulas based on the Einstein phenomenological theory and its generalizations [1–3]. For rarefied gas suspensions (the carrier gas is rarefied), such approaches are absent. In [4–6], we showed that the dynamics of even rarefied gas suspensions are generally described by a set of master equations involving multiparticle collision integrals. However, the set of Boltzmann master equations can be used to describe rarefied ultra-grained gas suspensions and, in certain cases, even fine-grained gas suspensions.

Study of the transport of nanoparticles in gases and fluids has long been of interest due to the development of nanotechnologies. The sizes of nanoparticles vary from ten to hundreds of Ångströms. Clusters, fullerenes, and large organic molecules can also be usually considered as such particles. Under ordinary conditions, the mean free path of carrier-gas molecules is much larger than the sizes of nanoparticles. Therefore, collisions between gas molecules and a nanoparticle can be adequately described in terms of pair collisions for a wide range of the parameters of rarefied gas suspensions. However, even in this case, the interaction of a gas molecule with a nanoparticle is collective, because it is necessary to take into account its simultaneous interaction with all atoms (molecules) of the particle. This can be done by using a specially constructed potential of the molecule–particle interaction [7–9]. This potential was used to study the diffusion of nanoparticles in rarefied gases in terms of the Boltzmann kinetic theory [9–11]. In particular, it was shown that the properties of the transport of nanoparticles differ radically from those of ordinary Brownian particles, and the Einstein theory, as well as the Cunningham–Millikan–Davies experimental correlation found on its basis, cannot be used to describe their diffusion. At the same time, kinetic theory with the potential proposed in [7–9] agrees well with available and specially obtained experimental data [11].

Since this theory with the potential from [7–9] is successfully used to calculate the diffusion of nanoparticles, one can be sure that it is also applicable to calculation and to analysis of the coefficients of viscosity for ultra-grained rarefied gas suspensions. Gas suspensions with nanoparticles as the dispersed component will be called gas nanosuspensions.

This study aims to analyze the coefficient of viscosity of rarefied gas suspensions by kinetic theoretical methods. The molecule–particle interaction is described by the potential taken from [7–9]. At present, there is no reliable potential of the interaction between dispersed particles (including certain models of the interaction). For this reason, we describe the particle–particle interaction by the hard-sphere potential. We analyzed the dependence of the viscosity coefficient on the radius of particles, their concentration, and the temperature of the carrier medium. It was shown that, depending on the concentration of nanoparticles and their sizes, the effective viscosity of gas nanosuspensions can be both larger and smaller than that of a pure carrier gas. Since the mass concentration of nanoparticles can be equal to about unity even for low particle number densities, the addition of nanoparticles with a certain size and composition to a gas can be used, in particular, to decrease the viscosity of the carrier gas. Thus, the addition of nanoparticles to a gas flow can be used to reduce the drag for bodies moving in the gas.

We consider a rarefied gas nanosuspension as a binary mixture of carrier-gas molecules and nanoparticles. As has been mentioned, the molecule–particle interaction is described by the potential [7–9]

$$\Phi(r) = \Phi_9(r) - \Phi_3(r),$$

$$\Phi_i(r) = C_i\{[(r-R)^{-i} - (r+R)^{-i}] - a_i[(r-R)^{-(i-1)} - (r+R)^{-(i-1)}]\}. \quad (1)$$

Novosibirsk State University of Architecture and Civil Engineering, Novosibirsk, 630003 Russia

* *e-mail: rudyak@ngasu.nsk.su*

** *e-mail: sergius@ngasu.nsk.su*

Here, $C_9 = \frac{4\pi\varepsilon_{ij}\sigma_{ij}^{12}}{45V}$, $C_3 = \frac{2\pi\varepsilon_{ij}\sigma_{ij}^{6}}{3V}$, $a_9 = \frac{9}{8r}$, $a_3 = \frac{3}{2r}$, V is the effective volume per molecule of a dispersed particle, and ε_{ij} and σ_{ij} are the parameters of the Lennard–Jones potential describing the interaction between molecules of the incident gas and each molecule (atom) of the nanoparticle with radius R. Particles interact with each other as hard spheres. The dynamics of such a disperse binary system is described by the conventional Boltzmann set of equations. As a result, in the first approximation of the expansion in Sonin polynomials, the coefficient of viscosity of the rarefied gas nanosuspension under consideration is described by the formula [12]

$$\eta = \frac{1+Z}{X+Y}, \tag{2}$$

where

$$X = \frac{x_1^2}{\eta_1} + 2\frac{x_1x_2}{\eta_{12}} + \frac{x_2^2}{\eta_2},$$

$$Y = 0.6A_{12}^*\left\{\mu\frac{x_1^2}{\eta_1} + 0.5x_1x_2\frac{(1+\mu)^2}{\mu}\frac{\eta_{12}}{\eta_1\eta_2} + \frac{1}{\mu}\frac{x_2^2}{\eta_2}\right\},$$

$$Z = 0.6A_{12}^*$$

$$\times\left\{\mu x_1^2 + 2x_1x_2\left[\frac{(1+\mu)^2}{4\mu}\left(\frac{\eta_{12}}{\eta_1} + \frac{\eta_{12}}{\eta_2}\right) - 1\right] + \frac{1}{\mu}x_2^2\right\},$$

$$\eta_i = \frac{5}{16}\frac{(\pi m_i kT)^{1/2}}{\pi\sigma_{ii}^2\Omega_i^{(2,2)*}}, \quad \eta_{12} = \frac{5}{16}\frac{(\pi m_{12} kT)^{1/2}}{\pi\sigma_{12}^2\Omega_{12}^{(2,2)*}}.$$

Here, x_1 and x_2 are the molar fractions of respective components (hereafter, subscript 2 refers to nanoparticles unless otherwise specified); $\mu = \frac{m_1}{m_2}$, where m_1 and m_2 are the masses of molecules of the carrier gas and particle, respectively; T is the temperature; $A_{12}^* = \frac{\Omega_{12}^{(2,2)*}}{\Omega_{12}^{(1,1)*}}$, where $\Omega_{12}^{(l,m)*}$ are the reduced Ω integrals; and $\sigma_2 = 2R$.

Thus, similar to the case of molecular gas mixtures, calculation of the transport coefficients for gas nanosuspensions reduces to calculation of the corresponding Ω integrals with potential (1). Since the atoms (molecules) of nanoparticles are generally not identical to carrier-gas molecules, it is necessary to use combination relationships (2) for determining the parameters of the interaction potential for the binary mixture from the parameters of potential (1) for pure gases. In this study, we used the relationships

$$\sigma_{ij} = \sqrt{\sigma_{ii}\sigma_{jj}}, \quad \varepsilon_{ij} = \sqrt{\varepsilon_{ii}\varepsilon_{jj}}.$$

The calculations for a number of binary mixtures (Cd–Ne, Zn–Ne, Cu_2O–Ne, Zn–Ar, Cu_2O–Ar, Ne–Xe, and Ne–UF_6) showed that all Ω integrals for potential (1) (contrary to the corresponding values for a rarefied gas) depend only weakly on both various combination relationships and very different data about the parameters of the intermolecular potentials.

The Ω-integral values are very sensitive to variation of radii of nanoparticles and differ only slightly from unity (by less than 5%) for almost all investigated pairs of molecules beginning with particle radii exceeding 100 Å. On the other hand, the Ω-integral values varies monotonically in the range 1.5–3.5 for particles with a radius of about 10 Å and increase with the constants C_3 and C_9.

The coefficient of viscosity (2) of the gas nanosuspension is a multiparameter function and varies substantially with the sizes of nanoparticles, their concentration, and the temperature of the gas suspension. However, the Boltzmann kinetic theory is applicable for describing gas nanosuspensions only when the number densities of dispersed particles are sufficiently low, more exactly, when the corresponding van der Waals parameter is small: $n_2R^3 \ll 1$ (R is the nanoparticle radius). For this reason, it is useful to study the behavior of the coefficient of viscosity (2) for small molar fractions of the dispersed phase: $x_2 \ll 1$. It is easy to show that, in the first approximation in x_2, coefficient (2) takes the form

$$\eta = \eta_1 + \Delta\eta = \eta_1\left\{1 + \frac{x_2}{1 + 0.6A_{12}^*\mu}\right.$$

$$\left.\times\left[0.3A_{12}^*\frac{(1+\mu)^2}{\mu}\frac{\eta_{12}}{\eta_1} + 2 - 12A_{12}^* - 2\frac{\eta_1}{\eta_{12}}\right]\right\}. \tag{3}$$

Function (3) depends strongly on the mass ratio μ, nanoparticle radius, temperature, and parameters of potential (1). In particular, function (3) can change sign for certain values of these quantities. This means that the addition of small volume fractions of dispersed solid particles to a gas can both increase and decrease the effective viscosity of the medium. As an example, Fig. 1 shows the R dependence of the derivative of function (3) with respect to the volume fraction φ of dispersed particles:

$$\eta' = \eta_1^{-1}\frac{d\eta}{d\varphi} = \frac{kT}{pV_p\eta_1}\frac{d\eta}{dx_2} \tag{4}$$

for the H_2–U gas nanosuspension (uranium particles of radius R in hydrogen). An analysis of Fig. 1 shows that derivative (4) actually changes sign near $R \simeq 360$ Å. Thus, the effective viscosity of this H_2–U gas nanosuspension with particles of a sufficiently large radius is lower than that of the carrier gas. On the other hand, the viscosity of the gas nanosuspension with fine particles is higher than that of the carrier gas. Finally, it should be stressed that derivative (4) is largest for particles of small radii ($R < 20$ Å) and varies noticeably for small R values. This means that even low concentrations of ultra-grained particles can noticeably modify the viscosity of the carrier gas. As an example, Fig. 2 shows the dependence of viscosity (2) for the H_2–U gas nanosuspension on a volume fraction of particles with radius $R = 5$ Å for temperatures T = (*1*) 200, (*2*) 300, (*3*) 400, (*4*) 500, (*5*) 600, (*6*) 800, and (*7*) 1000 K. For concentrations of about 2×10^{-4} and room temperatures, the viscosity of the gas nanosuspension exceeds that of the carrier gas by 90%. This effect depends strongly on temperature, and $\frac{\eta}{\eta_1} \sim 2.3$ at $T = 1000$ K for the same concentrations.

As was noted above, the addition of dispersed particles to a gas, depending on their size, can generally both decrease and increase the effective viscosity of the gas suspension. This circumstance is illustrated in Fig. 3, where the viscosity of the H_2–U gas suspension with uranium particles of radius $R = 700$ Å ($T = 300$ K) is shown as a function of the volume fraction of particles. The viscosity of the gas suspension actually decreases with increasing volume fraction of dispersed particles, and this effect increases with temperature.

The effect of dispersed particles on the behavior of the effective viscosity of the gas suspension is determined by its composition [ratio μ, parameters of potential (1), etc.], and the addition of small particles can both increase (Fig. 2) and strongly reduce the effective viscosity. Figure 4 shows effective viscosity (2) calculated for the Ne–Zn gas nanosuspension as a function of the volume fraction of particles with radius $R = 5$ Å for various temperatures. Curves *1*–*7* correspond to the same temperatures as respective lines in Fig. 2. The effective viscosity is lower than the viscosity of the carrier gas at room temperature and $\varphi = 2 \times 10^{-4}$ by approximately 15%, and this effect also increases with temperature.

In conclusion, it is necessary to note two circumstances. In this study, we used the hard-sphere potential for the calculation of particle interaction. This potential is generally inadequate for dispersed particles. First, these are van der Waals forces substantial at small distances. Second, the hard-sphere potential is known to give an improper temperature dependence of transport coefficients. However, the results and conclusions of this study are virtually independent of these circumstances, because the contribution of the particle–particle interaction to the effective coefficient of viscosity is negligible for small volume concentrations of the dispersed phase. This contribution is absent in formula (3), while the exact calculations show that the inclusion of these interactions modifies the result for small volume fractions of the dispersed phase (up to 10^{-3}) by fractions of a percent, and it is in practice negligible.

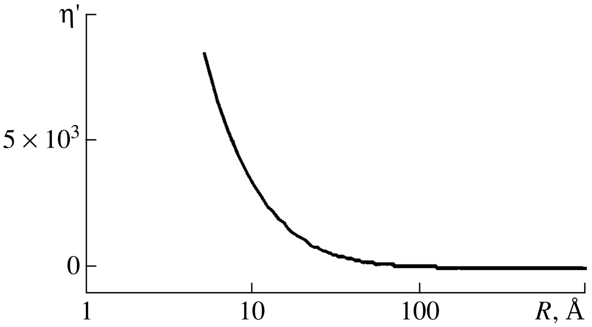

Fig. 1. Derivative of the viscosity of the gas suspension with respect to the volume fraction of uranium particles in H_2 vs. the radius (R = 5–1000 Å) for T = 300 K.

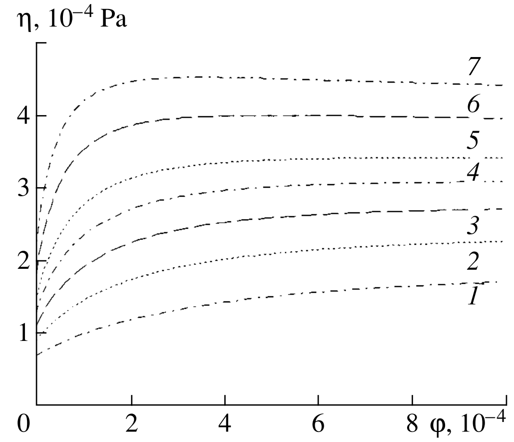

Fig. 2. Viscosity of the gas suspension of uranium particles (R = 5 Å) in H_2 vs. the volume fraction of dispersed particles for temperatures T = (*1*) 200, (*2*) 300, (*3*) 400, (*4*) 500, (*5*) 600, (*6*) 800, and (*7*) 1000 K.

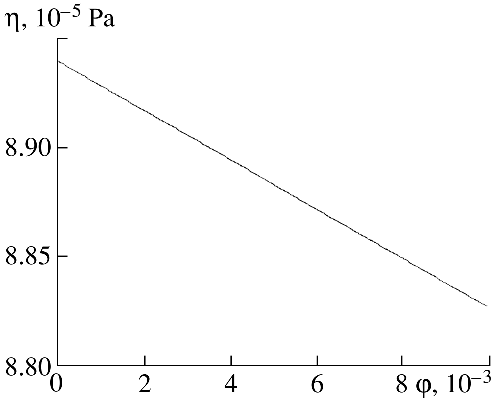

Fig. 3. Same as in Fig. 2, but for R = 700 Å and T = 300 K.

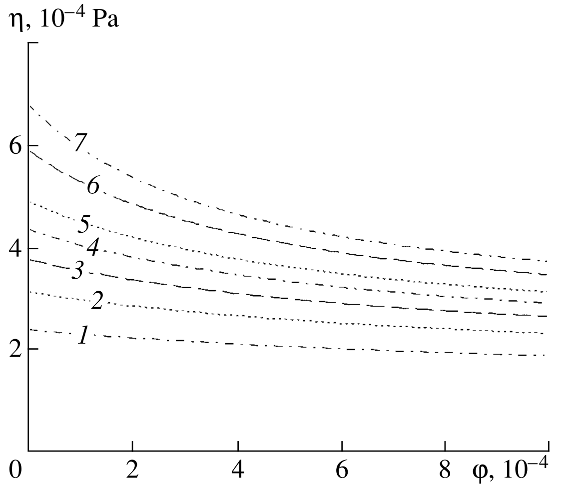

Fig. 4. Same as in Fig. 2, but for the gas suspension of zinc particles (R = 5 Å) in Ne.

We noted above that the behavior of the effective viscosity of a gas suspension is determined by its composition and parameters of components. Knowing these parameters, one can predict the behavior of the effective viscosity. For low particle number densities, formula (3) can be used for calculations. For the gas suspension, it involves small parameters, because usually

$$\mu = \frac{m_1}{m_2} \ll 1, \quad s = \frac{\sigma_1}{\sigma_2} \ll 1. \qquad (5)$$

Parameters (5) are generally related to each other so that $\mu\alpha = s^3$, where α is the ratio between the densities of the dispersed-particle material and carrier-gas molecules. In view of the smallness of parameters (5), formula (3) provides one more useful estimate in the form

$$\eta = \eta_1\left\{1 + x_2\left[1.2\sqrt{2}\frac{\alpha}{s}\frac{\Omega_1^{(2,2)*}}{\Omega_{12}^{(1,1)*}} + 2 - 1.2A_{12}^* - \frac{\sqrt{2}}{4}\frac{1}{s^2}\frac{\Omega_{12}^{(2,2)*}}{\Omega_1^{(2,2)*}}\right]\right\}. \qquad (6)$$

When the sizes of molecules of the carrier gas differ strongly from the sizes of nanoparticles, the last term in formula (6) can dominate, and a reduction in the effective viscosity as compared with the gas viscosity should be expected. Of course, it is necessary to take into account the parameter α and the values of the Ω integrals, which can vary by a factor of 2–3.

Finally, it should be noted that, as a rule, $\sigma_1 \sim \sigma_2$ for a gas mixture, and, for $\mu \ll 1$, it follows from Eq. (3) that

$$\eta = \eta_1\left[1 + 1.2\sqrt{2}x_2\frac{s^2}{\mu}\frac{\Omega_{12}^{(2,2)*}}{\Omega_{12}^{(1,1)*}} + O(1)\right].$$

Thus, a small addition of a heavier gas to a lighter gas increases the viscosity of the mixture as compared to that of the lighter component. However, such an increase depends nonmonotonically on the heavier-component concentration and substantially varies with temperature.

ACKNOWLEDGMENTS

We are grateful to Academician A.K. Rebrov for his interest in this study and for discussion and support. This work was supported in part by the Russian Foundation for Basic Research (project nos. 01-01-00045 and 03-01-06145) and the Council of the President of the Russian Federation for Support of Leading Scientific Schools (project no. NSh-964.2003.1.).

REFERENCES

1. A. A. Einstein, Ann. Phys. **19**, 289 (1906).
2. G. K. Batchelor, Annu. Rev. Fluid Mech. **6**, 227 (1974).
3. G. K. Batchelor, J. Fluid Mech., Part 1 **83**, 97 (1977).
4. V. Ya. Rudyak, Pis’ma Zh. Tekh. Fiz. **18** (20), 77 (1992) [Sov. Tech. Phys. Lett. **18**, 681 (1992)].
5. M. Yu. Gladkov and V. Ya. Rudyak, Zh. Tekh. Fiz. **64** (4), 170 (1994) [Tech. Phys. **39**, 441 (1994)].
6. M. Yu. Gladkov and V. Ya. Rudyak, Izv. Ross. Akad. Nauk, Mekh. Zhidk. Gaza, No. 2, 165 (1994).
7. V. Ya. Rudyak and S. L. Krasnolutskiĭ, Preprint No. 3(13)-98, NGASU (Novosibirsk State University of Architecture and Civil Engineering, Novosibirsk, 1998).
8. V. Ya. Rudyak and S. L. Krasnolutskiĭ, in *Proceedings of the XXI International Conference on Rarefied Gas Dynamics, Marseille, 1999*, Vol. 1, pp. 263–270.
9. V. Ya. Rudyak and S. L. Krasnolutskiĭ, Zh. Tekh. Fiz. **72** (7), 13 (2002) [Tech. Phys. **47**, 807 (2002)].
10. V. Ya. Rudyak and S. L. Krasnolutskiĭ, Dokl. Akad. Nauk **381**, 623 (2001) [Dokl. Phys. **46**, 897 (2001)].
11. V. Ya. Rudyak, S. L. Krasnolutskiĭ, A. G. Nasibulin, and E. I. Kauppinen, Dokl. Akad. Nauk **386**, 624 (2002) [Dokl. Phys. **47**, 758 (2002)].
12. J. O. Hirschfelder, C. F. Curtiss, and R. B. Bird, *Molecular Theory of Gases and Liquids* (Wiley, New York, 1954).

Translated by V. Bukhanov

Doklady Physics, Vol. 48, No. 10, 2003, pp. 587–589. Translated from Doklady Akademii Nauk, Vol. 392, No. 5, 2003, pp. 631–633.
Original Russian Text Copyright © 2003 by Batisheva.

MECHANICS

On the Derivation of Dynamic Equations for a Rigid Body in a Gas Reacting Nonuniformly with Its Surface

Ya. G. Batisheva

Presented by Academician V.V. Kozlov June 20, 2003

Received June 23, 2003

In this study, dynamic equations for a rigid body that moves in a gas [1] and reacts with it nonuniformly over the surface [2] are derived in the kinetic approach. The approach proposed makes it possible to take into account changes in the mass, inertia tensor, and geometrical shape of the body.

Let us consider the motion of a rigid body in the gas that is accompanied by nonuniform surface reactions [3]. The rigid body is characterized by its mass M, radius vector $\mathbf{R}$ of the center of mass, inertia tensor $\hat{J}$, momentum $\mathbf{Q}$, and angular momentum $\mathbf{K}$.

The total force $\mathcal{F}$ with which the gas acts on the body is the sum of microscopic changes of the momentum in individual collisions. In order to find this force, it is necessary to evaluate these microscopic changes for each collision and to integrate over the entire surface for all collisions. If there are several different kinds of interactions between the body and gas molecules (e.g., mirror reflection and absorption occurring with the corresponding probabilities), then local fluxes obtained for each kind of interaction should be added together with their weights and integrated over the surface. The same procedure must be performed for other flux quantities (fluxes of the angular momentum, mass, moment of inertia, and displacements of the center of masses).

The above approach is applicable to the calculation of flux quantities (forces, moments, mass, etc.) only if the frequency of collisions of gas molecules with the body surface is so high that the passage from summation over individual collisions to integration is justified. This condition means that the number of collisions during the minimum characteristic time must be equal to several orders of magnitude. The characteristic times are the rotation period, time taken to cover a single turn in motion along a spiral, relaxation times, i.e., the quantities inverse to the coefficients of the first terms of the expansion of dissipative forces and moments, and, perhaps, the times determined by the features of a particular problem.

The three main kinds of interaction between gas molecules and the surface—mirror, or elastic, reflection; diffuse reflection [5, 6]; and sorption—will be taken into account. The respective terms will be denoted by subscripts e, d, and s. The weighting functions β_i ($i = e$, d, and s) characterizing the relative number of collisions of each kind of interaction must meet the conditions

$$\beta_i \geq 0, \quad i = e, d, s \text{ and } \sum_{i = e, d, s} \beta_i = 1.$$

The weighting functions β_i can be functions of the surface coordinate $\mathbf{r}$ with respect to the center of mass, relative velocity $\mathbf{v}$, and normal $\mathbf{n}$ to the surface at the point where a gas molecule falls on the surface, i.e., $\beta_i = \beta_i(\mathbf{r}, \mathbf{v}, \mathbf{n})$.

The differential frequency of collisions of gas molecules with the body is the number of molecules in an elementary phase-space volume that fall externally on the body per unit time. It is defined by the expression

$$d\Omega = (\mathbf{v}, \mathbf{n}) \cdot \theta((\mathbf{v}, \mathbf{n})) \cdot f(\mathbf{r}, \boldsymbol{p}) d\mathbf{p} ds, \tag{1}$$

where n is the inward normal at the point $\mathbf{r}$ on the body surface, ds is the surface element, $\mathbf{v} = \frac{\mathbf{p}}{m} - \frac{\mathbf{Q}}{M} - [\omega, \mathbf{r}]$ is the relative velocity, m is the mass of a molecule, and ω is the angular velocity.

A change in the shape of a body with a smooth surface can be taken into account analytically. If

$$\mathcal{S} = m\rho^{-1}\int \beta_s(\mathbf{v}, \mathbf{n})\theta((\mathbf{v}, \mathbf{n})) f(\boldsymbol{r}, \mathbf{p}) d\mathbf{p} \tag{2}$$

is the flux of a sorbed substance per unit area, so that the layer with thickness $\mathcal{S}\delta t$ is precipitated on the surface

Keldysh Institute of Applied Mathematics,
Russian Academy of Sciences,
Miusskaya pl. 4, Moscow, 125047 Russia
e-mail: batisheva@newmail.ru

1028-3358/03/4810-0587$24.00 © 2003 MAIK “Nauka/Interperiodica”

Table 1

Parameter of the body	Elastic, or mirror, reflection	Diffuse (Maxwell) reflection
Momentum	$\Delta_e\mathbf{Q} = 2(M^{-1} + m^{-1} + ([\mathbf{r}, \mathbf{n}], \hat{J}^{-1}[\mathbf{r}, \mathbf{n}]))^{-1} \cdot (\mathbf{v}, \mathbf{n})\mathbf{n}$	$\Delta_d\mathbf{Q} = m\mathbf{v} + \mathbf{n}\sqrt{\frac{1}{2}\pi mkT_W}$
Angular momentum	$\Delta_e\mathbf{K} = 2(M^{-1} + m^{-1} + ([\mathbf{r}, \mathbf{n}], \hat{J}^{-1}[\mathbf{r}, \mathbf{n}]))^{-1} \cdot (\mathbf{v}, \mathbf{n})[\mathbf{r}, \mathbf{n}]$	$\Delta_d\mathbf{K} = m[\mathbf{r}, \mathbf{v}] + [\mathbf{r}, \mathbf{n}]\sqrt{\frac{1}{2}\pi mkT_W}$

during the time δt, then the change in the function defining the surface by the formula $\varphi(\mathbf{r}) = 0$ is described in the body reference frame by the equation

$$\frac{\partial\varphi}{\partial t} - \mathcal{S}|\nabla\varphi| = 0. \qquad (3)$$

Now, let us find the increments of the dynamic quantities for each kind of interaction.

The mirror, or ideally elastic, interaction satisfies all conservation laws of mechanics; i.e., the momentum, energy, and angular momentum are conserved. The dynamics of elastic collision of two bodies has already been studied by Maxwell [4]. Acting similarly to [4–6], we derive the formulas listed in the first column of Table 1.

Diffuse reflection, which was also considered by Maxwell for the first time, can be represented in the form of a successive sorption–desorption process with the Maxwellian distribution corresponding to the surface temperature. In this case, the velocities of molecules leaving the surface are assumed to be independent of their velocities before collision with the surface and to be distributed with the probability density [5, 6]

$$\mathcal{P}(\mathbf{p}) = \frac{-(\mathbf{p} - m\mathbf{v}_r, \mathbf{n}) \cdot \theta(-(\mathbf{p} - m\mathbf{v}_r, \mathbf{n}))}{2\pi m(kT_W)^2} \times \exp\left(\frac{(-\mathbf{p} - m\mathbf{v}_r)^2}{2mkT_W}\right). \qquad (4)$$

Here, $\mathbf{v}_r = \frac{Q}{M} + [\omega, \mathbf{r}]$ is the velocity of the surface at the collision point $\mathbf{r}$. The data obtained for the diffuse reflection are listed in the second column of Table 1.

Without going into particular physical and chemical mechanisms, sorption is treated as a collision in which a gas molecule is adsorbed and moves with the body as a whole. Since this interaction is inelastic, the mechanical energy is not conserved, while the momentum, angular momentum, and mass are conserved. In this case, the results are presented in Table 2.

Now the features of the dynamic of a solid body with variable mass geometry are considered. When mass geometry changes due to the absorption of gas molecules, the basis of the principal axes can rotate stepwise by considerable angles [7] even for an arbitrarily low ratio of masses. Therefore, it is reasonable to describe the orientation of the body in terms of the inertia tensor $\hat{J}$ rather than in terms of the Eulerian angles or principal axes used in the traditional description [8].

The corresponding equation can be written in the form

$$\frac{d\hat{J}}{dt} = \hat{\omega}\hat{J} - \hat{J}\hat{\omega} + \int\beta_s\Delta_s\hat{J}d\Omega.$$

Here, the cycling frequency tensor ω is related to the angular velocity as

$$\hat{\omega} = \begin{bmatrix} 0 & \omega_3 & -\omega_2 \\ -\omega_3 & 0 & \omega_1 \\ \omega_2 & -\omega_1 & 0 \end{bmatrix}. \qquad (5)$$

Its commutator with the inertia moment $\hat{J}$ describes the rotation of the body, and the integral term describes the variation of the inertia tensor due to mass absorption. Its microscopic variation $\Delta_s\hat{J}$ is presented in Table 2.

Table 2

Parameter of the body	Sorption
Momentum	$\Delta_s\mathbf{Q} = \mathbf{p} = m(\mathbf{v} + \mathbf{v_r})$
Angular momentum	$\Delta_s\mathbf{K} = \frac{Mm}{M+m}[r, \mathbf{v} + [\omega, \mathbf{r}]]$
Mass	$\Delta_s M = m$
Radius-vector of the center of masses	$\Delta_s \mathrm{R} = \frac{m\mathbf{r}}{M+m}$
Inertia tensor	$\Delta_s\hat{J} = \frac{Mm}{M+m}(\mathbf{r}^2\hat{E} - \mathbf{r}\otimes\mathbf{r}^{\mathrm{T}})$

The final system of equations generally has the form

$$\begin{aligned}
\frac{d\mathbf{R}}{dt} &= \frac{\mathbf{Q}}{M} + \int \beta_s \Delta_s \mathbf{R}\, d\Omega, \\
\frac{dM}{dt} &= \int \beta_s \Delta_s M\, d\Omega, \\
\frac{d\mathbf{Q}}{dt} &= \sum_{i = e, d, s} \int \beta_i \Delta_i \mathbf{Q}\, d\Omega + \mathcal{F}_{\text{external}}, \\
\frac{d\mathbf{K}}{dt} &= \sum_{i = e, d, s} \int \beta_i \Delta_i \mathbf{K}\, d\Omega + \mathcal{M}_{\text{external}}, \\
\frac{d\hat{J}}{dt} &= \hat{\omega}\hat{J} - \hat{J}\hat{\omega} + \int \beta_s \Delta_s \hat{J}\, d\Omega,
\end{aligned} \tag{6}$$

where $\hat{\omega}$ and $d\Omega$ are given by formulas (5) and (1), respectively, and microscopic variations in the quantities are listed in Tables 1 and 2. The system of equations is closed by Eqs. (1)–(3) describing the variation in the frequency of collisions along with the geometrical shape of the body.

Equations (1)–(3) and (6) describe the dynamics of a rigid body in a gas medium with allowance for variation in mass, mass geometry, and the surface geometry during the process.

ACKNOWLEDGMENTS

I am grateful to V.V. Vedenyapin, M.V. Maslennikov, and Yu.N. Orlov for valuable advice and remarks and to I.V. Melikhov and A.Ya. Gorbachevskiĭ for stimulating discussions. This work was supported by the Russian Foundation for Basic Research (project nos. 01-01-00407 and 02-03-33176).

REFERENCES

1. V. V. Beletskiĭ and A. M. Yanshin, *Effect of Aerodynamic Forces on Rotation of Satellites* (Naukova Dumka, Kiev, 1984).
2. Ya. G. Batisheva, V. V. Vedenyapin, I. V. Melikhov, and A. Ya. Gorbachevskiĭ, Mat. Model. **15** (6), 6 (2003).
3. I. V. Melikhov, E. F. Simonov, and A. A. Vedernikov, Zh. Fiz. Khim. **72**, 2300 (1998).
4. J. C. Maxwell, Philos. Mag. **1**, 377 (1860).
5. V. V. Vedenyapin, *Boltzmann and Vlasov Master Equations* (Fizmatlit, Moscow, 2001).
6. C. Cercignani, *Theory and Application of the Boltzmann Equation* (American Elsevier, New York, 1975; Mir, Moscow, 1978).
7. V. I. Arnold, *Mathematical Methods of Classical Mechanics* (Editorial URSS, Moscow, 2000; Springer, New York, 1989).
8. A. V. Borisov and I. S. Mamaev, *Dynamics of Solids* (NITs “Regul. Khaotich. Din.,” Izhevsk, 2001).

Translated by Yu. Vishnyakov

Doklady Physics, Vol. 48, No. 10, 2003, pp. 590–593. Translated from Doklady Akademii Nauk, Vol. 392, No. 5, 2003, pp. 634–637.
Original Russian Text Copyright © 2003 by Georgievskiĭ.

Small Perturbations of an Undeformed State in Media with Yield Stress

D. V. Georgievskiĭ

Presented by Academician I.F. Obraztsov June 11, 2003

Received June 11, 2003

The linearization of constitutive relationships, which is necessary when formulating the problems of stability with respect to small perturbations in continuum mechanics, implies the determination of a linear physical relationship between the increments $\delta\underset{\sim}{s}$ and $\delta\underset{\sim}{v}$ of the stress deviator $\underset{\sim}{s} = s_{ij}\mathbf{e}_i \otimes \mathbf{e}_j$ and the strain-rate tensor $\underset{\sim}{v} = v_{ij}\mathbf{e}_i \otimes \mathbf{e}_j$ coinciding with its deviator due to medium incompressibility. Here, $\mathbf{e}_1$, $\mathbf{e}_2$, and $\mathbf{e}_3$ are the unit vectors of the Cartesian coordinate system. For all media except viscous and perfect fluids, the linearized constitutive relationships involve the unperturbed-process parameters, marked hereafter by the symbol "°."

1. We consider a quite general class of continua that have the shear yield stress τ_s and hardening and satisfy the tensor (vector) linear constitutive relationships [1]

$$s_{ij} = \frac{2}{U}(\tau_s + F(U))v_{ij}, \quad U = \sqrt{2v_{ij}v_{ij}}. \tag{1}$$

The hardening function $F(U) > 0$ meets the conditions

$$\lim_{U \to 0^+} F(U) = 0 \text{ and } \lim_{U \to 0^+} \frac{F(U)}{U} < \infty,$$

i.e., near zero this function can be represented by its linear part

$$F(U) = \mu U + o(U), \quad 0 \le \mu < \infty. \tag{2}$$

Here, μ is the dynamic viscosity at the onset of deformation (starting) (figure, curve *1*). The class under consideration also includes the case of $\mu = 0$, where the material behaves as a perfectly plastic body at the starting time (figure, curve *2*) [2–5].

After linearization, the constitutive relationships have the form [6]

$$\begin{aligned}\delta s_{ij} &= \frac{2}{U^\circ}(\tau_s + F(U^\circ))\delta v_{ij} \\ &+ \frac{4}{U^\circ}v^\circ_{ij}v^\circ_{kl}\left(\frac{d}{dU}\frac{\tau_s + F(U)}{U}\right)_{U = U^\circ}\delta v_{kl} \\ &= \frac{2}{U^\circ}\Big[(\tau_s + F(U^\circ))\Delta_{ijkl} \\ &+ 2v^\circ_{ij}v^\circ_{kl}\left(\frac{d}{dU}\frac{\tau_s + F(U)}{U}\right)_{U = U^\circ}\Big]\delta v_{kl},\end{aligned} \tag{3}$$

where Δ_{ijkl} are the components of the fourth-rank unit tensor.

Multiplying tensor equality (1) by itself, we obtain the scalar constitutive relationship

$$\begin{gathered} T(U) \equiv \frac{1}{\sqrt{2}}\sqrt{s_{ij}s_{ij}} = \tau_s + F(U), \\ \lim_{U \to 0^+} T(U) = \tau_s \end{gathered} \tag{4}$$

between the maximum shear stress T and the highest slip velocity U. If the medium has no hardening ($F \equiv 0$),

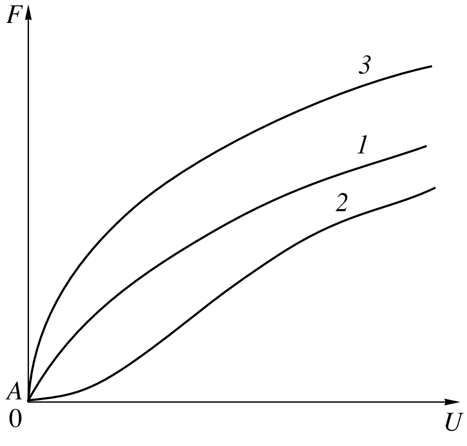

Types of the hardening functions $F(U)$.

Moscow State University,
Vorob'evy gory, Moscow, 119899 Russia
e-mail: georgiev@mech.math.msu.su

relationship (4) represents the von Mises–Hencky plasticity condition.

It is necessary to substitute relationship (3) into the linearized equations of motion (mass forces do not change)

$$-\delta p_{,i} + \delta s_{ij,\,j} = \rho\left(\frac{\partial \delta v_i}{\partial t} + v^{\circ}_{i,\,j}\delta v_j + v^{\circ}_j\delta v_{i,\,j}\right). \quad (5)$$

We also take into account the incompressibility condition

$$\delta v_{i,\,i} = 0 \quad (6)$$

and the Stokes relationship

$$\delta v_{ij} = \frac{1}{2}(\delta v_{i,\,j} + \delta v_{j,\,i}). \quad (7)$$

In this case, the set of four equations (5) and (6) for three velocity perturbations $\delta v_i(\mathbf{x}, t)$ and the pressure perturbation $\delta p(\mathbf{x}, t)$ is closed for the region Ω_f occupied by the flow. Generally speaking, this region is not known in advance, and the boundary separating it from the rigid region $\Omega_{\rm r}$, where $U \equiv 0$, is one of the desired objects of the boundary value problem [7].

A particular case of the field $\mathbf{v}^{\circ}$ can be a one-dimensional plane-parallel shear $v^{\circ}_1 = v^{\circ}(x_2, t)$, $v^{\circ}_2 = v^{\circ}_3 \equiv 0$ with the profile v° [8] preset from certain reasons.

The relation between increments (3) exists only for $U^{\circ}(\boldsymbol{x}, t) \neq 0$. If $U^{\circ} \equiv 0$, i.e., if $v^{\circ}_{ij} \equiv 0$, which corresponds to the undeformed initial state (rest or motion as an absolutely rigid body), according to Eq. (2), it is necessary to replace Eq. (3) with the relations

$$\delta s_{ij} = \frac{2}{\delta U}(\tau_{\rm s} + F(0) + F'(0)\delta U)\delta v_{ij}$$
$$= \frac{2\tau_{\rm s}}{\delta U}\delta v_{ij} + 2\mu\delta v_{ij}, \quad (8)$$

$$(\delta U)^2 = 2\delta v_{ij}\delta v_{ij}$$
$$\equiv \frac{2}{3}((\delta v_{11} - \delta v_{22})^2 + (\delta v_{22} - \delta v_{33})^2$$
$$+ (\delta v_{33} - \delta v_{11})^2 + 6(\delta v_{12})^2$$
$$+ 6(\delta v_{23})^2 + 6(\delta v_{31})^2). \quad (9)$$

Relationships (8) are nonlinear for $\tau_{\rm s} > 0$, and linearization (1) is no longer possible.

The ratios $\frac{\delta v_{ij}}{\delta U}$ in Eq. (8) are about unity, which is corroborated by the following continuum-mechanics parametrizations of space kinematics and spatial stress state in terms of δU and four angles $0 \le \varphi, \theta_1, \theta_2, \theta_3 < 2\pi$ [1–5, 9]:

$$\delta v_{11;\,22} = \frac{\delta U}{2}\cos\varphi\left(\pm\cos\theta_3 + \frac{1}{\sqrt{3}}\sin\theta_3\right),$$
$$\delta v_{33} = -\frac{\delta U}{\sqrt{3}}\cos\varphi\sin\theta_3,$$
$$\delta v_{12} = \frac{\delta U}{2}\sin\varphi\cos\theta_1\cos\theta_2, \quad (10)$$
$$\delta v_{23} = \frac{\delta U}{2}\sin\varphi\cos\theta_1\sin\theta_2,$$
$$\delta v_{13} = \frac{\delta U}{2}\sin\varphi\sin\theta_1;$$

$$\delta s_{11;\,22} = (\tau_{\rm s} + \mu\delta U)\cos\varphi\left(\pm\cos\theta_3 + \frac{1}{\sqrt{3}}\sin\theta_3\right),$$
$$\delta s_{33} = -\frac{2}{\sqrt{3}}(\tau_{\rm s} + \mu\delta U)\cos\varphi\sin\theta_3,$$
$$\delta s_{12} = (\tau_{\rm s} + \mu\delta U)\sin\varphi\cos\theta_1\cos\theta_2, \quad (11)$$
$$\delta s_{23} = (\tau_{\rm s} + \mu\delta U)\sin\varphi\cos\theta_1\sin\theta_2,$$
$$\delta s_{13} = (\tau_{\rm s} + \mu\delta U)\sin\varphi\sin\theta_1.$$

According to Eqs. (8) and (11), the shear yield stress is of the same order of smallness as variations δs_{ij}. Thus, the development of small perturbations near the undeformed state ($U^{\circ} \equiv 0$) can be studied only for a material with a low yield stress $\tau_{\rm s}$. Its degree of smallness in each problem is evidently determined by comparison with the corresponding combinations of other dimensional quantities.

Substituting Eq. (8) into Eq. (5), we obtain the equations of motion

$$-\delta p_{,i} + 2\tau_{\rm s}\left(\frac{\delta v_{ij}}{\delta U}(\delta\mathbf{v})\right)_{,\,j} + \mu\Delta\delta v_{ij}$$
$$= \rho\left(\frac{\partial\delta v_i}{\partial t} + v^{\circ}_{i,\,j}\delta v_j + v^{\circ}_j\delta v_{i,\,j}\right), \quad (12)$$

which are nonlinear with respect to the variations and, together with Eq. (6), form the closed set in the region $\Omega_{\rm f}$. The two last terms on the right-hand side of Eq. (12) can be nonzero (even if $v^{\circ}_{ij} \equiv 0$) when the unperturbed process is the motion of a perfect plastic medium as a perfectly rigid body.

2. Substituting $\theta_1 = \theta_2 = \theta_3 \equiv 0$ into Eq. (11), we obtain the following standard continuum-mechanics parameterization of the stress state for the plane deformation [in the (x_1x_2) plane]:

$$\delta\sigma_{11;\,22} = -\delta p \pm (\tau_{\rm s} + \mu\delta U)\cos\varphi,$$
$$\delta\sigma_{12} = (\tau_{\rm s} + \mu\delta U)\sin\varphi. \quad (13)$$

The set closed in the region Ω_f with respect to v_1, v_2, p, and φ consists of four equations (hereafter, the signs of variations are omitted for brevity):

$$
\begin{gathered}
-p_{,1} - \tau_s \varphi_{,1} \sin\varphi + \tau_s \varphi_{,2} \cos\varphi + \mu \Delta v_1 \\
= \rho\left(\frac{\partial v_1}{\partial t} + v^{\circ}_{1,J} v_J + v^{\circ}_J v_{1,J}\right), \\
-p_{,2} - \tau_s \varphi_{,1} \sin\varphi + \tau_s \varphi_{,2} \sin\varphi + \mu \Delta v_2 \\
= \rho\left(\frac{\partial v_2}{\partial t} + v^{\circ}_{2,J} v_J + v^{\circ}_J v_{2,J}\right), \\
v_{1,1} + v_{2,2} = 0, \\
\cos\varphi = \frac{2 v_{1,1}}{\sqrt{4 v_{1,1}^2 + (v_{1,2} + v_{2,1})^2}}.
\end{gathered}
\tag{14}
$$

The capital roman subscripts take the values 1 and 2.

Set (14) can be easily reduced to the following single nonlinear equation for the perturbation of the stream function $\psi(x_1, x_2, t)$ ($v_1 = \psi_{,2}$, $v_2 = -\psi_{,1}$, $v^{\circ}_1 = \psi^{\circ}_{,2}$, $v^{\circ}_2 = \psi^{\circ}_{,1}$):

$$
\begin{gathered}
\tau_s\left(L\frac{L\psi}{K\psi} + M\frac{M\psi}{K\psi}\right) + \mu\Delta\Delta\psi = \rho\frac{\partial\Delta\psi}{\partial t} \\
+ \rho\epsilon_{JL}(\Delta\psi^{\circ}_{,J}\psi_{,L} + \Delta\psi_{,J}\psi^{\circ}_{,L} + \psi^{\circ}_{,JM}\psi_{,LM} + \psi_{,JM}\psi^{\circ}_{,LM}),
\end{gathered}
\tag{15}
$$

where ϵ_{JL} is the Levi-Civita two-dimensional symbol and

$$
\begin{gathered}
L = \frac{\partial^2}{\partial x_2^2} - \frac{\partial^2}{\partial x_1^2}, \quad M = \frac{2\partial^2}{\partial x_1 \partial x_2}, \\
K\psi = \sqrt{(L\psi)^2 + (M\psi)^2}.
\end{gathered}
\tag{16}
$$

In more detail, we discuss the case where the basic state of a medium is rest ($v^{\circ}_I \equiv 0$) in a gravitational field with a hydrostatic distribution of stresses. In this case, the right-hand side of Eq. (15) is simplified. We rewrite this equation in the dimensionless form assuming that $\tau_s = \frac{\tau}{\rho g h}$ (g is the gravitational acceleration and h is the characteristic linear size) is a small parameter:

$$
\begin{gathered}
\tau\left(L\frac{L\psi}{K\psi} + M\frac{M\psi}{K\psi}\right) + \nu\Delta\Delta\psi = \frac{\partial\Delta\psi}{\partial t}, \\
\nu = \frac{\mu}{\rho\sqrt{gh^3}}.
\end{gathered}
\tag{17}
$$

Equations similar to Eq. (17) arise in the theory of hydrodynamic stability when investigating inviscid flows ($\tau = 0$ and $\nu = 0$), where

$$
\frac{\partial\Delta\psi}{\partial t} = 0 \tag{18}
$$

or the flows of Newtonian viscous fluid [10], where

$$
\nu\Delta\Delta\psi = \frac{\partial\Delta\psi}{\partial t}. \tag{19}
$$

In this paper, we consider only small perturbations of kinematics near the point A in the figure, where the curve $T(U)$ specified by Eq. (4) is discontinuous. Therefore, Eqs. (17)–(19) have only local meaning near the undeformed state.

The question arises as to the character of perturbations in a pair of parameters τ and ν in terms with the higher derivatives in Eq. (17) with respect to Eq. (18) and perturbation of τ in Eq. (17) with respect to Eq. (19). It is known that Eq. (19) is a singularly perturbed biparabolic equation [11, 12] in the inviscid limit $\nu \to 0$. In particular, since the small parameter ν appears in the term with the higher derivative, two of four branches of the solutions of Eq. (19) do not tend to solutions of Eq. (18) for $\nu \to 0$ [13, 14]. In this case, the numbers of boundary conditions necessary for the formulation of the corresponding spectral problems differ from each other by two. The mechanical meaning is that only a single quantity (normal component of either the velocity or stress vector) can be set at every point of the boundary in a perfect fluid. At the same time, all components of any of these vectors can be set in a viscous fluid (in the plane case, these are two conditions at each point of the boundary).

Similar to the case of a perfect fluid, in a medium behaving at the initial time of flow ($U \to 0^+$) as a perfectly plastic body ($\nu = 0$), the tangential components of neither the velocity nor stress vector can be set. Therefore, the number of boundary conditions for Eq. (18) is equal to that for Eq. (17), where it is necessary to put $\nu = 0$. If $\nu > 0$, the number of boundary conditions is the same for Eqs. (19) and (17).

Therefore, it is natural to assume that the dependence of solutions of Eq. (17) on τ is regular:

$$
\psi = \psi_0 + \tau\psi_1 + \tau^2\psi_2 + \ldots, \tag{20}
$$

where ψ_0 is the solution of Eq. (18) or Eq. (19) if $\nu = 0$ or $\nu > 0$, respectively. Substituting asymptotic expansion (20) into Eq. (17) and equating the coefficients of

τ powers, we obtain the sequence of inhomogeneous linear equations for $\psi_1, \psi_2, \ldots$

$$\frac{\partial\Delta\psi_1}{\partial t} - \nu\Delta\Delta\psi_1 = L\frac{L\psi_0}{K\psi_0} + M\frac{M\psi_0}{K\psi_0},$$

$$\frac{\partial\Delta\psi_2}{\partial t} - \nu\Delta\Delta\psi_2$$
$$= L\left[\frac{L\psi_1}{K\psi_0} - \frac{L\psi_0}{(K\psi_0)^3}(L\psi_0 L\psi_1 + M\psi_0 M\psi_1)\right]$$
$$+ M\left[\frac{M\psi_1}{K\psi_0} - \frac{M\psi_0}{(K\psi_0)^3}(L\psi_0 L\psi_1 + M\psi_0 M\psi_1)\right].$$

3. We consider separately the case where the function $F(U)$ near $U = 0$ cannot be represented as Eq. (2); i.e.,

$$\lim_{U \to 0^+} F(U) = 0, \quad \lim_{U \to 0^+} \frac{F(U)}{U} = \infty$$

(figure, curve *3*) so that the hardening function has, for example, the form

$$F(U) = \eta U^\gamma, \quad 0 < \gamma < 1, \quad \eta > 0. \qquad (20)$$

It is necessary to replace relation (8) between the increments $\delta \underset{\sim}{s}$ and $\delta \underset{\sim}{v}$ with the relation

$$\delta s_{ij} = \frac{2\tau_s}{\delta U}\delta v_{ij} + \frac{2\eta}{(\delta U)^{1-\gamma}}\delta v_{ij} \qquad (21)$$

and to replace the factor $\tau_s + \mu\delta U$ with $\tau_s + \eta(\delta U)^\gamma$ everywhere in parameterizations (11) and (13) of the stress state.

Substituting Eq. (21) into Eq. (5), we obtain the following equations of motion in variations instead of Eq. (12):

$$-\delta p_{,i} + 2\tau_s\left(\frac{\delta v_{ij}}{\delta U}(\delta \mathbf{v})\right)_{,j} + 2\eta\left(\frac{\delta v_{ij}}{(\delta U)^{1-\gamma}}(\delta \mathbf{v})\right)_{,j}$$
$$= \rho\left(\frac{\partial \delta v_i}{\partial t} + v^\circ_{i,j}\delta v_j + v^\circ_j \delta v_{i,j}\right),$$

which, together with Eq. (6), close the set in the region Ω_f.

The inclusion of the hardening function in the form of Eq. (20) in the plane problem does not lead to a single compact operator equation of the type of Eq. (15) with respect to the perturbation in the stream function.

ACKNOWLEDGMENTS

This work was supported by the Russian Foundation for Basic Research, project nos. 02-01-00780 and 02-01-00567.

REFERENCES

1. A. A. Il'yushin, *Plasticity* (Gostekhizdat, Moscow, 1948).
2. V. V. Sokolovskiĭ, *Theory of Plasticity* (Vysshaya Shkola, Moscow, 1969).
3. M. I. Erkhov, *Theory of Ideally Plastic Bodies and Constructions* (Nauka, Moscow, 1978).
4. A. Yu. Ishlinskiĭ and D. D. Ivlev, *Mathematical Theory of Plasticity* (Fizmatlit, Moscow, 2001).
5. V. G. Zubchaninov, *Mathematical Theory of Plasticity* (Tversk. Gos. Tekh. Univ., Tver, 2002).
6. D. V. Georgievskiĭ, Izv. Ross. Akad. Nauk, Mekh. Tverd. Tela, No. 5, 21 (2001).
7. D. V. Georgievskiĭ, *Stability of Deformation of Viscoplastic Solids* (URSS, Moscow, 1998).
8. D. V. Georgievskiĭ, Prikl. Mat. Mekh. **58**, 171 (1994).
9. D. V. Georgievskiĭ, Vestn. Mosk. Univ., Ser. 1: Mat., Mekh., No. 3, 45 (2001).
10. H. Lamb, *Lehrbuch der Hydrodynamik* (Verlag-Teubner, Leipzig, 1931; Cambridge University Press, Cambridge, 1932; Gostekhizdat, Moscow, 1947).
11. S. A. Lomov, *Introduction to the General Theory of Singular Perturbations* (Nauka, Moscow, 1981).
12. B. R. Veĭnberg, *Asymptotic Methods in Equations of Mathematical Physics* (Mosk. Gos. Univ., Moscow, 1982).
13. C.-C. Lin, *The Theory of Hydrodynamic Stability* (Cambridge University Press, Cambridge, 1966; Inostrannaya literature, Moscow, 1958).
14. R. Betchov and W. O. Criminale, Jr., *Stability of Parallel Flow* (Academic Press, New York, 1967; Mir, Moscow, 1971).

Translated by V. Bukhanov

Doklady Physics, Vol. 48, No. 10, 2003, pp. 594–597. Translated from Doklady Akademii Nauk, Vol. 392, No. 6, 2003, pp. 767–770.
Original Russian Text Copyright © 2003 by V. Babeshko, O. Babeshko.

MECHANICS

Factorization Method for Boundary Value Problems in Unbounded Domains

Academician V. A. Babeshko and O. M. Babeshko

Received June 18, 2003

The factorization method described in [1, 2] for investigating boundary value problems for partial differential equations is applied to boundary value problems in unbounded multiply connected domains. Unbounded domains traditionally complicate analysis of boundary value problems and are specified by the conditions for the behavior of solutions at infinity. In this work, we demonstrate that the factorization method is applicable in such domains and, therefore, is universal. It is important that the factorization method provides the construction of regularized sets of integral equations for boundary value problems for partial differential equations with piecewise varying coefficients in arbitrary domains with relief boundaries. Moreover, the approach has the standard form independent of the domain of the boundary value problem.

The selection of a single solution in an unbounded domain that is determined by the requirement of radiation or decrease in the solution, depending on the type of the problem, is particularly simple in the factorization method. Basic information concerning the application of the factorization method in unbounded domains is given and illustrated by an example. It has been shown that particular cases of the boundary value problem under consideration, which were solved by other methods, follow from the factorization method.

Numerous boundary value problems of the mechanics of deformable solids, hydromechanics, mathematical physics, seismology, ecology, and other fields considered in layered domains with flat boundaries can be investigated in domains with relief boundaries and arbitrary internal cavities and inclusions by the factorization method.

We note that other, predominantly numerical, methods of analysis of boundary value problems in complex domains only integrally take into account the effect of certain parameters specifying the boundary value problem under consideration on the solution, in particular, the effect of the form of the boundary of the domain of the problem or certain coefficients of differential equations. In contrast, the factorization method can separately trace their effects. In this respect, the factorization method is not only a computational method, but also a method for analysis in arbitrary domains, and is similar to the method of the set of ordinary differential equations with constant coefficients in the one-dimensional case.

In this work, formulas for construction of solutions of boundary value problems in both unbounded and semibounded domains with arbitrary internal cavities and relief boundaries are presented, and the problems of selection of physically justified solutions are discussed.

1. We consider two types of unbounded domains with smooth boundaries. The first type is the entire space with excluded bounded cavities with smooth boundaries. These domains are called unbounded. The second type of domain with the relief boundary includes sets that are embedded in any type of hyperboloids, cylinder, cone, layer, or half-space. At least one boundary of such domains generally extends unboundedly, while the internal zones can contain the cavities described above. Such domains are called semibounded. Thus, similar to [2], the unbounded multiply connected domain Ω has the composite smooth boundary Γ consisting of parts Γ_1 with nonnegative curvature and parts Γ_2 with at least one negative principal curvature.

In these domains, we formulate the boundary value problem for a set of partial differential equations with constant coefficients, which is specified by Eqs. (1) and (2) in [2] with the same notation, but with additional conditions at infinity, which will be presented below. Boundary conditions satisfy the complementarity condition for elliptic systems [3]. The boundary value problem is analyzed in spaces of slowly increasing generalized functions $\mathbf{H}_s(\Omega)$ described in [1].

To apply the approach that was developed in [1, 2] and is based on the methods of manifold geometry to the case of an unbounded domain, it is necessary to compactify this domain. This can be achieved by known procedures using either the homeomorphism of the 3D space to a 3D sphere complemented by an infi-

---

Kuban State University,
ul. Karla Libknekhta 149, Krasnodar, 350640 Russia
e-mail: babeshko@kubsu.ru

nitely distant point or the introduction of the vicinity of the infinitely distant point. The second variant is preferable for practical applications, and we introduce the vicinity of the infinitely distant point that is described by the exterior of spheres whose radii tend to infinity. The infinitely distant point is internal and is the boundary for the first and second types of domains, respectively.

In this case, introducing topology generated by the Euclidean space, we consider the domain as an oriented chain with an oriented boundary.

Since the domain of the boundary value problem is unbounded, it is necessary to comment on the application of the factorization method in such domains. First, we consider the class of problems where the determinant $Q(\alpha)$ of all possible unitary transformations of space has only complex zeros $\alpha_{3\nu}^{\pm}$ in the notation from [2]. For simplicity, we assume that the number of zeros $\alpha_{3\nu}^{\pm}$ of $Q(\alpha)$ in the upper and lower half-planes are equal to each other. We seek the solution of this problem that belongs to $\mathbf{H}_s(\Omega)$ and decreases at infinity.

The case where there are real zeros among $\alpha_3^{\pm}$, which is characteristic for problems of steady oscillations in unbounded media, will be discussed separately. To analyze the boundary value problem in a first-type domain, we introduce an exterior vector form $\omega(\alpha, x)$ whose components are specified as

$$\begin{gathered}
\omega_m(\alpha, x) = R_m dx_1 \wedge dx_2 \\
+ Q_m dx_1 \wedge dx_3 + P_m dx_2 \wedge dx_3, \\
P_m = \sum_r e^{i\langle\alpha, x\rangle}[a_{mr11}(\partial x_1\varphi_r - i\alpha_1\varphi_r) \\
- a_{mr12} i\alpha_2\varphi_r + a_{mr13}\partial x_3\varphi_r + b_{mr1}\varphi_r], \\
Q_m = -\sum_r e^{i\langle\alpha, x\rangle}[a_{mr22}(\partial x_2\varphi_r - i\alpha_2\varphi_r) \\
- a_{mr23} i\alpha_3\varphi_r + a_{mr12}\partial x_1\varphi_r + b_{mr2}\varphi_r], \\
R_m = \sum_r e^{i\langle\alpha, x\rangle}[a_{m33}(\partial x_3\varphi_r - i\alpha_3\varphi_r) \\
- a_{mr13} i\alpha_1\varphi_r - a_{mr23} i\alpha_2\varphi_r + b_{mr3}\varphi_r].
\end{gathered} \tag{1}$$

According to the above discussion, the vicinities of the infinitely distant point are introduced as the parts of the domain Ω that are extended to infinity and are cut by the large-radius sphere. In the constructed bounded domain, we apply the Stokes formula and then let the radius of the sphere go to infinity. Solutions decrease on the parts of this sphere, and this boundary disappears. We recall that, similar to [1, 2], the exterior form contains the relations describing the specified boundary conditions, as well as the functions that must be determined or their normal derivatives with boundary values. Assuming that the vector function φ satisfies the set of differential equations (1) from [2], we arrive at the expression

$$\begin{gathered}
\varphi(\mathbf{x}) = \frac{1}{8\pi^3}\iiint_{\sigma} Q^{-1}(\alpha)\cdot\mathbf{D}(\alpha)\cdot\iint_{r} e^{-i\langle\alpha, \mathbf{x}\rangle} \\
\times\omega(\alpha, \xi)d\alpha_1\wedge d\alpha_2\wedge d\alpha_3, \\
\mathbf{Q}^{-1}(\alpha) = Q^{-1}(\alpha)\mathbf{D}(\alpha), \quad \mathbf{D}(\alpha) = \mathbf{D}(\alpha_1, \alpha_2, \alpha_3), \\
\omega(\alpha, \xi) = \omega(\alpha_1, \alpha_2, \alpha_3, \xi_1, \xi_2, \xi_3).
\end{gathered} \tag{2}$$

2. Taking into account that Ω is exterior with respect to the closed surface Γ, we apply generalized factorization to separate classes of functions with the support in $\overline{\Omega}$. Using notation from [1, 2] and omitting the manipulations presented in those works, we can represent Eqs. (5) in the form

$$\begin{gathered}
\iint_{\Gamma}\overset{0}{\mathbf{D}}_k(\gamma_1, \gamma_2, \overset{+}{\gamma}_{3r})\{e^{i\langle\alpha(\gamma), \xi(\eta)\rangle_+}\}_k^{+}\overset{0}{\omega}(\gamma_1, \gamma_2, \overset{+}{\gamma}_{3r}, \eta) = 0, \\
r = 1, 2, \ldots, M, \quad k = 0, 1, 2, \ldots, \\
\gamma_3 = \overset{+}{\gamma}_{3r}(\gamma_1, \gamma_2), \quad \mathrm{Im}\overset{+}{\gamma}_{3r}(\gamma_1, \gamma_2) > 0, \\
\overset{0}{\mathbf{D}}_{2k}(\gamma_1, \gamma_2, \gamma_3) = \overset{0}{\mathbf{D}}(\gamma_1, \gamma_2, \gamma_3)\overset{0}{Q}(\gamma_1, \gamma_2, -\gamma_3) \\
+ \overset{0}{\mathbf{D}}(\gamma_1, \gamma_2, -\gamma_3)\overset{0}{Q}(\gamma_1, \gamma_2, \gamma_3), \\
\overset{0}{\mathbf{D}}_{2k+1}(\gamma_1, \gamma_2, \gamma_3) = \overset{0}{\mathbf{D}}(\gamma_1, \gamma_2, \gamma_3)\overset{0}{Q}(\gamma_1, \gamma_2, -\gamma_3) \\
- \overset{0}{\mathbf{D}}(\gamma_1, \gamma_2, -\gamma_3)\overset{0}{Q}(\gamma_1, \gamma_2, \gamma_3),
\end{gathered} \tag{3}$$

where $\gamma_3 = \overset{+}{\gamma}_{3r}(\gamma_1, \gamma_2)$ $[\mathrm{Im}\overset{+}{\gamma}_{3r}(\gamma_1, \gamma_2) > 0]$ and $\gamma_3 = \overset{-}{\gamma}_{3r}(\gamma_1, \gamma_2)$ are the zero sets of the function $Q^0(\gamma_1, \gamma_2, \gamma_3)$ $Q^0(\gamma_1, \gamma_2, -\gamma_3)$ in the new coordinates

$$\begin{gathered}
\alpha = \alpha(\gamma), \quad \gamma = \{\gamma_1, \gamma_2, \gamma_3\}, \\
\xi = \xi(\eta), \quad \eta = \{\eta_1, \eta_2, \eta_3\};
\end{gathered}$$

and

$$\begin{gathered}
\{e^{i\langle\alpha(\gamma), \xi(\eta)\rangle}\}_k^{+} = \left(\frac{1}{2\pi i}\int_{-\infty + io}^{\infty + io}\frac{e^{i\langle\alpha(\gamma), \xi(\eta)\rangle}}{\gamma_3 - \overset{+}{\gamma}_3}d\gamma_3\right)_k, \\
\mathrm{Im}\overset{+}{\gamma}_3 > 0
\end{gathered} \tag{4}$$

according to the application procedure of generalized factorization [2]. Further investigations of the set of integral equations (3) repeat the approach developed in [1, 2], because the surface Γ is bounded, i.e., compact.

We now analyze the case of steady harmonic oscillations of an unbounded medium. It is known that, for the solution to be single, it must satisfy the radiation condition in a certain form. Among these forms are

(i) the Sommerfeld condition that the solution satisfies the limiting differential relation at infinity, (ii) the Ignatovskiĭ principle of limiting absorption that presents the transition to the system without absorption through the system with artificial internal friction, (iii) the limiting-amplitude principle, i.e., the consideration of steady oscillations as the time-limiting solution of the Cauchy problem, and (iv) the Mandelstam energy-emission principle. For an example of dynamic mixed problems for an inhomogeneous strip, all these conditions were analyzed in detail in [4–6], where it was found that the Ignatovskiĭ and Mandelstam principles are equivalent to each other for all anomalous cases associated with the propagation of waves in complex media and domains. Therefore, the factorization method allows extremely simple selection of single solutions similarly to the one-dimensional case. Indeed, in this case, the zeros of the determinant $Q(\alpha)$ also lie on the real axis [4]. Attributing these zeros $\overset{+}{\alpha}_{3k}$ and $\overset{-}{\alpha}_{3k}$ to the upper and lower half-planes if

$$\mathrm{Re}\overset{+}{\alpha}_{2\mathrm{K}} \geq 0, \quad \mathrm{Im}\overset{+}{\alpha}_{3\mathrm{K}} \geq 0,$$

$$-\infty \leq \alpha_1, \alpha_2 \leq \infty,$$

$$\mathrm{Re}\overset{-}{\alpha}_{3\ \mathrm{K}} \leq 0, \quad \mathrm{Im}\overset{-}{\alpha}_{3\ \mathrm{K}} \leq 0,$$

respectively, and using Eqs. (8) and (9) form [2], we automatically satisfy the required emission conditions. For many-valued functions, the calculation of zeros of the dispersion (characteristic) equation requires the choice of necessary branches. Since some problems include physically justified anomalous situations, where real and imaginary parts have opposite signs, it is necessary to perturb the original set of differential equations by setting the terms responsible for internal friction to zero. As a result, all zeros $\overset{\pm}{\alpha}_{3\mathrm{K}}$ will be in the necessary half-planes. Therefore, the sets of integral equations will be correctly derived by the factorization method, and radiation conditions at infinity will be satisfied in the limiting case.

The construction of the set of integral equations (8) from [2] is specific for semibounded domains. Separating the vicinity of the infinitely distant point as described above, we repeat the manipulations preceding the derivation of the set. We arrive at boundaries extended to infinity. At these boundaries, we separate parts cut by large-radius spheres and give them local coordinate systems. Repeating manipulations from the work indicated above, including those in the vicinities of the infinitely distant point, we conclude that the methods of classical or generalized factorization leading to the mentioned sets are applicable.

3. Example. We consider a boundary value problem for the differential equation

$$(A_{11}\partial^2 x_1 + A_{22}\partial^2 x_2 + A_{33}\partial^2 x_3 + A_0)\varphi^0 = 0,$$

specified in the Cartesian coordinate system in a cylindrical domain with unbounded wedge-shaped section

$$|x_1| \leq \infty, \quad \Gamma_0(x_2) \leq x_3 \leq 0, \quad \Gamma_0(-c) = 0.$$

Here, the smooth curve

$$x_3 = \Gamma_0(x_2) \leq -(x_2 + c)\tan\sigma, \quad x_2 \geq -c, \quad \sigma > 0,$$

that lies in the upper half-plane is concave and approaches the asymptotic function

$$L_0\colon x_3 + (x_2 + c)\tan\sigma = 0, \quad x_2 \to \infty$$

from below. For simplicity, we consider that one of the natural boundary conditions for the function or its derivative is specified at the boundary.

This boundary value problem corresponds to out-of-plane vibrations of an anisotropic body. The curve Γ_0 forms the lower relief base of the domain, which transforms to the straight line L_0 under upward deformation. After the application of the Fourier transform in x_1, the boundary value problem becomes two-dimensional,

$$(A_{22}\partial^2 x_2 + A_{33}\partial^2 x_3 + A)\varphi = 0 \tag{5}$$

and the corresponding exterior form is specified by the relations

$$\omega = R dx_2 + Q dx_3,$$

$$R = A_{33} e^{\langle \alpha, x \rangle}(\partial x_3 - i\alpha_3)\varphi,$$

$$Q = -A_{22} e^{\langle \alpha, x \rangle}(\partial x_2 - i\alpha_2)\varphi$$

in the original coordinate system. The absence of zeros in Eq. (5) is associated with renaming in the Fourier transform.

Performing manipulations described in [1, 2] and decomposing unity with local, identically oriented, Cartesian coordinate systems with the ordinate normal to the boundary of the domain, we arrive at the set of integral equations

$$\int_{-c}^{\infty} R dx_2 + \int_{\Gamma_o} \sum_k e_k \{ (A_{33} C_\psi^2 + A_{22} S_\psi^2) \partial x_{3\psi} + i(\alpha_3 A_{33} C_\psi$$
$$+ \alpha_2 A_{22} S_\psi) \} \varphi_\psi \exp i \{ x_{2\psi} (\alpha_3 S_\psi - \alpha_2 C_\psi)$$
$$- H_\psi \alpha_3 - h_\psi \alpha_2 \} dx_{2\psi} = 0,$$

$$\int_{-c}^{\infty} A_{33} [\partial x_3 + i(\alpha_{3\psi} C_\psi - \alpha_{2\psi} S_\psi)] \varphi \exp i \{ H_\psi (\alpha_{2\psi} S_\psi$$
$$- \alpha_{3\psi} C_\psi) - x_2 (\alpha_{2\psi} C_\psi + \alpha_{3\psi} S_\psi) \} dx_2$$
$$+ \int_{\Gamma_o} \sum_k e_k \{ (A_{33} C_\psi^2 + A_{22} S_\psi^2)(\partial x_{3\psi} - i\alpha_{3\psi}) \tag{6}$$
$$+ i(A_{22} - A_{33}) C_\psi S_\psi \alpha_{2\psi} \} \varphi_\psi \exp i \{ x_{2\psi} \alpha_{2\psi}$$

$$-h_\psi(\alpha_{2\psi}C_\psi+\alpha_{3\psi}S_\psi)\}dx_{2\psi} = 0,$$

$$C_\psi = \cos\sigma_\psi, \quad S_\psi = \sin\sigma_\psi,$$

$$\sigma_\psi > \sigma, \quad \sigma_\psi = \pi-\psi, \sum e_k = 1.$$

Here, σ_ψ are acute angles between the angle ox_2 and tangents that are constructed at the origins of the local coordinate systems to the elements of the unity decomposition of the curve Γ_0 and σ is the acute angle between the asymptotic line L_0 and ox_2. The most right-handed element of the decomposition of this curve is semi-infinite and is the vicinity of the semi-infinite point. Relations show that the ray $(-c, \infty)$ is one of the decomposition elements. It is one more vicinity of the infinitely distant point for which the original coordinate system is taken as the local coordinate system. Here, $x_{2\psi}o_\psi x_{3\psi}$ are local right-hand Cartesian coordinate systems with the origin at $o_\psi(h_\psi, H_\psi)$ (in the x_2ox_3 system) and outer normal $o_\psi x_{3\psi}$. As was mentioned above, boundary values of either functions or normal derivatives are unknown in the set of integral equations. As was described in [1], the set is regularized by sequentially inverting the Fourier transforms of unknown functions with respect to the parameters α_2 or $\alpha_{2\psi}$ in the local coordinate systems. Deforming Γ_0 to L_0, $\sigma_\psi \to \sigma$, we arrive at the problem in the wedge-shaped domain, for which set (6) was derived by other methods.

Taking $h_\psi \to 0, H_\psi \to -c(\tan\sigma) = \text{const}, \sigma \to 0$, and $c \to \infty$ in this set, we obtain the problem of the out-of-plane vibration of an anisotropic layer. Setting $h_\psi = 0$, $H_\psi = 0, c = 0$, and $\sigma \to \pi$ in this system, we arrive at this problem for a half-space. This example, where classical factorization was applied, illustrates the above conclusion that it is convenient to deform the boundary contour and to simultaneously trace the role of each zero of the characteristic (or dispersion for oscillation problems in unbounded domains) equation, which directly presents the properties of the coefficients of the original differential equation of the boundary value problem.

However, we emphasize that contours must be deformed carefully in this particular case in view of the application of classical factorization rather than generalized factorization. Indeed, the entire contour can be deformed to a parabola, branch of a hyperbola, or similar infinitely expanded curve (with the corresponding transformations of exterior forms, vicinities, and zeros $\alpha_{r\psi}^{\pm}$ under deformation) with the condition that contour points with negative curvature must not arise. Otherwise, the form of the equations somewhat changes (see Note 2 in [1]).

ACKNOWLEDGMENTS

This work was supported by the Ministry of Education of the Russian Federation (project nos. E02-4.0-190, Z/N-241, 379, 380, GN-374); the Russian Foundation for Basic Research (project no. 03-01-00694); the R2003YuG Program, the Russian Foundation for Basic Research (project nos. 03-01-96537, 03-01-96527, 03-01-96519, 03-01-96584); the “Integratsiya” Program (project no. B0121); and the US Civilian Research and Development Foundation for the Independent States of the Former Soviet Union (grant no. REC-004).

REFERENCES

1. V. A. Babeshko and O. M. Babeshko, Dokl. Akad. Nauk **389**, 184 (2003) [Dokl. Phys. **48**, 134 (2003)].
2. V. A. Babeshko and O. M. Babeshko, Dokl. Akad. Nauk **392** (2003) (in press).
3. S. Agmon, A. Douglis, and L. Nirenberg, Commun. Pure Appl. Math. **12**, 623 (1959); *Estimates of Near-Boundary Solutions of Elliptic Equations* (Inostrannaya Literatura, Moscow, 1962).
4. I. I. Vorovich and V. A. Babeshko, *Dynamic Mixed Problems of Elasticity Theory in Unlimited Domain Regions* (Nauka, Moscow, 1979).
5. I. I. Vorovich, Dokl. Akad. Nauk SSSR **245**, 817 (1979) [Sov. Phys. Dokl. **24**, 302 (1979)].
6. I. I. Vorovich, Dokl. Akad. Nauk SSSR **245**, 1076 (1979) [Sov. Phys. Dokl. **24**, 304 (1979)].

Translated by R. Tyapaev